FILTRATION MECHANICS PROJECT

Annual Report – 1965

(Phase II – Final)

Prepared for

George C. Marshall Space Flight Center

National Aeronautics and Space Administration

Huntsville, Alabama

Fluid Power Controls Laboratory

School of Mechanical Engineering

OKLAHOMA STATE UNIVERSITY

Stillwater, Oklahoma

Technical Summary Report (Phase II - 1965)

Date Submitted: 1 March 1966

Contractor: Oklahoma State University
School of Mechanical Engineering
Fluid Power and Controls Laboratory

STUDY OF FILTRATION MECHANICS AND SAMPLING TECHNIQUES

CONTRACT: NAS 8 11009

Prepared for: George C. Marshall Space Flight Center
Huntsville, Alabama

Prepared by: Roger H. Tucker, Project Leader
Peter Dransfield, Faculty Associate
Kirby L. Stone, Project Associate

E. C. Fitch, Project Director

FOREWORD

This Technical Summary Report was prepared by the Fluid Power and Controls Laboratory of the School of Mechanical Engineering, Oklahoma State University. The study, begun in September, 1963, was initiated by the George C. Marshall Space Flight Center, Huntsville, Alabama, and accomplished under Contract NAS 8 11009.

The contract is entitled "Study of Filtration Mechanics and Sampling Techniques." It is under the technical monitorship and guidance of Mr. Victor Neiland, Chief, Engine Control Systems Section, R-P&VE-PAE, and Mr. Royce Church, Chief, Research Unit, R-P&VE-PAE. The work on the project at OSU has been the duties of Dr. E. C. Fitch, Project Director; Mr. R. H. Tucker and Mr. R. E. Reed, Project Leaders; Dr. P. Dransfield, Faculty Associate; Mr. K. L. Stone, Project Associate; and Mr. R. Khatti, Project Assistant.

Special appreciation is expressed to the following members of the filter industry for making samples of media available for testing: Bendix Filter Division; G. Bopp & Co.; Pall Corporation; Purolator Products, Inc.; and the Wintec Corporation.

This report covers work conducted from 1 January 1965 through 31 December 1965.

ABSTRACT

25533

The report describes the activities and results of research conducted under Phase II of Contract NAS 8 11009. In Phase I, an equation was developed to describe the flow resistance of a filter media in terms of properties such as pore diameter, porosity, and permeability. Tests were developed to measure these properties. In the present report, some of the factors which affect the flow and filtration properties of wire cloth media and elements are investigated. Specific areas of investigation include:

1. examination of the modes of filtration applicable to wire cloth media,
2. the effects of housing design and element configuration on performance,
3. the effect of sintering on filtration properties,
4. the effect of flow variations on filtration performance,
5. the variation of filter efficiency as the filter media becomes loaded with contaminant.

The low pressure sampling technology developed in Phase I was used to develop a sampling device capable of extracting a representative sample of oil from systems working at up to 3,000 lb/in^2. The design and performance of the high pressure sampler are described.

An initial evaluation of the Silting Index Apparatus used for low micron contaminant analysis is included.

TABLE OF CONTENTS

LIST OF TABLES

LIST OF FIGURES

CHAPTER I

THE FILTRATION MECHANISMS OF WIRE-CLOTH MEDIA

1.1 Introduction

In defining or specifying filter performance, it is insufficient to describe only the sizes of particles which the filter will intercept from the fluid passing through it. It is necessary also to describe the quantity of contamination which the filter will handle while still performing satisfactorily. It is axiomatic that a filter in service will gradually clog with contaminant and that its resistance to the passage of the fluid flowing through it will increase, as indicated by a rising pressure drop across the filter for a constant flow-rate through it. It is common to specify a maximum pressure drop at a given flow-rate, at which the filter element must be serviced or replaced. When this condition is reached, the filter element is said to be loaded. The contamination capacity of a filter element can be considered as the quantity of contaminant which has been presented to it when it reaches the loaded condition. Thus, capacity describes a pressure drop--flow rate--contamination loading relationship. It is apparent that contamination capacity will depend on the physical size and type of element, on the flow-rate conditions through it (including surging), and on the type and size of contaminant being presented to it.

For a contamination capacity specification to be meaningful, the procedure associated with it must be closely established. For example,

Military Specifications MIL-F-23656A and MIL-F-8815 for the testing of oil hydraulic system filters require:

1. a constant flow-rate of oil through the filter element,
2. the injecting of known weights of a specified standard contaminant into the fluid, upstream of the test filter,
3. measurement of the pressure drop across the filter after each injection of contaminant.

The pressure drop is plotted against the weight of contaminant added to yield a contaminant capacity relationship. The contaminant capacity can be simplified by quoting the weight of contaminant added to cause the pressure drop to reach a specified value, e.g., 50 lb/in^2, at the particular steady flow-rate used. It should be noted that the contaminant capacity so quoted is the weight presented to, and not the weight of contaminant actually held by the filter element. Figure 1.1 shows a typical contaminant capacity curve with the capacity rated numerically at 50 lb/in^2 pressure drop.

The most common artificial contaminant used in filter capacity tests is composed of accurately controlled mixtures of silica particles. In particular, commercially available mixtures of Arizona Road Dust are used. The most common mixtures are AC Fine and AC Coarse test mixtures, whose particle distributions are shown in Table 1.1.

The experimental work associated with the present Section concerns the contaminant capacity characteristics at constant flow rate of a pleated wire cloth filter element, for a wide range of silica test contaminant size ranges and distributions. The test filter dimensions are shown in Figure 1.2, and the specific flow rate of fluid through the filter was maintained at 0.1 gpm/in^2 of wire cloth in the filter element. The

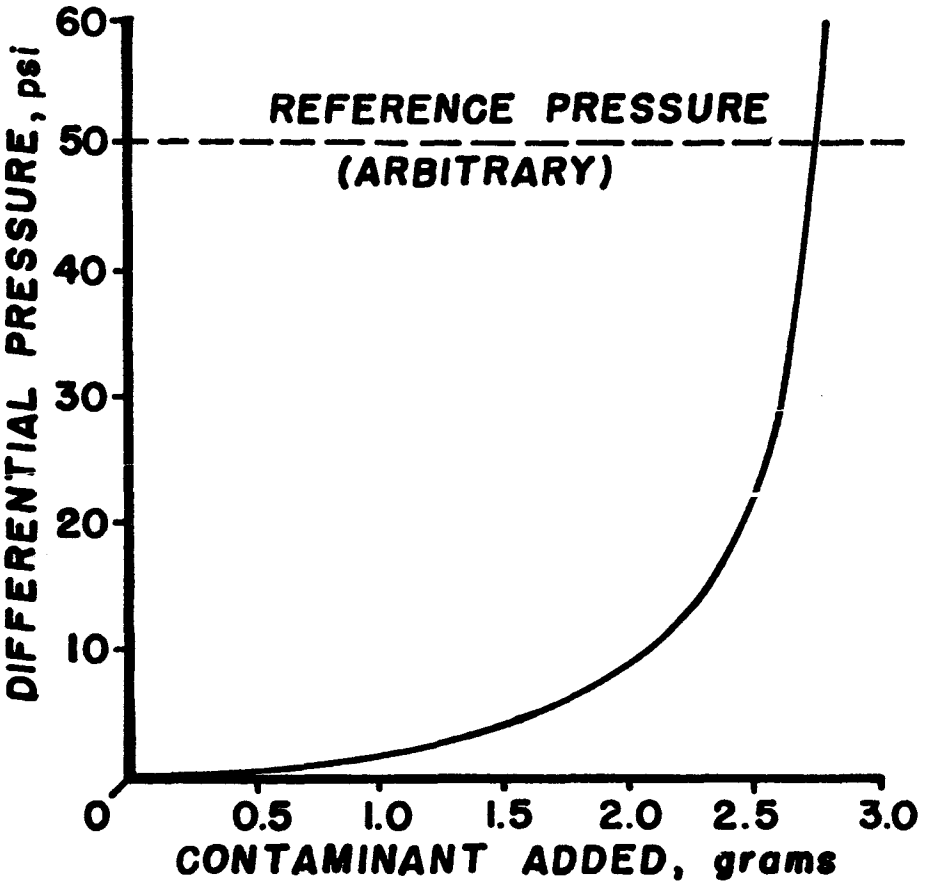

Figure 1.1. A Typical Contaminant Capacity Characteristic.

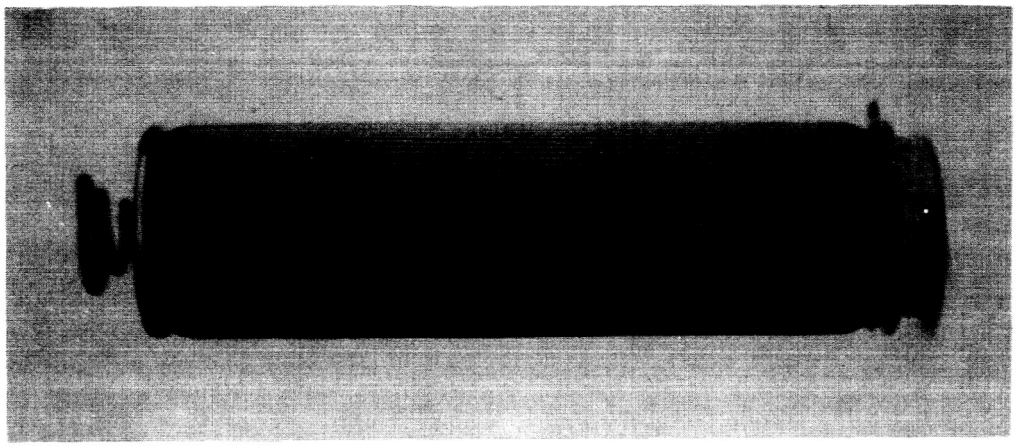

Figure 1.2. The Test Filter Element.

Length	4 in.
O. D.	1.15 in.
Pleat Depth	0.125 in.
No. of Pleats	85
Filter Media	165 x 1400 Dutch Twill Wire Cloth.

TABLE 1.1

PARTICLE SIZE DISTRIBUTIONS OF AC FINE AND AC COARSE TEST DUSTS

AC Fine		AC Coarse	
Size Range, Micron	% by Weight	Size Range, Micron	% by Weight
0-5	39 ± 2	0-5	12 ± 2
5-10	18 ± 3	5-10	12 ± 3
10-20	16 ± 3	10-20	14 ± 3
20-40	18 ± 3	20-40	23 ± 3
40-80	9 ± 3	40-80	30 ± 3
		80-200	9 ± 3

test element was cleaned between tests, using an ultrasonic bath to remove particles from its pores.* The sizes and distributions of contaminants used in the tests are tabulated on Table 1.2.

TABLE 1.2

TEST CONTAMINANT SIZES USED

Test No.	1	2	3	4	5	6	7	8	9
Contaminant Size Range, Micron	0-5	5-10	10-15	15-20	20-25	25-30	30-40	ACF	ACC

1.2 Theoretical Considerations

Hermans and Bredée (1935)[1]** examined experimental filter contamination cycles and proposed the following series of possible filtration mechanisms:

*See Appendix C for details.

**See Section 1.5 for References.

1. Complete Blocking, which occurs when the individual particles are large enough to directly plug the filter pores.
2. Standard Blocking, which occurs when contamination particles in streamlines adjacent to the walls of the pores adhere to the walls. The deposited particles can be smaller than the pore size. A continuous deposition of particles will eventually block the pore.
3. Cake Filtration, which occurs when solid particles of contaminant retained at the filter surface build up as more contaminated fluid is presented at the filter, to form a porous cake. Impingement and consequent stacking of the particles gradually thickens the cake, which acts as the primary barrier to flow through the filter element.
4. Intermediate Blocking, which is loosely defined as a filtration mode between standard blocking and cake filtration.

It is suggested that these mechanisms can be used to describe the various parts of an actual filtration cycle lasting from the clean filter condition over the useful filter life. Each mechanism can be described by mathematical relationships stemming from the basic filtration rate equations.*

$$\frac{d^2t}{dV^2} = K\left(\frac{dt}{V}\right)^n \qquad (1.1)$$

for constant pressure-drop filtration, and

$$\frac{d\Delta P}{dV} = K\Delta P^n \qquad (1.2)$$

for constant flow-rate filtration,

*A general nomenclature is given in Appendix A.

where t is time,

V is the volume of filtrate which has passed,

K is a constant depending on the type and size of contaminant present, the filter medium parameters, and on flow parameters such as flow-rate, viscosity, etc.,

n is an exponent dependent on the mechanism of filtration occurring.

It is suggested that n has the values

n = 2 for complete blocking,

n = 1.5 for standard blocking,

n = 1 for intermediate blocking,

n = 0 for cake filtration.

From Equations (1.1) and (1.2), a series of relationships can be developed to describe different filter operation modes (i.e., constant pressure drop, constant flow-rate, etc.) and different filtration mechanisms (i.e., standard blocking, cake filtration, etc.). The constant flow-rate mode, Equation (1.2), is more appropriate to the present work, and the following relationships can be developed from it:

For complete blocking, n = 2,

$$\frac{\Delta P_o}{\Delta P} = 1 - \frac{K_b V}{Q} \tag{1.3}$$

For standard blocking, n = 1.5,

$$\left(\frac{\Delta P_o}{\Delta P}\right)^{\frac{1}{2}} = 1 - \frac{K_s V}{2} \tag{1.4}$$

For intermediate blocking, n = 1,

$$\log_e \left(\frac{\Delta P_o}{\Delta P}\right) = K_i' V \tag{1.5}$$

For cake filtration, $n = 0$,

$$\frac{\Delta P}{\Delta P_o} = K_c Q V + 1 \qquad (1.6)$$

where K_b, K_s, K_i, and K_c are the appropriate plugging constants, Q is the constant flow-rate, and ΔP_o is the pressure drop required to promote flow-rate Q of uncontaminated oil through the filter.

Gonsalves (1950)[2] confirmed the filtration Equations (1.1) and (1.2), although different assumptions were made for the physical mechanisms of pore blocking. Thus, while the relationships of Hermans and Bredée are confirmed as applicable to the results of the filter performance, an area of doubt exists as to the actual mechanism of pore blocking.

Use of Equations (1.1) to (1.6) to predict filter performance requires assessment of the plugging constants K, and this has proven to be a very difficult requirement.

Grace (1953)[3] considered cake filtration to be described generally by the filtration-rate equation

$$\frac{dV}{dt} = Q = \frac{Ag\Delta P}{\mu\left(\frac{\alpha w V}{A} + R_m\right)} \qquad (1.7)$$

where A is the surface area of the filter and cake normal to flow,

g is acceleration due to gravity,

μ is viscosity of fluid flowing,

α is the specific cake resistance to flow,

R_m is resistance to flow of the filter medium,

the other symbols having been defined previously. Equations (1.7) and (1.6) are of similar form.

The specific cake resistance α is difficult to predict, as it is subjected to wide variations even under nominally constant operating conditions. The only clear fact is that α varies with filtration pressure, which is a reflection of the compressibility of the filter cake. Grace quotes many references concerned with establishing α relationships, and considers that the most successful outcome is the Kozeny-Carman Equation for viscous flow in grannular beds. The relationship assumes that the bed is composed of randomly packed discreet particles of random size and shape, and can be written,

$$\frac{Q}{A} = \frac{\epsilon^3}{(1 - \epsilon)^2 \, BS_o^2} \cdot \frac{\Delta Pg}{L} \qquad (1.8)$$

where Q/A represents the mean flow velocity through the filter,

ϵ is the average cake porosity or void fraction,

L is the cake thickness,

S_o is the specific surface of the contaminant particles

$$= \frac{\text{surface area of particle}}{\text{solid volume into which particle will fit}}$$

B is a constant depending on (1) particle shape and its orientation, (2) ratio length of flow path/cake thickness. B is fairly well established at $5 \pm 10\%$ for particles down to 5μ in an incompressible cake.

Neglecting filter medium resistance R_m as small relative to cake resistance $\alpha wV/A$, Equations (1.7) and (1.8) are combined to give

$$Q = \frac{\epsilon^3 \rho_s}{(1 - \epsilon)^2 \, KS_o^2} \cdot \frac{A\Delta Pg}{\mu \frac{W_o V}{A}} \qquad (1.9)$$

where W_o is the total weight of solid particles in the cake, ρ_s is the density of the solid particles of contaminant, and specific cake resistance has been expressed in terms of the cake properties,

$$\alpha = \frac{(1 - \epsilon)^2 KS_o^2}{\epsilon^3 \rho_s} . \qquad (1.10)$$

Grace (1956)[4] considered that

1. the caking mechanism of filtration was a widely established experimental fact,
2. the standard blocking mechanism fitted experimental data for a significant portion of the filtration cycle,
3. the complete blocking and intermediate blocking mechanisms have limited application, and the regions of a filtration cycle to which they can be applied are ill-defined and of short duration. Complete blocking is only significant in the few situations where only particles larger than the filter pore size are involved.

Grace extended Equation (1.4) for standard blocking to

$$\left(\frac{\Delta P_o}{\Delta P}\right)^{\frac{1}{2}} = 1 - \left[\frac{a/(1 - \epsilon)}{\pi N A h r^2}\right] V \qquad (1.11)$$

where a is the volume of solid particles of contaminant removed, per unit volume of filtrate,

N is the number of pores per unit area of filter medium,

h is the pore length,

r is the effective initial pore radius,

and other symbols are as used previously.

Grace carried out experiments on a wide range of filter media ranging from felt to tightly woven cloth. He concluded that

In general, the data for all media exhibit an initial region of filtration during which neither the standard blocking or cake-filtration apply. Over this initial region a large number of feed particles appear in the filtrate, and this number decreases very rapidly as filtration proceeds. Following this, a transition into a region of standard blocking appears to occur with all media except the Albany 220 felt. The duration of this region of standard blocking varies depending on the character and tightness of the filter medium, ----. ----the period of standard blocking was followed by a transition region which yielded to a prolonged region of cake filtration; this continued until the end of the run. ------. The data -------therefore, show that the filtration cycle generally passes through a number of modes. In each case, a portion of the cycle can be satisfactorily represented by the mode of standard blocking, while one or more regions appear to follow the mode of cake filtration, even though a true cake does not exist in a macroscopic sense. ------. Attempts to apply the complete blocking law to the initial region of filtration period failed in each case.

Bennett and Myers (1962)[5] expressed the filter medium resistance R_m of Equation (1.7) in terms of the hypothetical layer of cake associated with a hypothetical quantity of filtrate, V_m, to give

$$R_m = \frac{\alpha w V_m}{A} \tag{1.12}$$

For an incompressible cake, α is constant and Equation (1.7) was simplified to

$$\Delta P = (K_1 V + K_2)Q \tag{1.13}$$

SUMMARY The modes of blocking which occur in filter media appear to be well established. Each mode can be described mathematically and physically. It seems probable that several modes exist in the life cycle of a filter media, with steady transition from one mode to another. In particular, it seems that cake filtration plays an important part in the life cycle of many filter media.

1.3 The Experiments

1.31 Procedure

The test filter element of Figure 1.2 was fitted to the housing illustrated on Figure 1.3. The housing design permits easy removal of the element for examination and cleaning purposes. The plexiglass housing cylinder allows visual inspection of any build up of contaminant on the surface of the element. A description of the test stand and its operation procedure is given in Appendix B. Briefly, the system oil can be initially filtered to a cleanliness condition below the level on which the test filter is effective. Measured quantities of graded contaminant can be added to the system oil upstream of the test element, and presented to the element as a dispersed suspension. Oil temperature and its flow-rate through the filter element can be maintained constant.

The resistance of the test element to flow of uncontaminated oil at the specified flow-rate was measured. This pressure drop was subtracted from the measured pressure drop across the element to obtain the pressure drop due to the presented contaminant. The increments of artificial contaminant injected varied somewhat for the various particle size distritions used (Table 1.2), and ranged from 0.3 gm of AC Fine Test Dust to 1 gm of the 30-40 micron size cut. In all cases, the increments were sufficiently small to give sufficient points from which to plot the pressure drop--contaminant added relationships (Figure 1.4). The narrow band cuts of silica particles used were separated from AC Test Dust with the Roller Particle Size Analyzer, described in the 1964 Report.* Increments of a required size range were weighed to within 0.005 gm of the required

*Annual Report, 1964, Contract NAS 8 11009, "Study of Filtration Mechanics and Sampling Techniques. Prepared at Oklahoma State University.

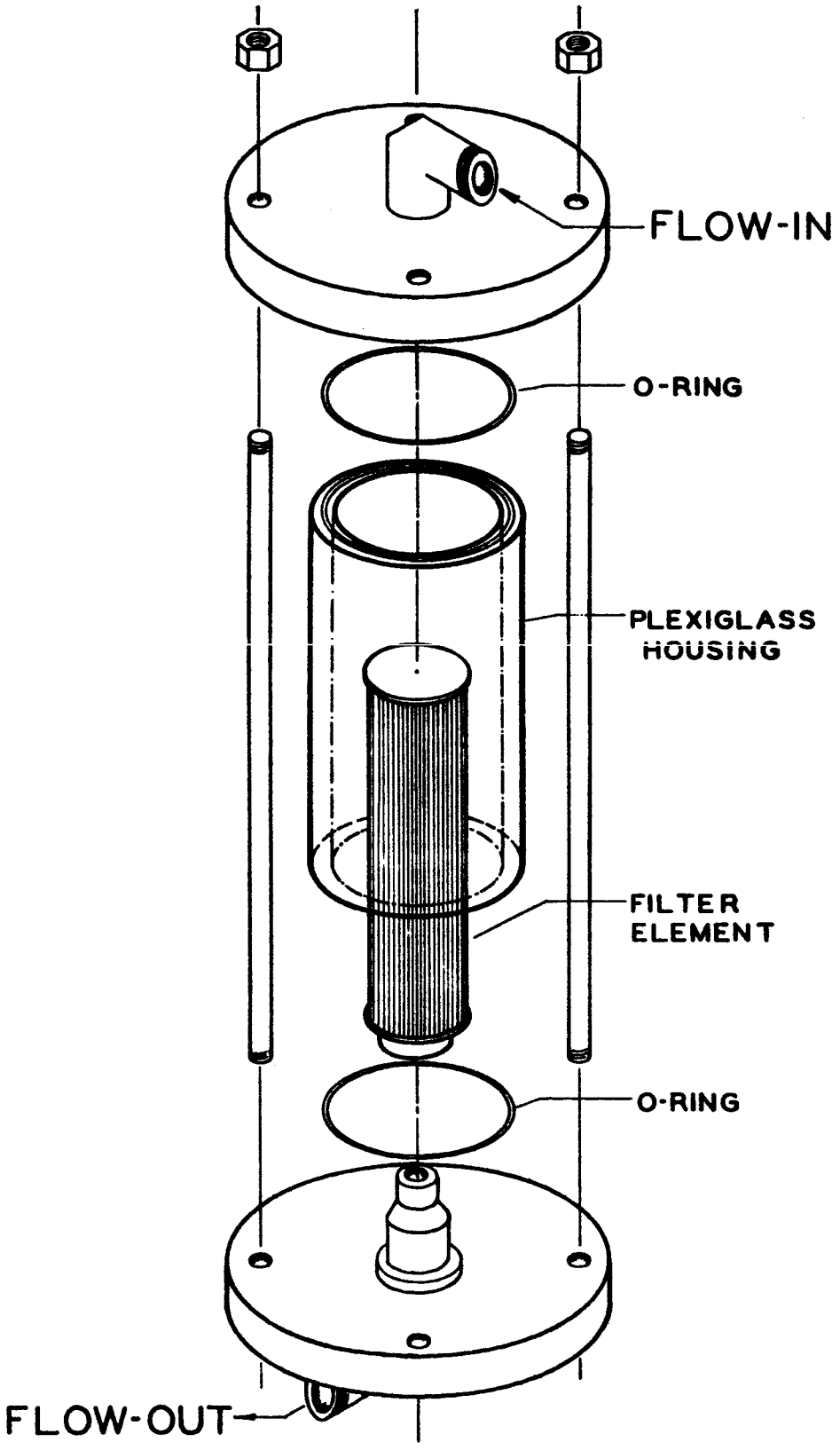

Figure 1.3. The Test Housing.

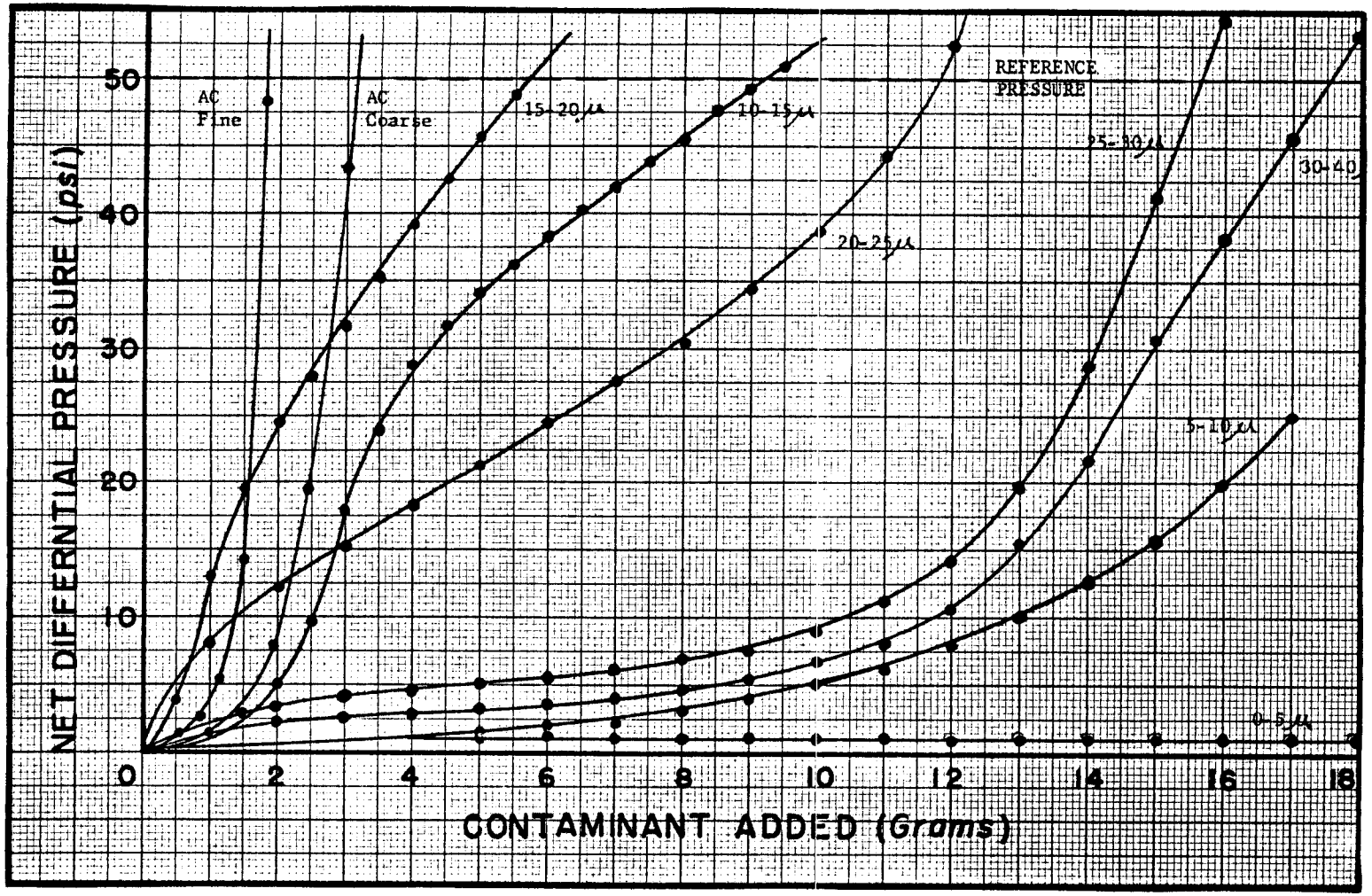

Figure 1.4. ΔP--Contaminant Capacity for Various Contaminant Size Distributions.

value, and placed into pre-cleaned 150 ml sample bottles. Pre-cleaned oil was added to the bottles. Just prior to its use, the contaminant was dispersed in the oil by vigorous shaking following by insertion of the bottle in an ultrasonic vibration tank.

The resultant slurry was added to the system upstream of the test filter. Allowing about 1 minute to ensure that all of the slurry was presented to the filter, the pressure drop across the element was observed. The procedure was repeated until sufficient contaminant had been injected to cause the pressure drop to rise 50 lb/in^2. On completion of a test, the test housing was dismantled and the element removed for cleaning prior to the next test. For the particle size cuts 0-5μ, 5-10μ, most of the contaminant passed through the filter, and the 50 lb/in^2 increase in pressure drop was not achieved with the amounts of contaminant added (Figure 1.4).

1.32 The Results

Figure 1.4 shows the contaminant capacity results obtained for the test filter element exposed to the nine silica particle distributions of Table 1.2 It is important to realize that contaminant capacity refers to the weight of contaminant presented to the filter, and not to the weight of contaminant retained by it.

For the narrow size cuts of contaminant, the contaminant capacity decreases as size increases to the region of the 15-20 cut, after which contamination capacity increases with particle size. The contaminant capacity values for 50 lb/in^2 increase in pressure drop across the filter are shown on Figure 1.5. The high values of contaminant capacity associated with the smaller particle size cuts reflects the passage through

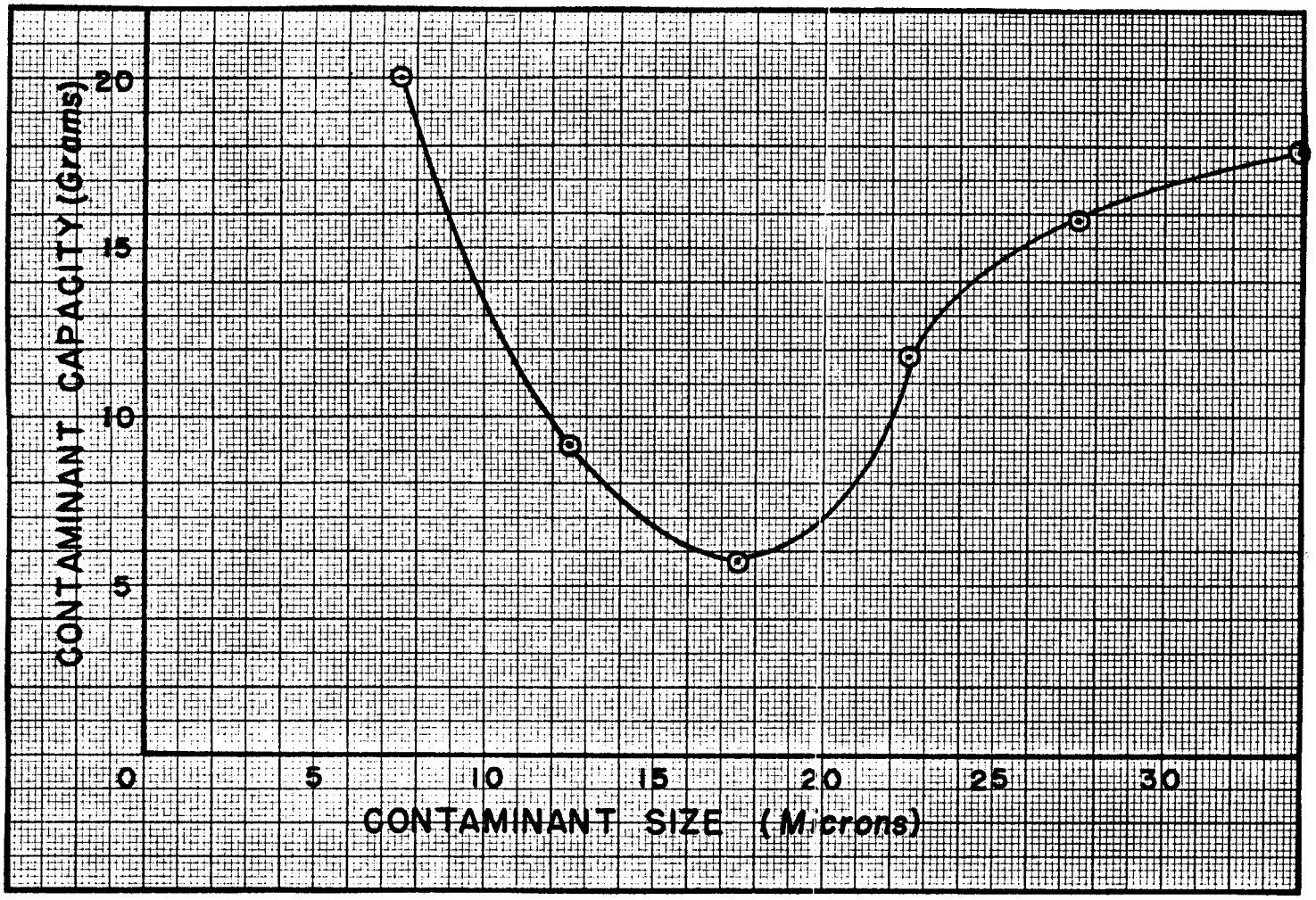

Figure 1.5. Contaminant Capacity (ΔP = 50 lb/in^2)--Particle Size Characteristic.

the filter of most of the contaminant, indicating the inefficiency of the filter at these particle size ranges.

A flat section of the wire cloth from which the filter element was made was subjected to an efficiency test and to a porosimeter test, the results of which are shown on Figure 1.6.

1.33 Discussion

Figure 1.6 indicates that the mean pore size of the test filter is of the order 20-25 microns. Figure 1.5 shows that the reference contamination capacity (arbitrarily chosen at $\Delta P = 50$ lb/in^2 in the present case) when narrow size cuts of silica are used as the test contaminant, reaches a minimum in a region of particle size just below the mean pore size. If the reference capacity was taken at $\Delta P = 40$ lb/in^2, the minimum occurs at the same particle size region. It appears that the nominal capacity versus particle size relationship experiences a discontinuity just below the indicated mean pore size of the filter. The relationship could be modeled by a relationship of the form shown on Figure 1.7, which could readily be described mathematically if further experimental results confirmed the model.

For the present experiments, the contamination level of the oil presented to the filter is nominally constant. The flow rate is also constant. Hence, the volume of oil passing through the filter (i.e., the filtrate V) and the weight of contaminant presented to the filter (W) are proportional. Equations (1.3) through (1.6), which describe various mechanisms of filtration, can be written in terms of W,

for complete blocking,

$$\frac{\Delta P_o}{\Delta P} = 1 - K_b' W \qquad (1.14)$$

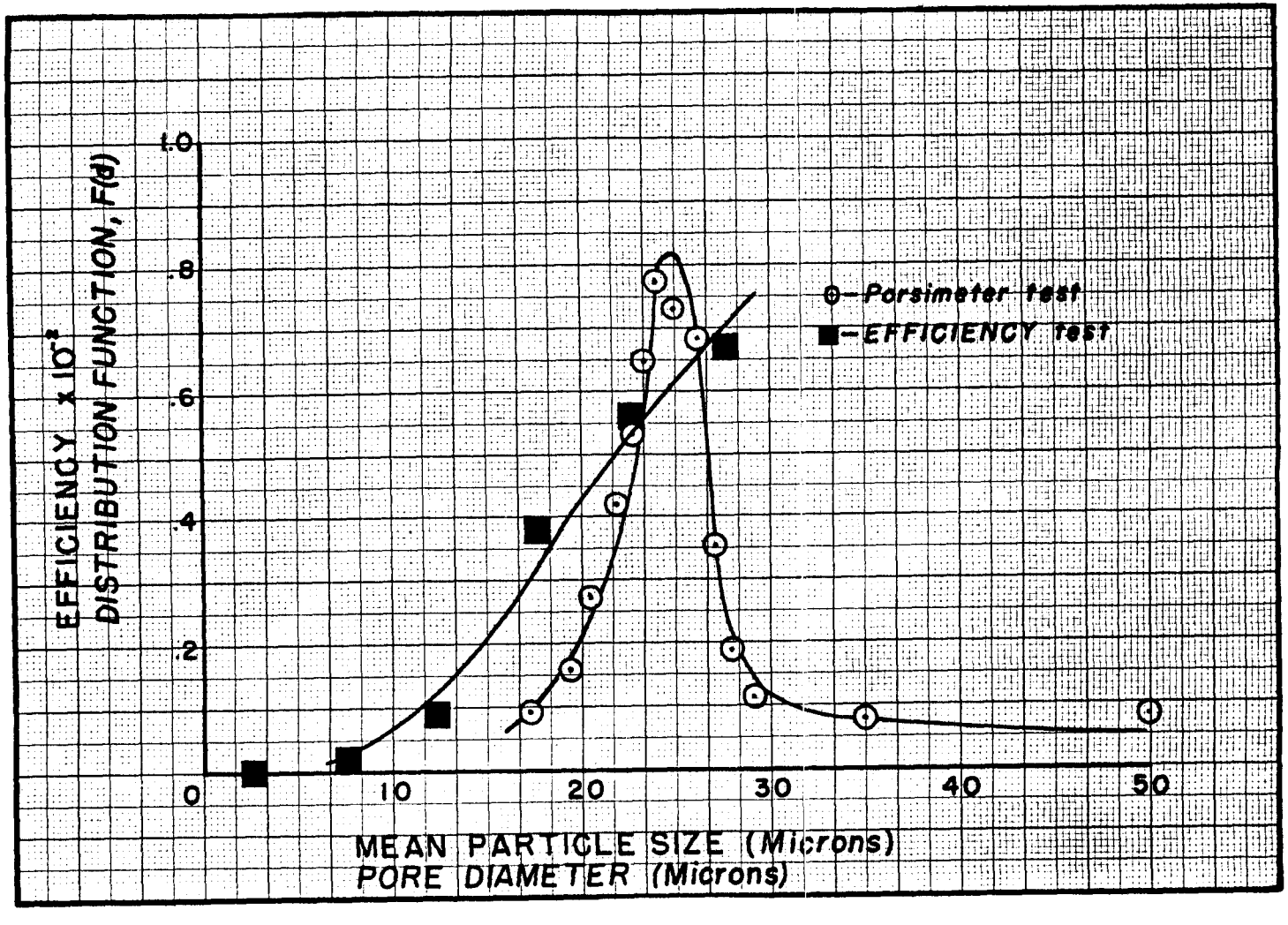

Figure 1.6. Pore Size Distribution and Efficiency Test Results for Test Medium.

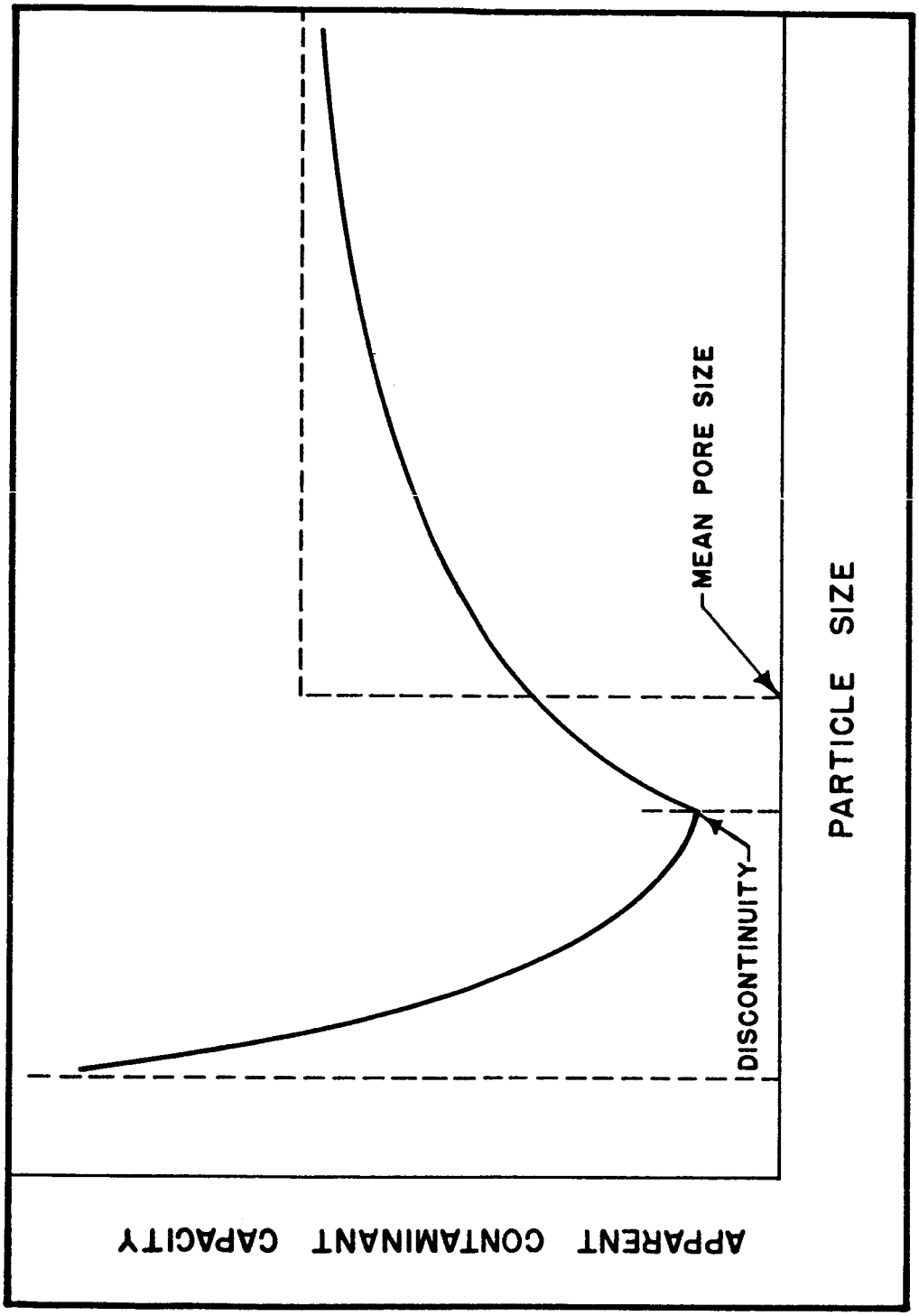

Figure 1.7. Typical Model for Contaminant Capacity--Particle Size Relationship.

for standard blocking,

$$\left(\frac{\Delta P_o}{\Delta P}\right)^{\frac{1}{2}} = 1 - K_s'W \qquad (1.15)$$

for intermediate blocking,

$$\log_e\left(\frac{\Delta P}{\Delta P_o}\right) = K_i'W \qquad (1.16)$$

for incompressible cake filtration,

$$\frac{\Delta P}{\Delta P_o} = K_c'W + 1 \qquad (1.17)$$

where $K_b' = \frac{K_b}{Q}k$; $K_s' = \frac{K_s k}{2}$; $K_i' = K_i k$;

$$K_c' = K_c Q k ,$$

are the respective plugging constants, k being the constant ratio V/W.

The form of relationships (1.14) through (1.17) are illustrated on Figure 1.8. The linear portions of the curves of Figure 1.4 fit the cake filtration mechanism. Some of the nonlinear portions of each of the curves of Figure 1.4 can be associated with one of the other mechanisms of filtration.

Inflections in a particular curve of Figure 1.4 indicate that changes occur in the mechanism of filtration for the contaminant size cut associated with that curve. The different shapes of the curves for different size cuts indicate that the order of filtration mechanisms varies with particle size cut. For example, the inflections of the 10-15μ and 20-25μ curves are in opposing senses.

The 0-5μ, 5-10μ, 10-15μ, and 15-20μ curves of Figure 1.4 seem to follow a pattern allowing for the incompleteness of the 0-5μ, 5-10μ

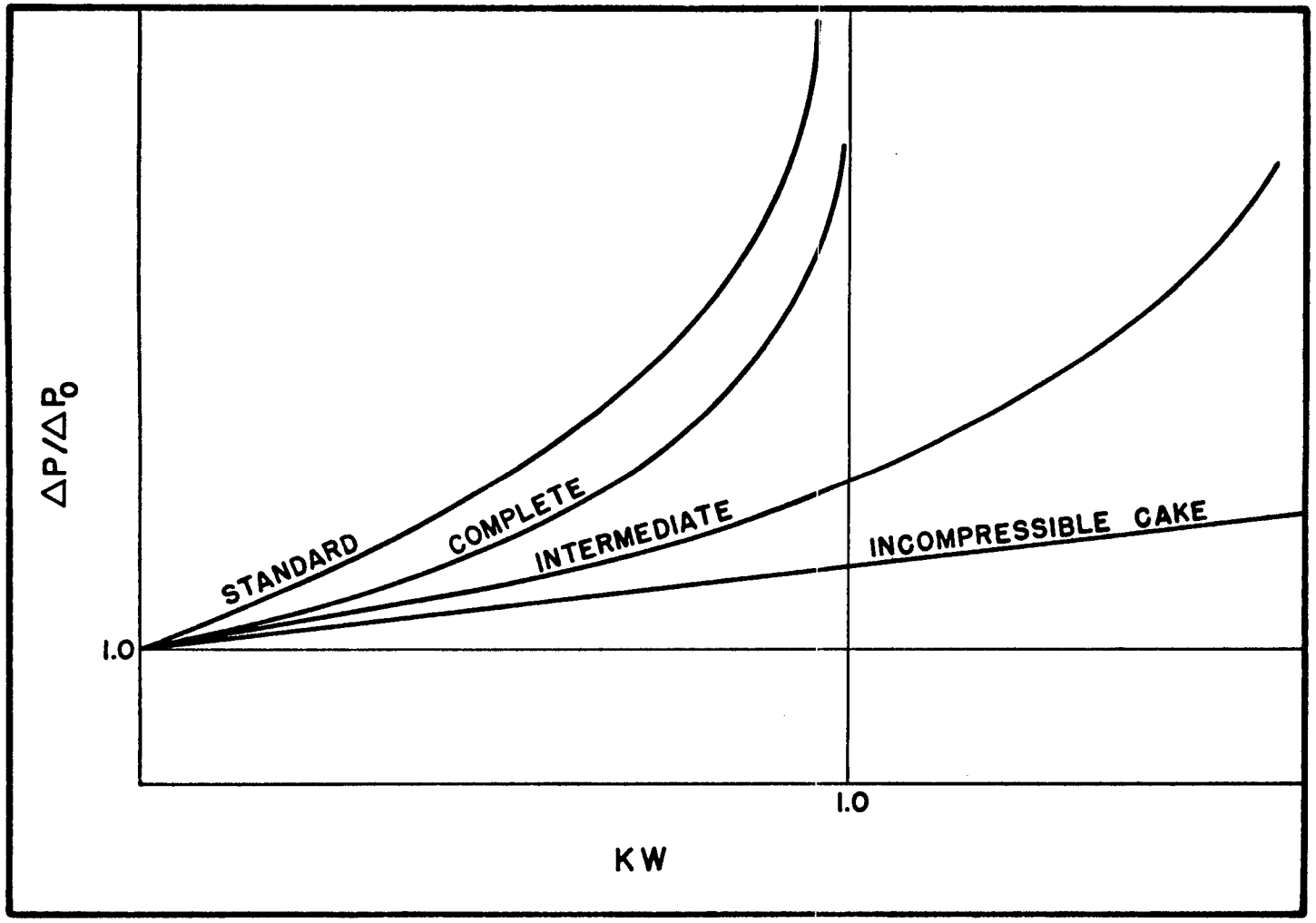

Figure 1.8. Typical Contaminant Capacity Curves for Various Filtration Modes.

curves. It is suggested that an initially upward curving relationship transforms to a linear relationship, the transition occurring earlier and more rapidly for increasing size cut. The contaminant capacity decreases with size cut, as reflected in Figure 1.5.

The 20-25μ, 25-30μ, and 30-40μ curves follow a pattern significantly different to that associated with the smaller size cuts. The curves show an initial increasing but decaying form (i.e., slope positive but decreasing) before entering a linear region. As the contamination cycle proceeds further, the slope begins to increase. The contamination capacity increases with size cut as reflected on Figure 1.5.

The slopes of the AC Fine and AC Coarse curves on Figure 1.4 increased continually with particle size cut.

It is apparent that the linear sections of the 10-15μ, 15-20μ, 20-25μ, 25-30μ, and 30-40μ curves, shown on Figure 1.9, fit the incompressible cake filtration model. Equation 1.17 can be written,

$$P = C_1 W + C_2 \qquad (1.18)$$

where $C_1 = K_c' \cdot \Delta P_o$ is the slope; $C_2 = \Delta P_o$ is the ΔP intercept value at $W = 0$ associated with the linear portion of the ΔP - W curve. It is inferred that, after an initial nonlinear region of filtration, each cycle enters a region of cake filtration. The initial filtration mechanism for the size cuts greater than 20 micron is different than for those less than 20μ.

Formation of a cake on the surface of the filter was physically apparent for the larger particle size cuts 25-30μ and 30-40μ. Figure 1.10 shows a sequence of closeup photographs taken during a test, which

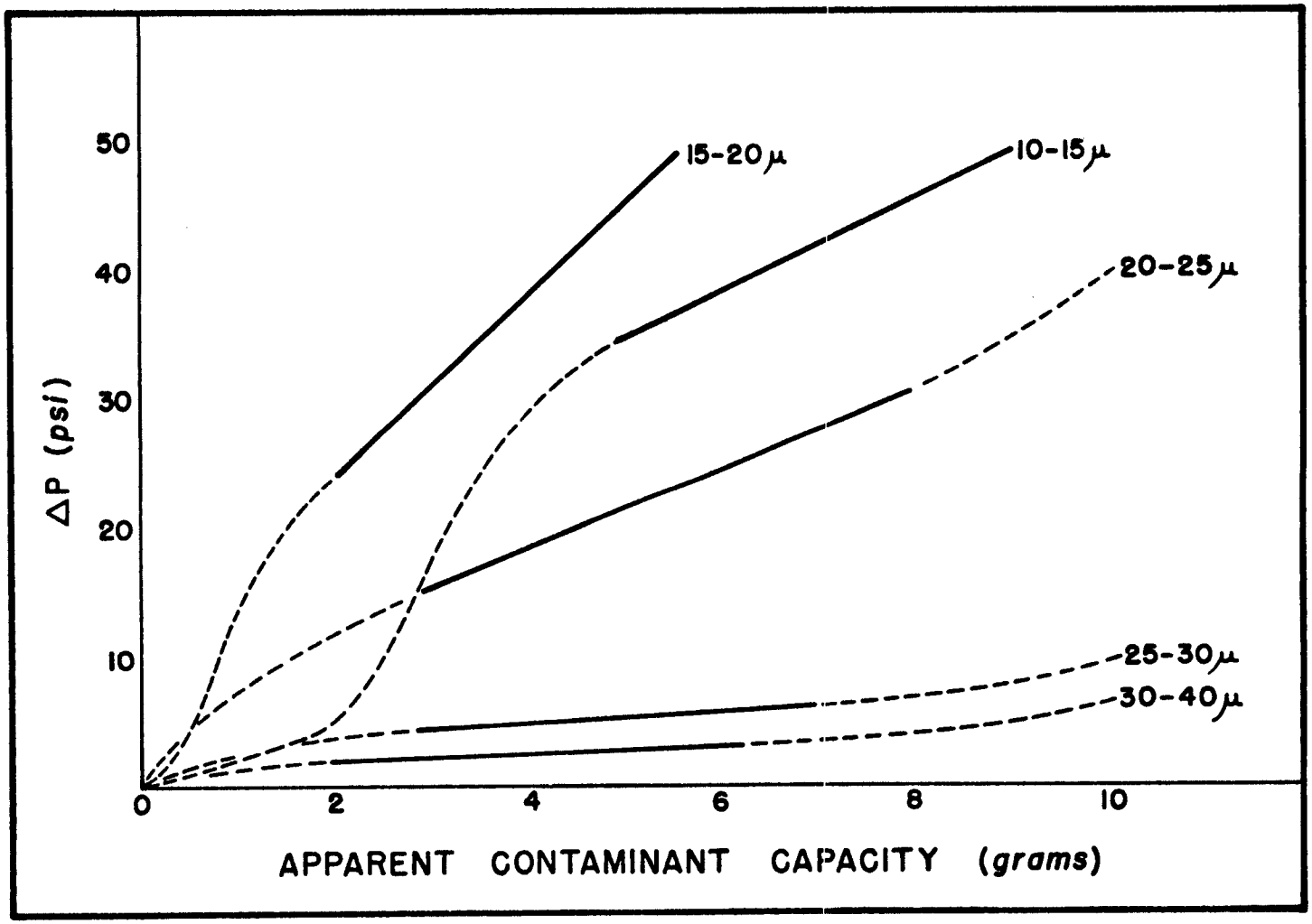

Figure 1.9. Contaminant Capacity Curves Showing Incompressible Cake Filtration Modes.

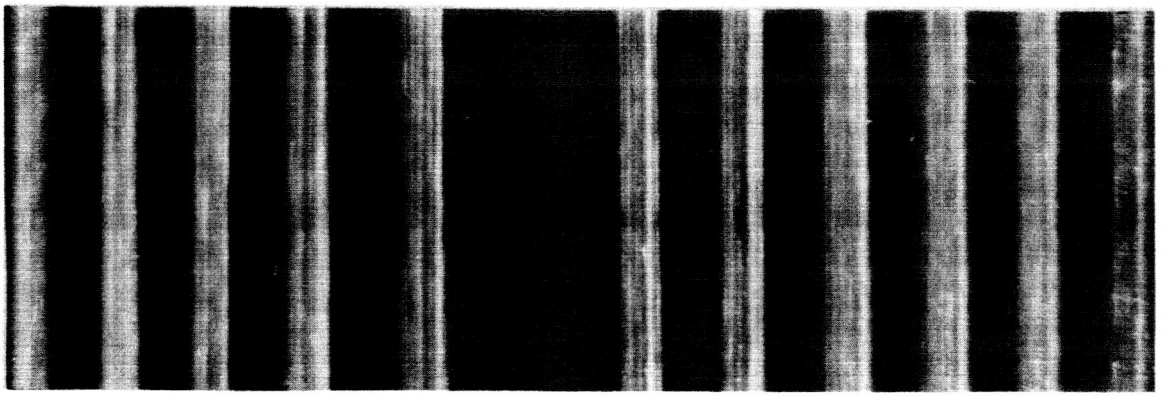

Filter Element Before Contaminant Capacity Test.

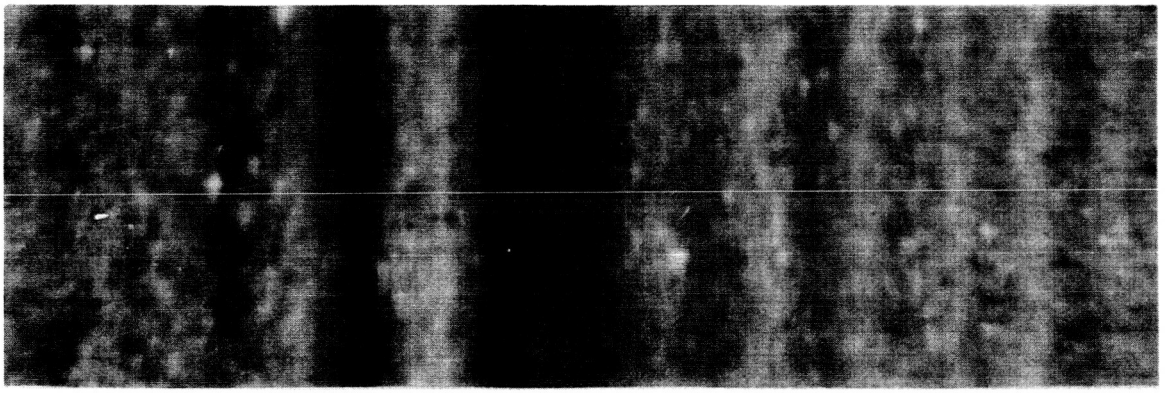

Element and Partial Filter Cake During Actual Experiment.

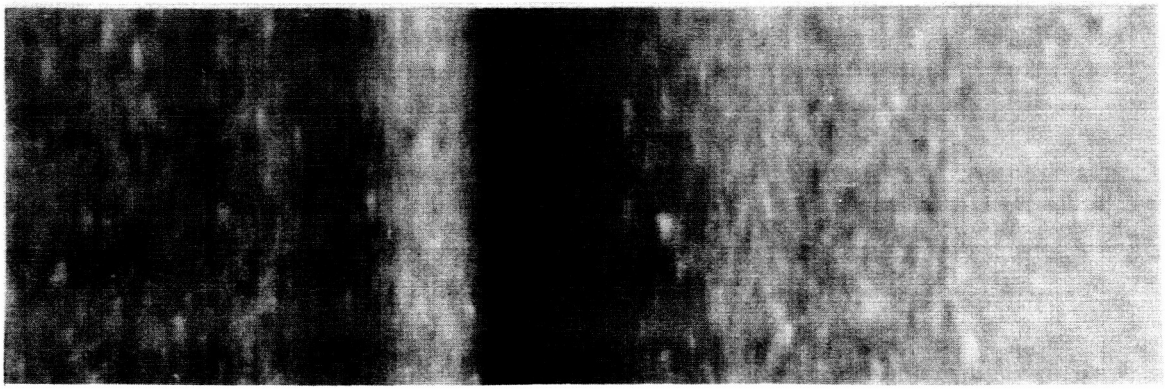

Element and Filter Cake at End of Experiment.

Figure 1.10. Formation of Filter Cake on Surface of Test Element.

illustrates the formation of a filter cake. The bands on the first photograph are the edges of the element pleats, viewed radially.

The crystalline nature of the silica particles used as the test contaminant would lend itself to the formation of an incompressible filter cake. It appears that cake filtration is an identifiable mechanism for part of the contaminant cycle experienced when narrow size cuts of silica are used to examine wire cloth filters.

The rapid increase in slope at the ends of the linear sections of the 20-25μ, 25-30μ, and 30-40μ curves is considered to be due to the structural collapse of the cake under the increasing pressure drop. Such a compression of the cake would act to increase the cake resistance to flow, with a corresponding increase in slope of the ΔP - W relationship. This type of sudden increase in cake resistance during a filter contamination cycle has been noted by previous workers[1,5]. It is suggested that the 15-20μ, 10-15μ, and smaller size-cut curves could experience a similar transition from incompressible cake to compressible cake filtration, if the contaminant addition cycle was extended sufficiently.

Equation (1.16) for intermediate blocking can be written

$$\log_{10} \Delta P = C_3 + C_4 W \qquad (1.19)$$

where $C_3 = 2{\cdot}3 \log_{10} \Delta P_o$; $C_4 = 2{\cdot}3 K_i'$.

Figure 1.11 shows a $\log_{10} \Delta P$ - W plot for the initial region of the 10-15 size cut relationship, together with the full plots for AC Fine and AC Coarse mixed size contaminant. Figure 1.11 also shows the $\log_{10} \Delta P$ - W plot of the 5-10 data. It is apparent that each case illustrated on Figure 1.11 fits the intermediate blocking mechanism of filtration.

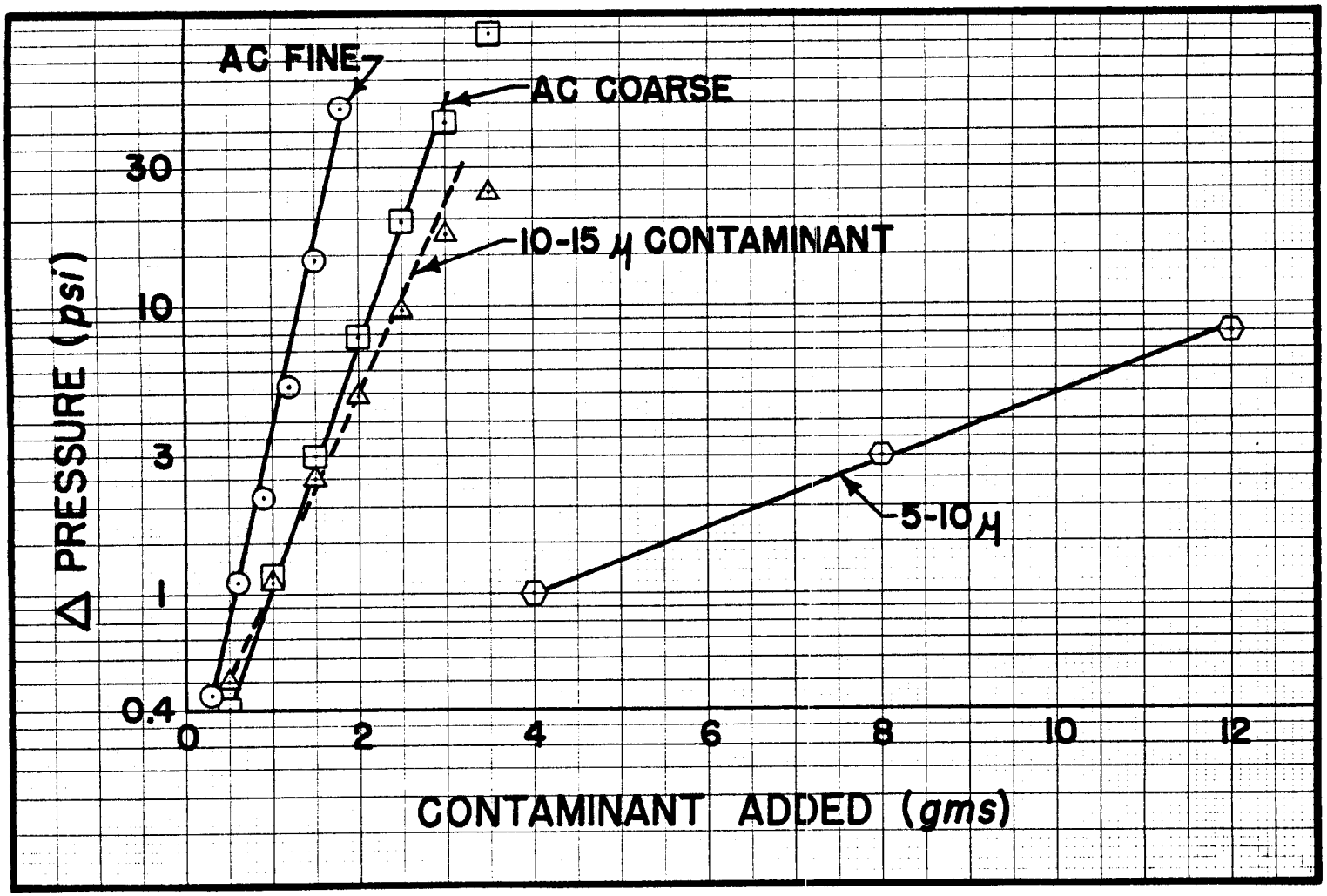

Figure 1.11. Contaminant Capacity Curves Showing Intermediate Blocking Filtration Modes.

It is possible also that the initial portion of the 15-20μ curve of Figure 1.4 would fit the intermediate blocking model if sufficient experimental points were available to justify a plot.

The initial shape of the ΔP - W curves for the larger particle size cuts (20-25μ, 25-30μ, 30-40μ of Figure 1.4) does not appear to fit any of the proposed filtration mechanisms (Figure 1.8). However, as the duration of the initial region is very short and the plots contain few points, the initial shape is somewhat obscure and can be regarded as a transition region leading to the cake mechanism.

1.4 Conclusions

(a) When a wire cloth filter is exposed to oil carrying contaminant of a narrow size band, the possible mechanisms of filtration appear to be similar to those proposed by Herman and Bredee[1] from data associated with textile depth filter media.

(b) A wire cloth filter is most susceptible to particles in a size range just below the mean pore size indicated by efficiency or porosimeter tests on the wire cloth.

(c) When subjected to narrow size cut particles in the ranges of size about its mean pore size the wire cloth contamination cycle includes a substantial amount of cake filtration. For size cuts below the mean pore size, the filter initially experiences the intermediate blocking mechanism for a region of the cycle which decreases as particle size range increases, following which it enters the incompressible cake filtration region. For particle size cuts around and greater than the mean pore size of the wire cloth, the initial mechanism of filtration is indeterminate and of short duration prior to development of the

incompressible cake mechanism. If sufficient contaminant is added, the increasing pressure drop can cause an incompressible cake to compress, increasing its resistance to flow through it.

(d) Mixed size contamination causes much more rapid blocking of the filter. For the mixed contaminants used, the filter contamination cycle followed the intermediate blocking mechanism, inferring that this was the mechanism most likely to occur in actual filter performance.

1.5 References

1. Hermans, P. H., and Bredée, H. L., Rec. Tran. Chim., Vol. 54, 1935, p. 680.

2. Gonsalves, V. E., Rec. Tran. Chim., Vol. 69, 1950, p. 873.

3. Grace, H. P., "Resistance and Compressibility of Filter Cakes," Chem. Eng. Prog., Vol. 49, Nos. 6 & 7, 1953, pp. 303-376.

4. Grace, H. P., "Structure and Performance of Filter Media," A.I.Ch.E. Jrnl., Vol. 2, No. 3, 1956, pp. 307-336.

5. Bennett, C. D., and Myers, J. E., Momentum, Heat, and Mass Transfer, McGraw-Hill, 1962, pp. 184-208.

CHAPTER II

EFFECTS OF ELEMENT CONFIGURATION AND HOUSING DESIGN UPON FILTER PERFORMANCE

2.1 Introduction

The basic ingredient in a filter element is the medium from which the element is constructed. In general, the type of medium selected determines quantity and sizes of the contaminant which will be removed from a system. There are, however, design practices which can have an effect upon the performance of a filter element from both a contaminant removal and flow resistance standpoint. These effects result both from element design and housing design. In this regard, a series of tests were devised and conducted to determine the effects on performance resulting from various housing and element configurations.

2.2 Housing Design Tests

2.21 Procedure

To facilitate the investigation of housing effects, an experimental test housing (Figure 1.3) was designed and constructed in such a manner that the housing of the cylindrical section encasing the filter element could be selected arbitrarily. Four plexiglass housings of different diameters were used in order to investigate the effect upon contaminant capacity of different annular clearances between the filter housing and the filter element. Figure 2.1 illustrates the experimental filter housing and two of the additional plexiglass housings. The commercial

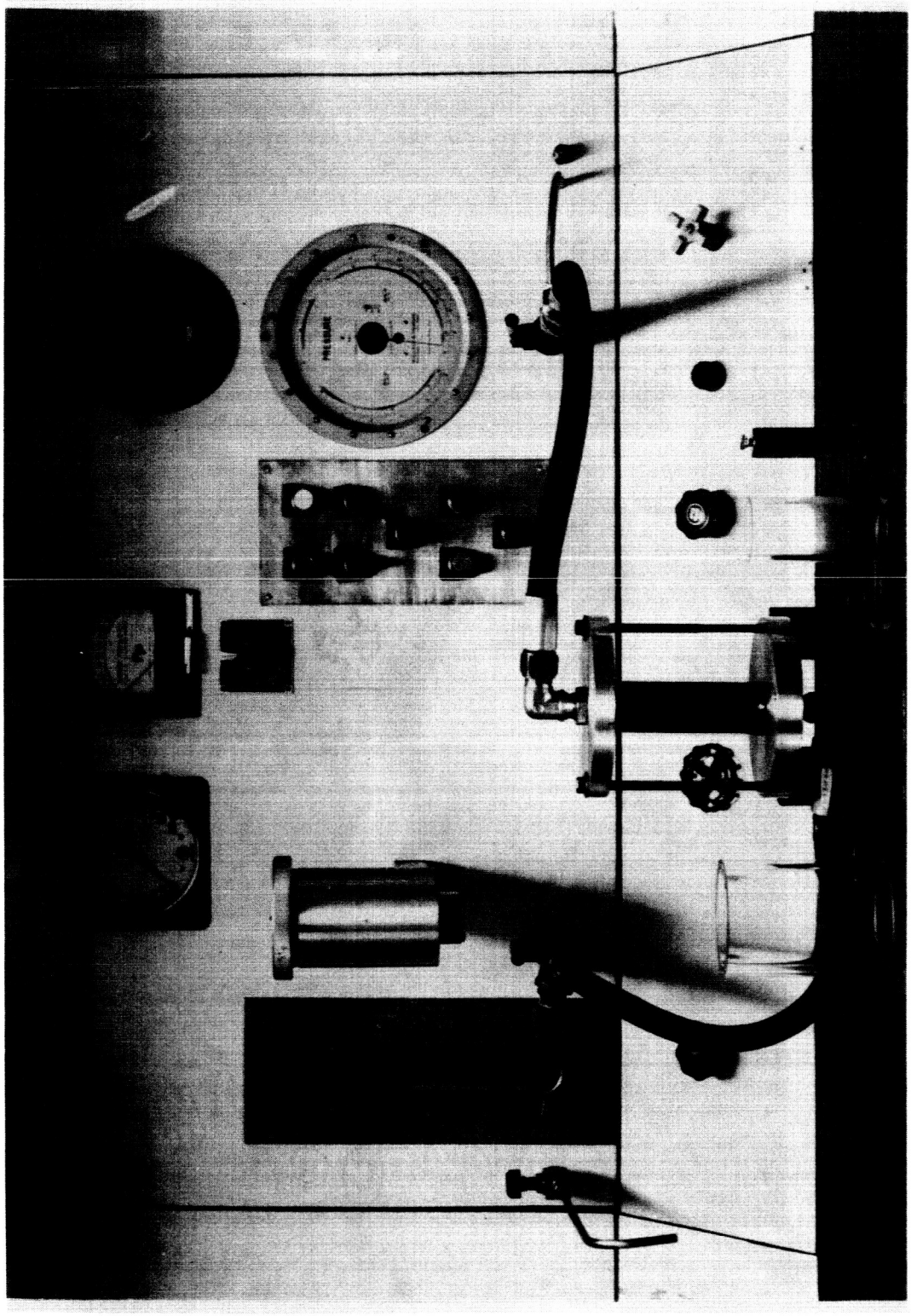

Figure 2.1. Experimental Test Housings.

housing designed for the wire cloth element used in the tests was used as an additional test housing. The filter element for the experiments described in Chapter I was also used in the housing tests. The ultrasonic cleaning procedure used to clean the element after each test is given in Appendix C. The housing dimensions and identification codes are shown in Table 2.1 and Figure 2.2.

TABLE 2.1

FILTER HOUSING MEASUREMENTS

Filter Housing Designation	Filter Housing Inside Diameter	Diametral Ratio, D/d
D-1 Plexiglass	1.25 inches	1.11
D-1 Plexiglass	1.50 inches	1.33
D-3 Plexiglass	2.00 inches	1.78
D-4 Plexiglass	3.75 inches	3.35
C-1 Commercial	1.35 inches	1.20

Note: The outside diameter of the filter element, d = 1.125 inches.

In all of the tests concerning the effects of annular clearance, the fluid entered the housing in such a manner that it was distributed evenly around the circumference of the element. However, the entrance ports in many commercial filter housings are located in such positions that they cause an uneven velocity distribution over the surface of their companion filter element. In order to investigate some of the effects of housing entrance flow conditions on the contaminant capacity of a filter element,

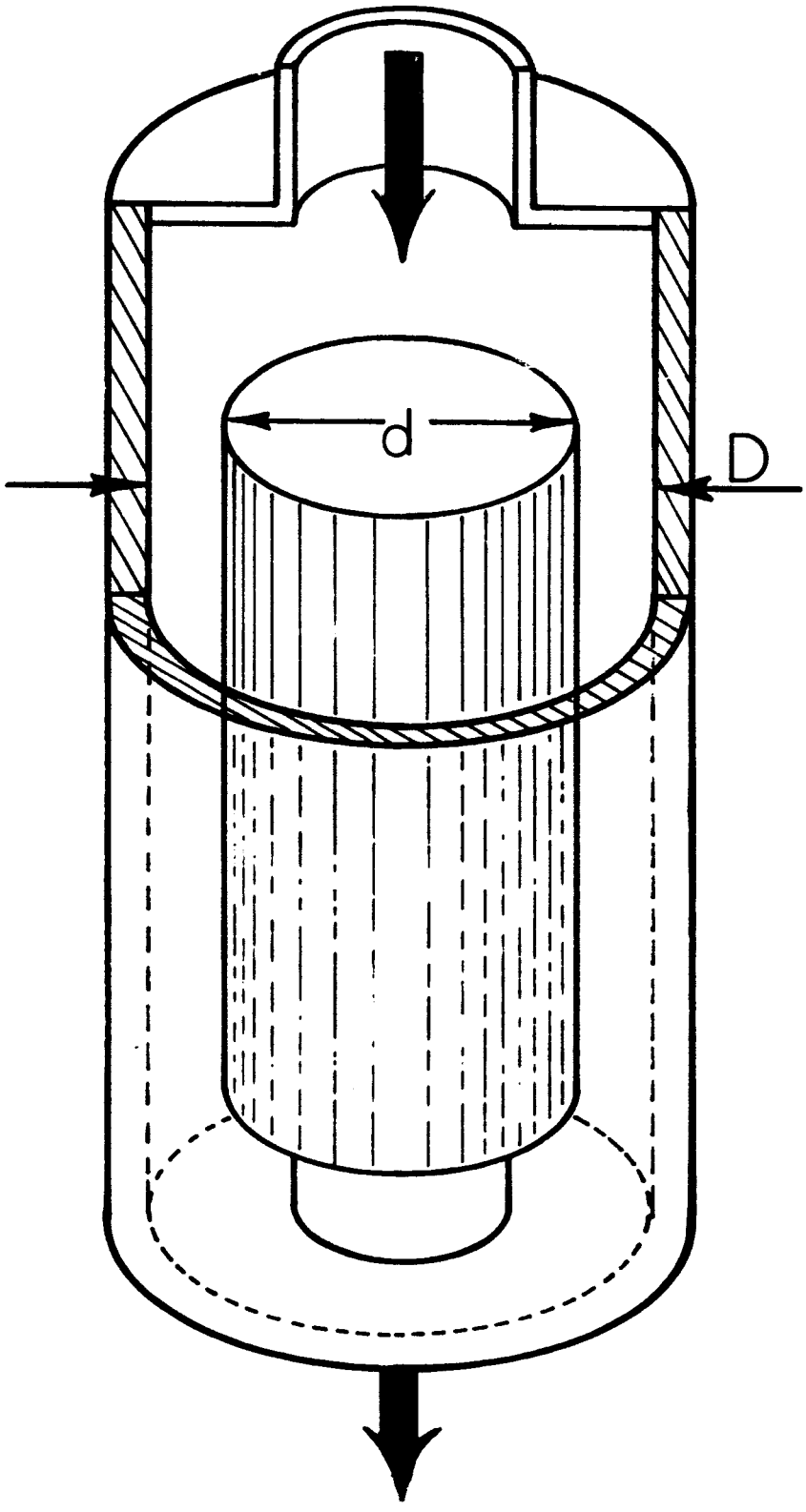

Figure 2.2. Housing Dimensions.

a thin disk baffle containing an orifice slot was placed on top of the filter element as shown in Figure 2.3.

The experimental housing models were installed in the test section of the Filter Evaluation Test Stand and contaminant capacity tests were conducted. The quantity of contaminant necessary to produce a predetermined pressure drop across the element constituted the contaminant capacity of the element. Detailed explanations of the Filter Evaluation Test Stand and the procedures for determining the contaminant capacity are described in Appendix B. The experimental contaminant used in all the contaminant capacity tests was classified AC test dust, which had been processed to obtain a 20-40 micron size range. The technique used for size classification of the test dust is described in the 1964 report. Classified test dust was used in order to minimize the confusion created by injecting a wide range on contaminant sizes in contaminant capacity determinations. Moreover, since the 20-40 micron test dust had previously exhibited a tendency to form a filter cake, the effect of housing configuration on the apparent cake mode of filtration occurring with the wire cloth element could be observed with graded contaminant of this size range.

2.22 Results

The results for the various filter housing configurations are shown in Figure 2.4 as a plot of the net differential pressure across the element versus the contaminant added. Figure 2.5 is an expansion of a region of the curves of Figure 2.4 near the reference differential pressure. A plot of the contaminant capacity versus the diametral ratio of the housing and element is shown in Figure 2.6. For the larger clearances between the element and housing, i.e., larger D/d ratios, the trend of the results

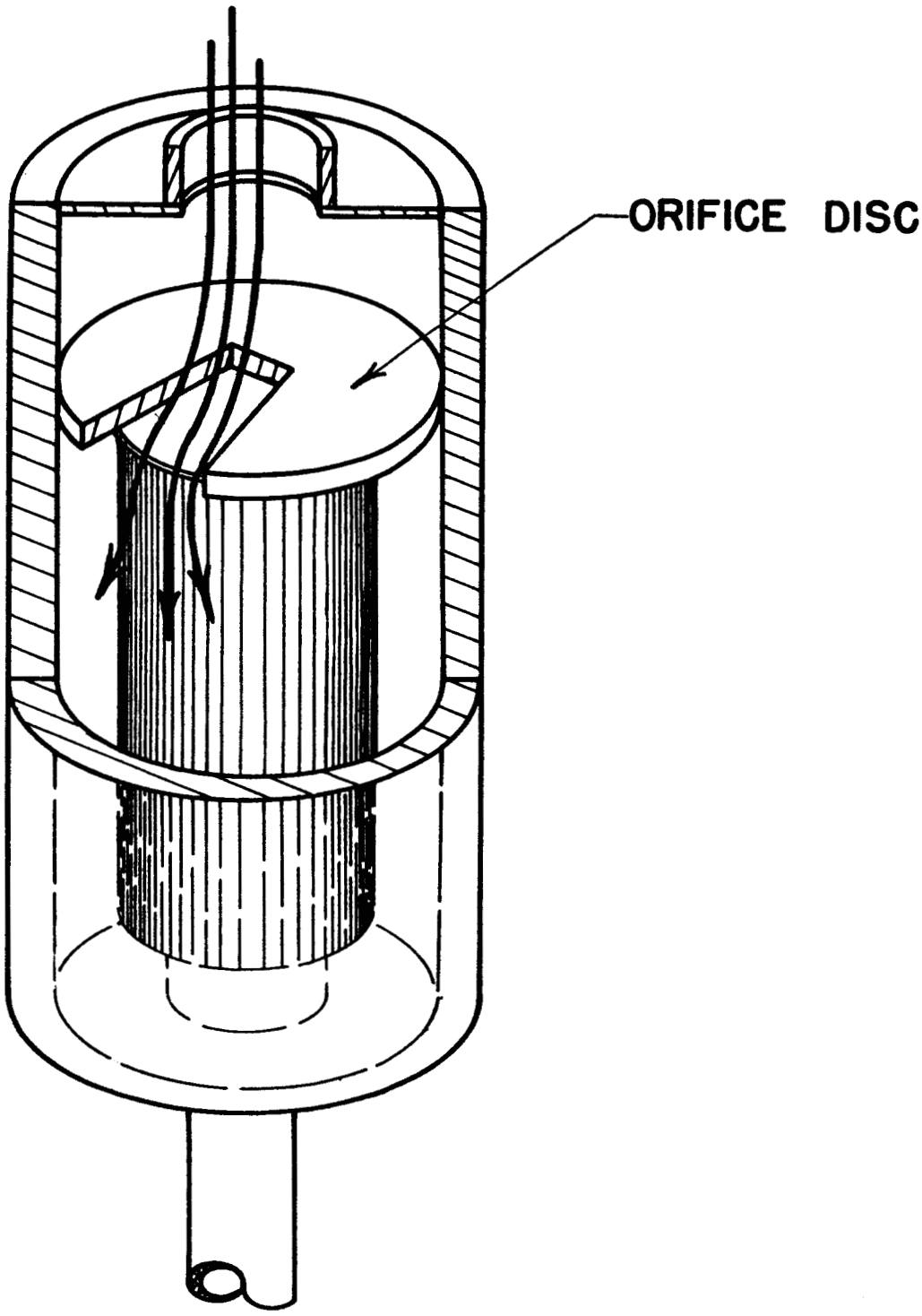

Figure 2.3. Housing With Orifice Disc.

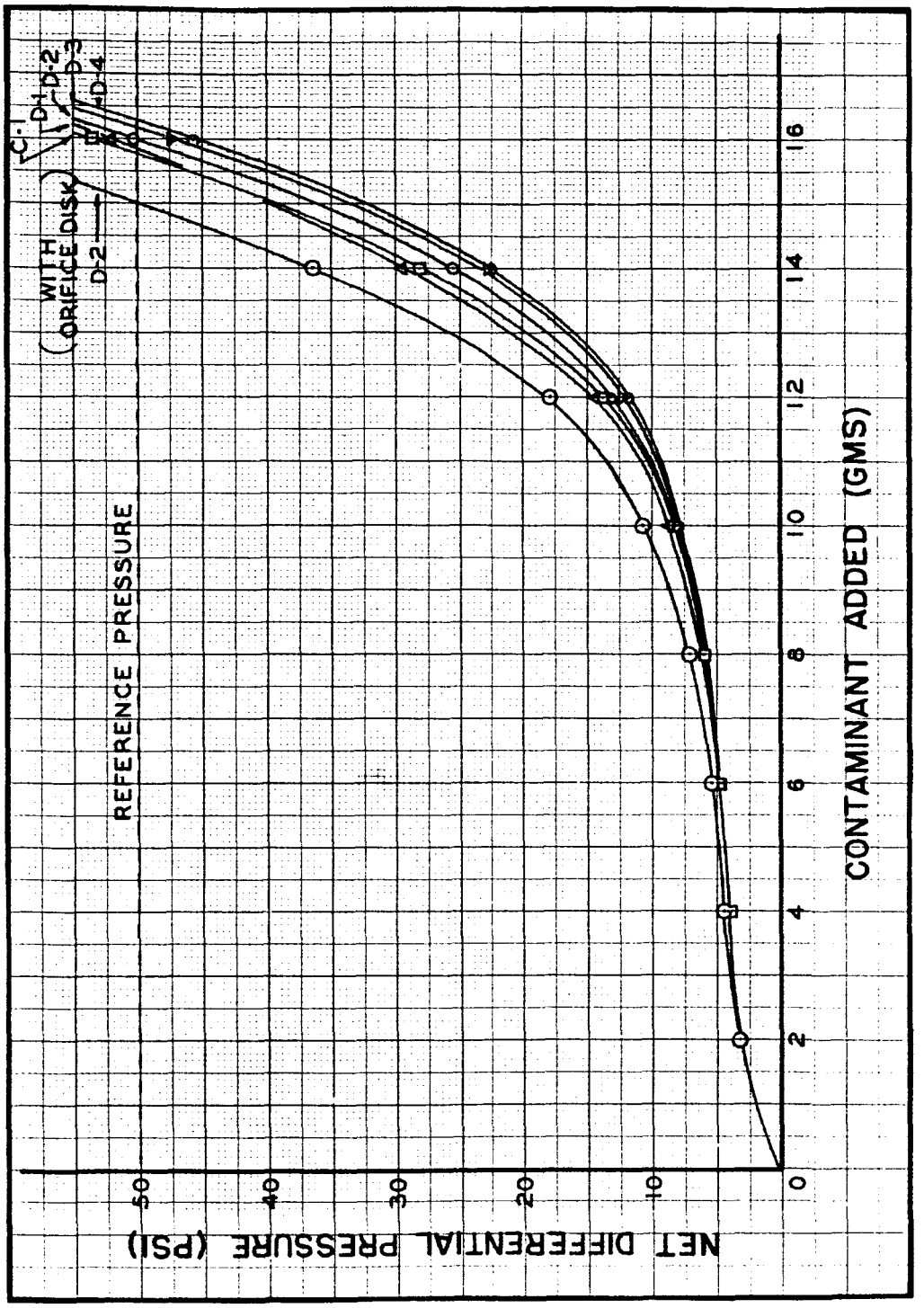

Figure 2.4. Contaminant Capacity Curves As a Function of Housing Size.

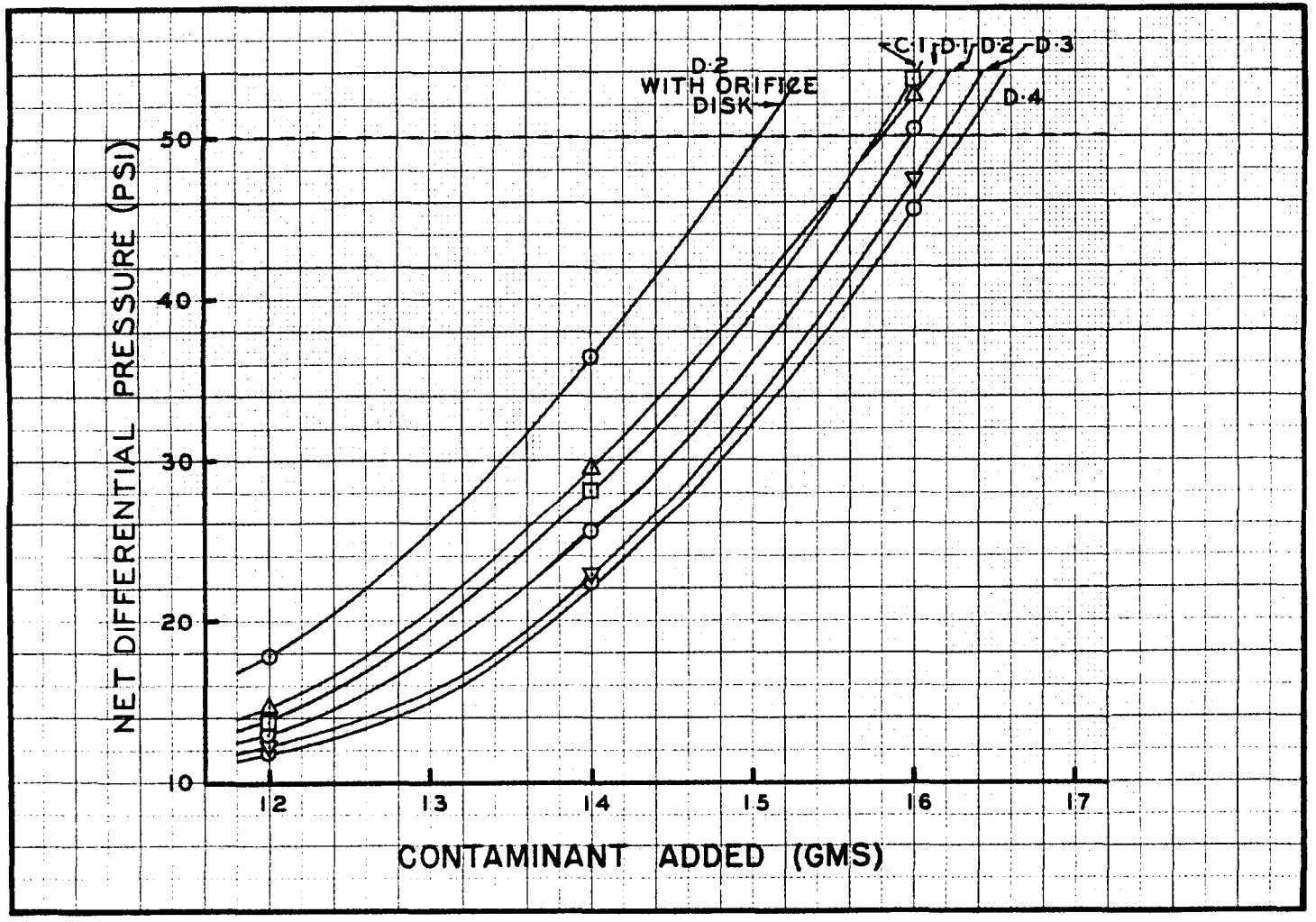

Figure 2.5. Expansion of Figure 2.4 in the Region of the Reference Pressure.

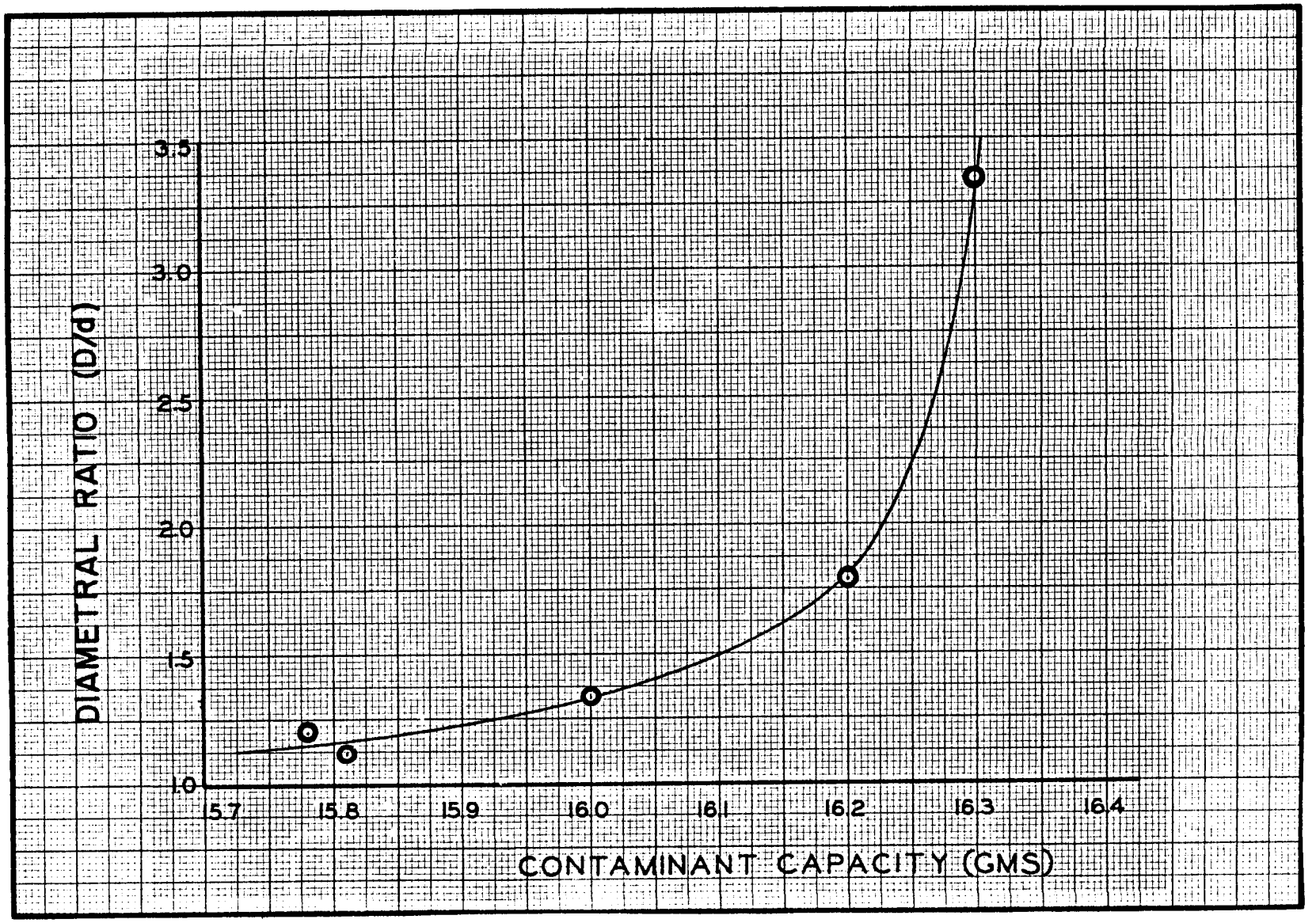

Figure 2.6. Contaminant Capacity as a Function of Diametral Ratio.

indicates that the contaminant capacity approaches a limiting value. Further increases in the filter housing inside diameter would have a negligible effect on the over-all contaminant capacity. As the diametral ratio approaches unity, the contaminant capacity decreases. These results reveal a design parameter which is important in the selection or design of a filter element housing.

From Figure 2.5 it can be seen that the maximum variation in the contaminant capacity at a reference differential pressure of 50 psi is approximately 8.45%. The maximum contaminant capacity occurred with experimental housing D-4, which had the largest D/d ratio. By comparing the contaminant capacity of housing D-1 with the orifice disk installed to its capacity without the orifice, it can be seen that the entrance effects induced by the disk resulted in a decrease in the contaminant capacity of the element. A reduction of 6.1% was observed when 20-40 micron test dust was used as the experimental contaminant; another test with 20-30 micron test dust resulted in a similar reduction in the contaminant capacity of the filter element. Similar results could be expected with commercial housings having an unsymmetrical entrance port arrangement.

The reduction in contaminant capacity of the element when used with the orifice disk, and also in test housings with smaller diametral ratios, appears to be related to the fluid velocity distribution over the surface of the filter element. The orifice disk induces a higher fluid velocity in the region of the filter surface adjacent to the orifice. It was visually observed that the increased turbulence in the fluid streamlines resulting from the assymmetric velocity distribution reduced the caking

ability of the contaminant on the surface of the element. In turn, the observed reduction in thickness of the filter cake beneath the orifice was reflected by the decrease in the contaminant capacity of the element. The housings having smaller diametral ratios cause a higher tangential fluid velocity over the surface of the element due to a smaller annular clearance between the element and the housing. The higher fluid velocity and the resultant reduction in caking ability may explain, in a manner similar to that observed with the orifice disk, the decrease in contaminant capacity as D/d decreases.

2.23 Conclusions

The use of housings which provide for a symmetrical fluid flow into the element can result in an increased contaminant capacity. Increasing the clearance between element and housing also yields an increased capacity. The results of the tests reported herein indicate that the change in contaminant capacity induced by changes in housing design is less than 10%. In most applications, housing size requirements would take precedence over the desire for such a slight improvement in capacity.

2.3 Element Design Effects

The effects of element design upon the filtration and flow performance of wire cloth filter elements was investigated by testing a number of filter elements. These elements, which were made available by the Wintec Corporation of Inglewood, California, were constructed to OSU specifications. The dimensions (Table 2.2) were selected in order to assess the relative results of variations in area, pleat depth, and number of pleats on the performance of an element.

TABLE 2.2

CHARACTERISTICS OF TEST FILTERS

Element No.	Number of Pleats	Nominal Depth (in.)	Nominal Area (sq.in.)
1	107	0.125	105
2	74	0.125	70
3	36	0.125	35
4	42	0.080	30
5	114	0.070	70
6	40	0.250	70
7	80	0.250	140
8	Cylindrical Element		14.3

Note: All elements were constructed from 165 x 1400 wire cloth and had an inside diameter of 1.125 in. Inner support tube was constructed from 20 mesh (.016 in. wire).

2.31 Flow Performance Tests

Two types of tests were carried out to measure the changes in filtration performance and flow performance resulting from element design variations. The first was a pressure drop versus flow rate test which was conducted on the Filter Media Performance Stand. The elements were installed in the test fixture of Figure 1.3 with the 3.75 in. I.D. housing in place. The test fluid, Mil-H-5606, was maintained at 100°F (viscosity = 12.0 cp) throughout the test.

The pressure differential across the test section was recorded at 2.5 gpm intervals. A correction for the pressure loss due to housing

losses was determined by measuring the pressure-flow relationship across a "dummy" filter element installed in the housing. The "dummy" element consisted of the 20 mesh support screen and end fittings which were identical to those of the test elements. Subtracting this pressure correction resulted in the pressure-flow contribution (ΔP versus Q) of the medium itself. Figure 2.7 shows the ΔP versus Q curves for each of the eight elements tested. From this data, a specific flow conductance term was calculated for each element from the following definition,

$$\text{Specific Flow Conductance (SFC)} = \frac{Q}{A\Delta P}\left(\frac{\text{gpm}}{\text{psi-sq.in.}}\right) \qquad (2.1)$$

Table 2.3 gives the SFC for the test elements.

TABLE 2.3

SPECIFIC FLOW CONDUCTANCE RESULTS

Element Number	Specific Flow Conductance (gpm/psi-sq.in.)
1	.079
2	.223
3	.212
4	.211
5	.183
6	.213
7	.093
8	.238

Figure 2.8 is a graph of the Specific Flow Conductance versus the number of pleats for elements 2, 5 and 6. These elements each have an area

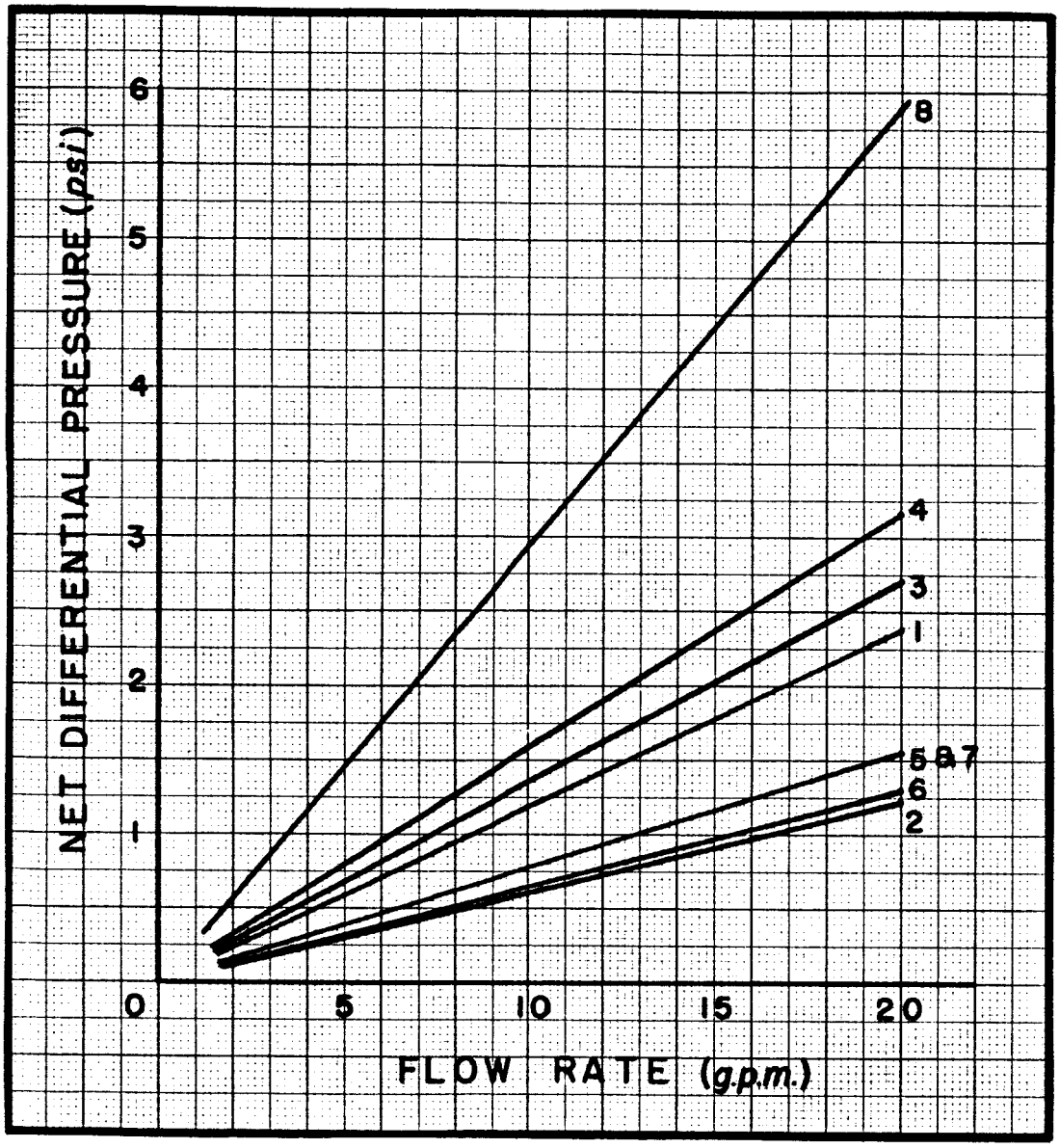

Figure 2.7. ΔP vs. Q Results for Test Elements.

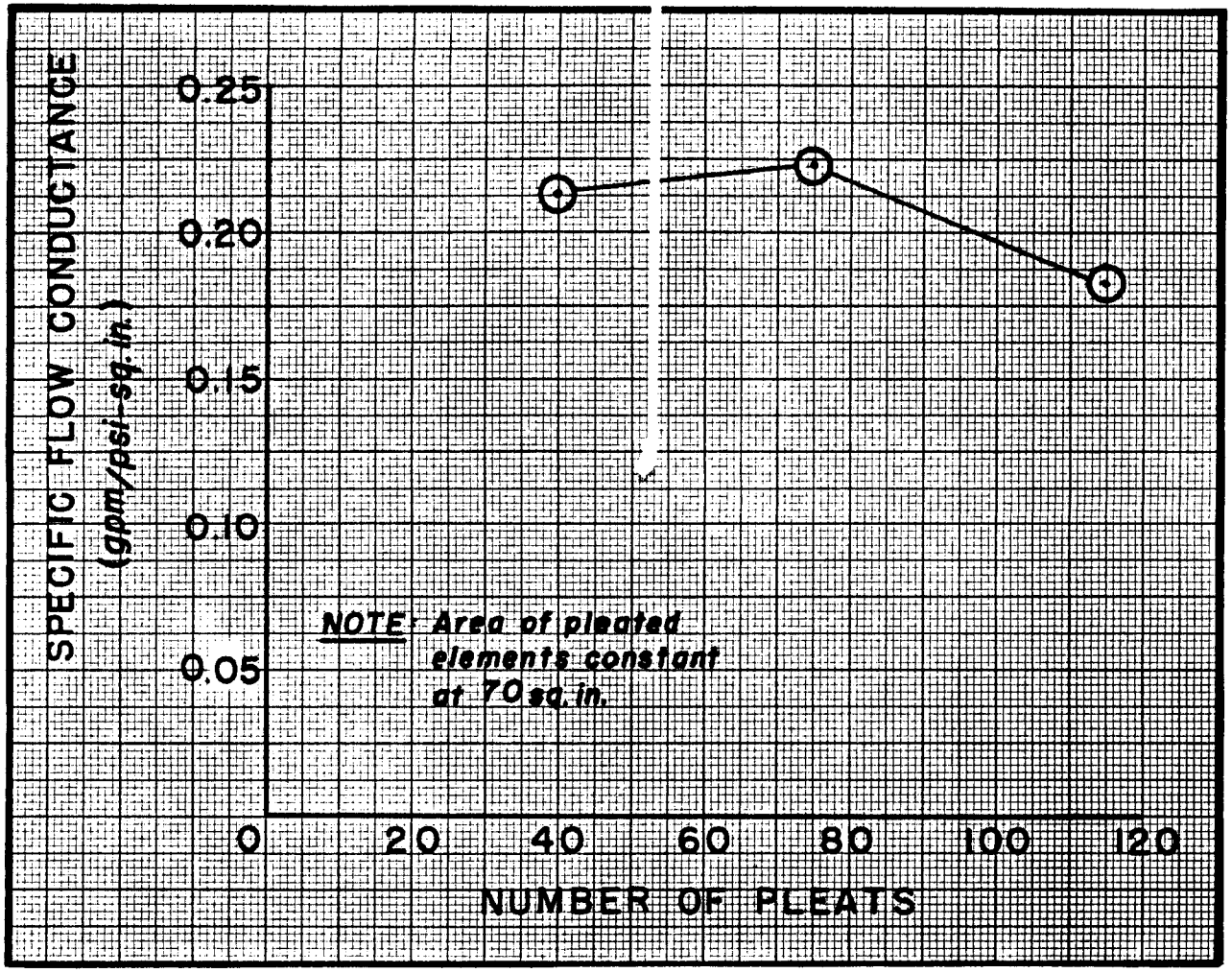

Figure 2.8. Specific Flow Conductance Vs. Number of Pleats With Area Constant.

of 70 sq. in. but differ in both number of pleats and pleat depth. The results in this case show a trend toward a decrease in conductance with an increase in the number of pleats. The decrease in the conductance term, which represents an increase in the pressure loss per unit of filter area at a given flow, can be attributed primarily to the fact that the fluid is passing through narrower drainage channels between pleats as the number of pleats increases. These narrowed drainage channels serve to restrict the flow and therefore reduce the conductance of the element.

Figure 2.9 is a plot of SFC versus number of pleats for elements 1, 2, and 3 which have a common pleat depth of 0.125 in., and for elements 6 and 7 which have a 0.250 in. depth. The same trend may be noted as occurred in Figure 2.8, namely, that the specific conductance decreases with increasing pleat numbers. Figure 2.10 is a graph of the conductance data for elements 3, 4, and 6. These filters have approximately the same number of pleats (36, 42, and 40 respectively), but their areas and pleat depths vary. This figure shows that no change in conductance resulted from varying the areas and pleat depths while holding the number of pleats constant. However, as the number of pleats increase, the effects of changes in depth upon the specific conductance may become significant as the length of narrowed drainage channel between pleats increases.

It is interesting to note that the specific conductance of the cylindrical element is greater than that of any of the pleated elements. This result is in harmony with the above hypothesis since an element with no pleats should have the greatest conductance. The conductance of a 2 inch diameter flat sample of the same medium was determined to be 0.293 gpm/psi-sq. in. This value is greater than that for the plain cylinder

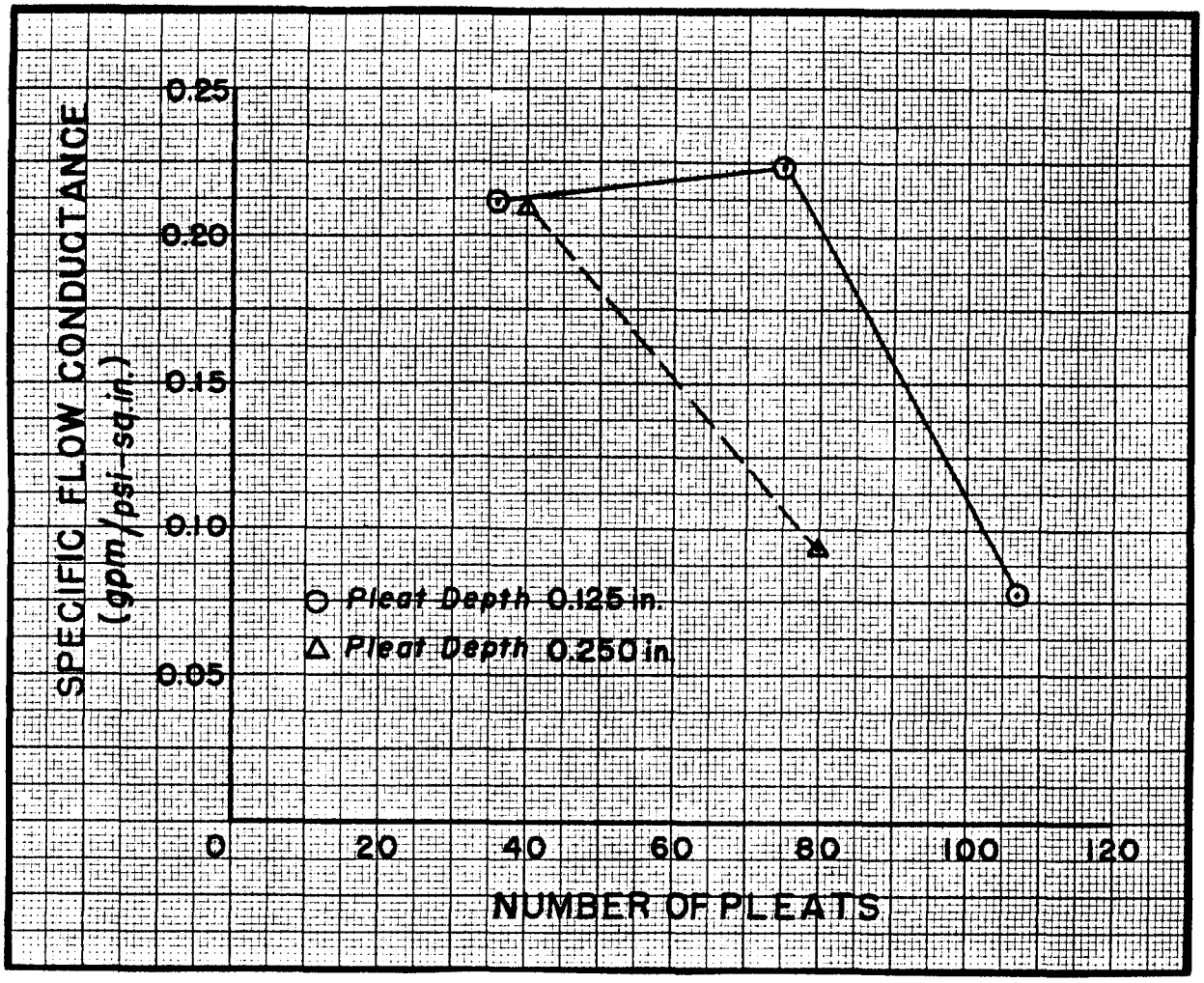

Figure 2.9. Specific Flow Conductance Vs. Number of Pleats With Pleat Depth Constant.

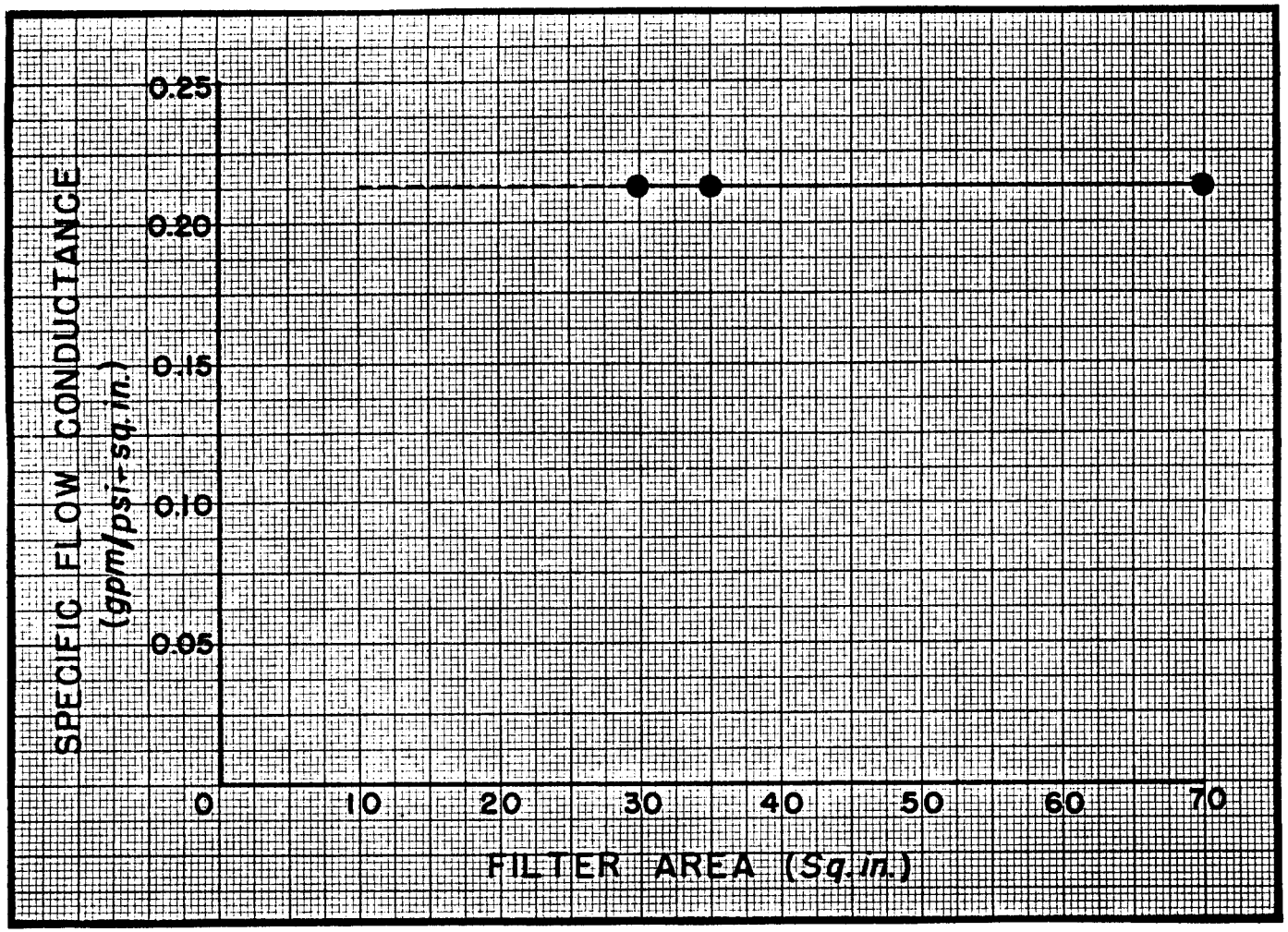

Figure 2.10. Specific Flow Conductance Vs. Area With Number of Pleats Constant.

because no pressure losses due to a change in flow direction were involved in flowing through the flat specimen.

2.32 Filtration Performance Tests

The second type of test conducted on each of the elements was a contaminant capacity test. These tests were performed on the Filter Evaluation Test Stand (Appendix B). A constant specific flow rate of 0.1 gpm per sq. in. of filter area was maintained throughout each test, and the fluid temperature was held constant at 100°F. The quantity of contaminant which was added incrementally was 0.00286 gram per sq. in. of filter area. This was done in order to present the same contaminant level to each filter during the injection cycle.

Figure 2.11 shows the contaminant capacity curves for each of the test elements. Table 2.4 gives the contaminant capacity of each element at the reference pressure of 40 psid, and the specific contaminant capacity for each element as defined by:

$$\text{Specific Contaminant Capacity (SCC)} = \frac{\text{Contaminant Capacity at 40 psid}}{\text{sq. in. of Filter Area}} \left(\frac{\text{gms}}{\text{sq. in.}} \right)$$

Also shown in the table is the capacity and specific capacity of the 2-inch diameter flat sample.

Figure 2.12 is a graph of SCC versus area for each of the elements tested. The figure shows that a significant loss of capacity accompanies any pleating process but that the nature of the variations caused by changes in filter area, number of pleats, and pleat depth is relatively insignificant once an element is convoluted. The cylindrical element had a specific capacity equal to that of the flat medium, 0.0383 gms/sq. in., while the average of the specific capacities of the seven pleated

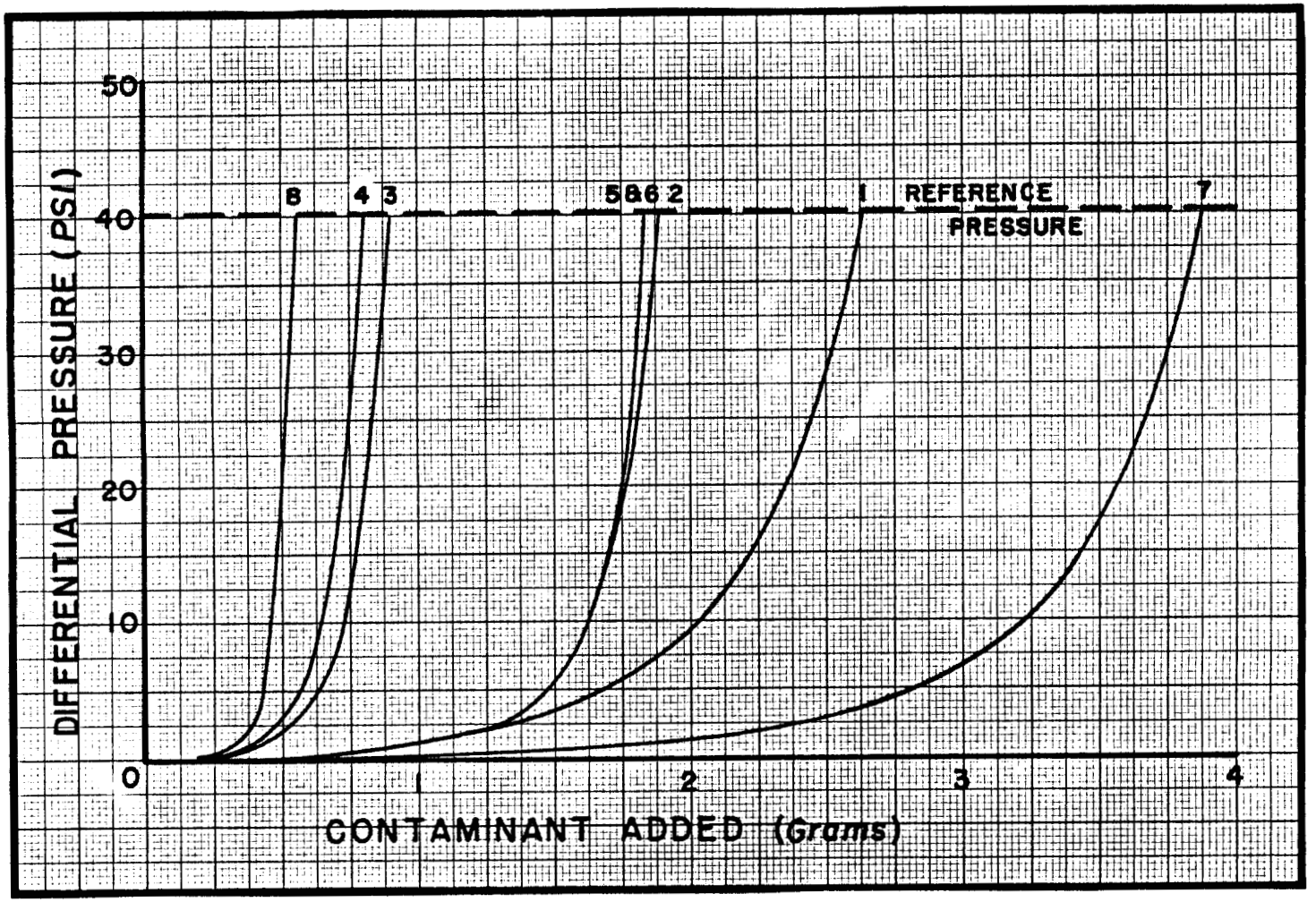

Figure 2.11. Contaminant Capacity Curves for the Test Elements.

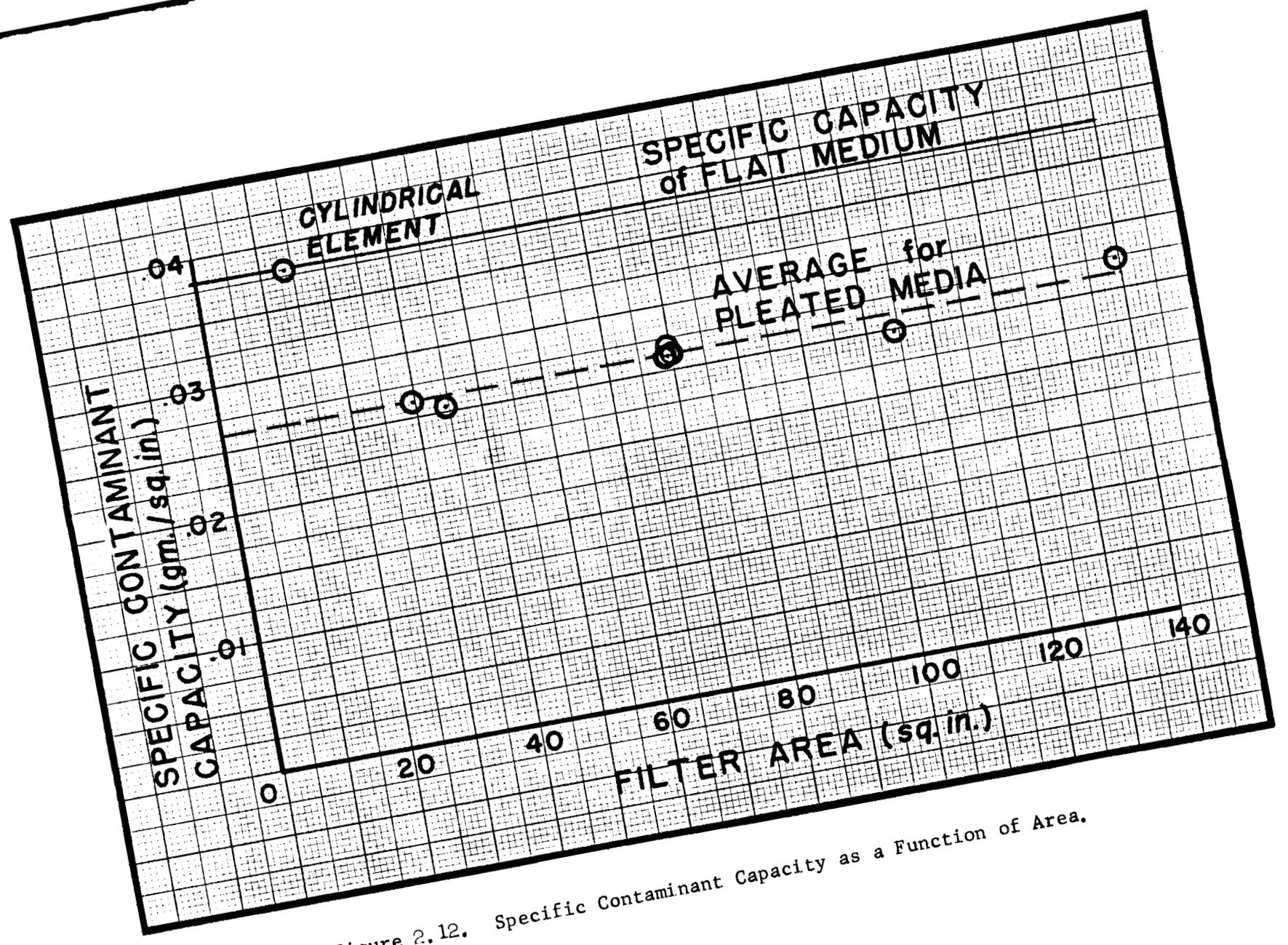

Figure 2.12. Specific Contaminant Capacity as a Function of Area.

TABLE 2.4

SPECIFIC CONTAMINANT CAPACITY RESULTS

Element Number	Contaminant Capacity to 40 psid	Specific Contaminant Capacity
1	2.63 gms	0.0250 gms/sq. in.
2	1.88	0.0269
3	0.89	0.0254
4	0.80	0.0266
5	1.84	0.0263
6	1.84	0.0263
7	3.87	0.0276
8	0.55	0.0384
Flat	0.12	0.0383

elements was 0.0263 gms/sq.in. The results indicate that from a capacity standpoint, a pleated element will have 70% of the capacity calculated from capacity tests performed on a flat sample of media. The 30% reduction in capacity resulting from pleating may be a characteristic of the type of wire cloth used; however, the reductions using other sizes of cloth can be expected to be of the same order.

2.33 Conclusions

The following conclusions are apparent regarding the effects of housing and element design upon the performance of a filter element:

1. The convolution of a wire cloth medium results in a loss of flow efficiency when compared with a flat medium. That is to say,

the pressure loss through a convoluted medium at a given flow rate will be greater than the pressure loss through a flat medium of the same area at the same flow rate. This reduction in flow efficiency, which is represented by a decrease in the specific conductance term, becomes increasingly pronounced as the number of pleats increases.

2. The specific contaminant capacity of a pleated element is reduced by approximately 30% over that of a flat or cylindrical element. On the basis of the data presented, this reduction is virtually constant and independent of changes in area, pleat depth, and the number of pleats.

CHAPTER III

FACTORS AFFECTING THE PERFORMANCE OF WIRE CLOTH MEDIA

3.1 Introduction

The results reported in the 1964 report were primarily generated during the development of methods to measure the properties of wire cloth filter media. Since the 1964 report was written, numerous other filter media have been tested to determine their properties. Table 3.1 is a summary of the data obtained from the media tested during the past year as well as a repetition of most of the test data from the 1964 report. Of the group tested, several different pairs of media were examined which were identical except that one member of each pair was sintered while the other was unsintered. An analysis of the effect of the sintering process upon the properties of the media is discussed in Section 3.2.

Two test programs were conducted to measure the filtration performance of wire cloth media. In the first of these programs, the specific contaminant capacity of a number of samples of dutch twill media were tested. The average pore diameters of these media ranged from 12 to 30 microns. The second program involved the measurement of the specific contaminant capacity of a given type of cloth as a function of flow rate. The results of these programs are presented in Section 3.3 and 3.4, respectively.

TABLE 3.1

PROPERTIES OF FILTER MEDIA

Specimen Number	Porosity ϕ (%)	Average Diameter (Microns)		Permeability (μ^2)		
		Porosimeter Test D_1	Boiling Test D_2	Measured	Theoretical $D_1^2/32$	Theoretical $D_2^2/32$
1	53.1	51.0	54.5	98.0	81.3	93.0
2	60.5	35.5	35.0	42.4	39.4	38.2
3	38.4	23.5	25.5	16.3	17.3	20.3
4	36.7	12.0	11.5	4.1	4.5	4.1
5	37.8	19.5	17.0	9.9	11.9	9.0
6	37.8	13.0	11.5	4.6	5.3	4.1
7S	52.5	32.0	37.0	46.8	32.0	42.8
8S	42.2	16.5	16.5	9.5	8.5	8.5
9S	37.9	23.5	24.5	16.7	17.3	18.7
10S	42.3	14.5	12.5	6.3	6.6	4.9
11S*	66.5	17.0	18.0	18.1	9.0	10.1
12S	74.2	64.0	52.5	176.5	128.0	86.0
13S*	72.8	13.5	19.5	29.9	5.7	11.9
14S*	62.4	11.0	14.0	5.3	3.8	6.1
15S	16.5	9.0	13.5	3.5	2.5	5.7
16S	66.8	46.5	34.0	47.6	67.5	36.1
17	49.8	21.0	21.5	12.7	13.8	14.4
18S*	55.8	14.5	11.5	4.0	6.6	4.1
19S*	57.2	15.0	13.5	6.8	7.0	5.7
20S	53.5	11.0	14.5	3.2	3.8	4.5
20	49.0	10.5	14.0	3.2	3.4	6.1
21	26.2	23.5	22.0	16.8	17.2	15.1
21S	25.7	22.0	22.5	20.7	15.1	15.8
22S	57.3	22.0	24.0	16.1	15.1	18.0
22	57.0	23.5	25.0	15.6	17.2	19.5
23S	36.4	19.5	18.0	11.2	11.9	10.1
23	36.2	19.5	17.0	10.7	11.9	9.0
24	51.8	26.0	36.0	48.3	21.1	40.5
24S	51.8	28.0	36.5	56.5	24.5	41.7
25S	51.8	46.5	46.0	62.2	67.5	66.1
25	52.6	41.0	42.5	51.8	52.5	56.4
26S	61.0		71.2	152.0		158.0
26	59.6		64.0	108.0		128.0
27S	74.6		80.5	350.0		202.0
28	72.9		99.3	198.0		308.0
28S	65.2		103.0	338.0		332.0

S - Sintered Medium

* - Layered Medium

3.2 Effects of Sintering on the Properties of Wire Cloth Media

Figure 3.1 is a graph of the average diameter of the sintered media versus the average diameter of the corresponding unsintered media. The line drawn on the graph is the line of equivalent diameters. It is apparent from the fact that the data points fall slightly above this line, that the sintering process can result in a small increase in the average diameter. This effect is further apparent in Figure 3.2 which shows the measured permeability of the sintered media to exceed that of the unsintered media. Recalling from the 1964 report that a medium's permeability is proportional to the square of its average diameter, the diameters of the sintered media are again shown to exceed those of the unsintered.

3.3 Specific Contaminant Capacities of Dutch Twill Media

A series of tests were conducted on a group of dutch twill media having various average diameters. The purpose of these tests was to measure the specific contaminant capacity of dutch twill media as a function of average diameter. In order to perform the tests on the Filter Media Performance Stand, an auxilliary injection system was constructed (see Figure 3.3). A 2-inch diameter sample of each medium was used in each case, and a specific flow rate of 0.1 gpm/sq. in. was maintained throughout the test. The fluid temperature was held constant at 100°F.

Table 3.2 is a summary of the data giving the average diameter (porosimeter test) and specific contaminant capacity for each medium tested. Figure 3.4 is a graph of this data. The increase in specific capacity with increased diameter is due to the nature of the definition of contaminant capacity which is commonly in use. The samples having the larger diameters are merely less affected by contamination because

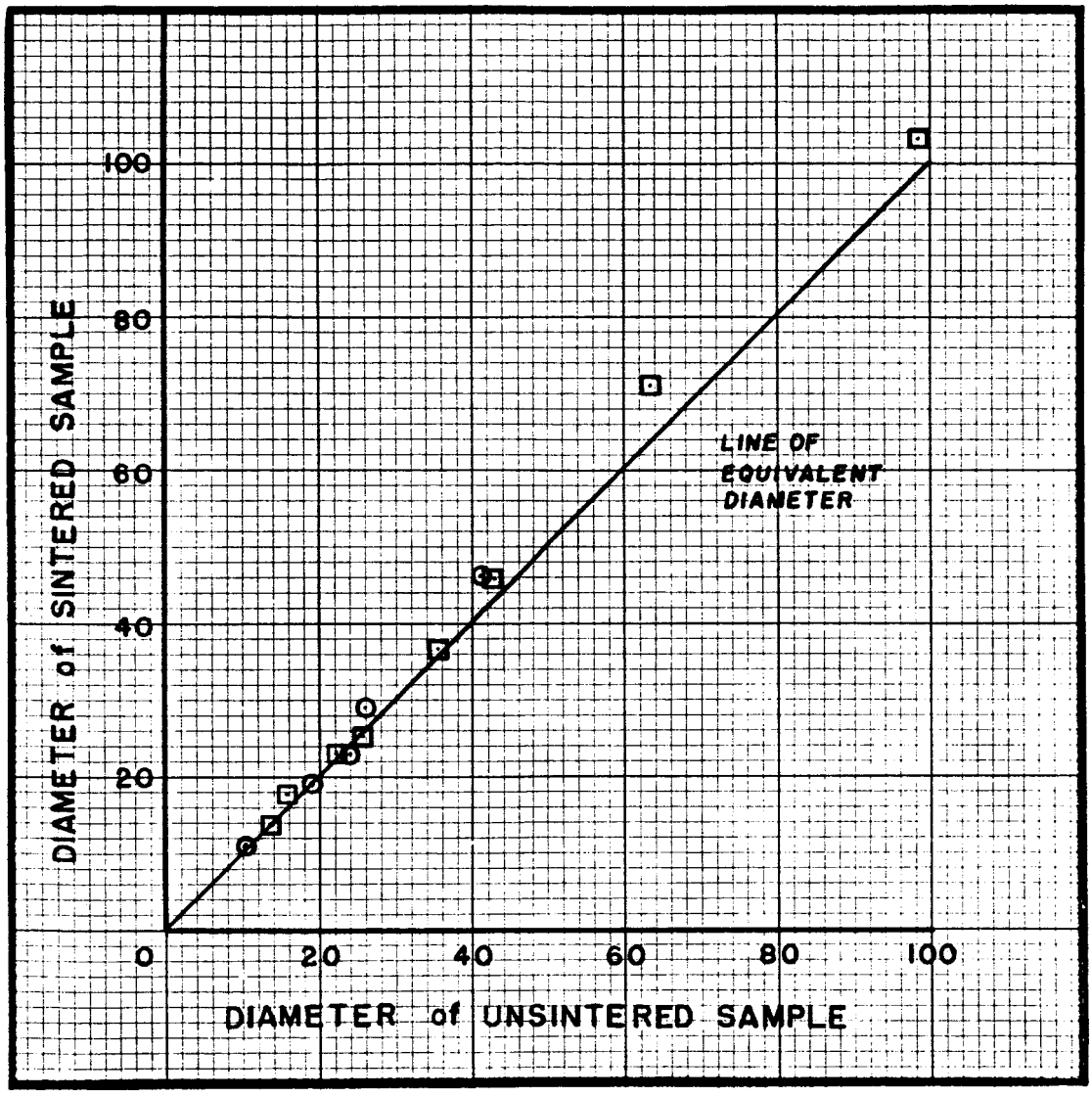

Figure 3.1. Effects of Sintering on Media Diameters.

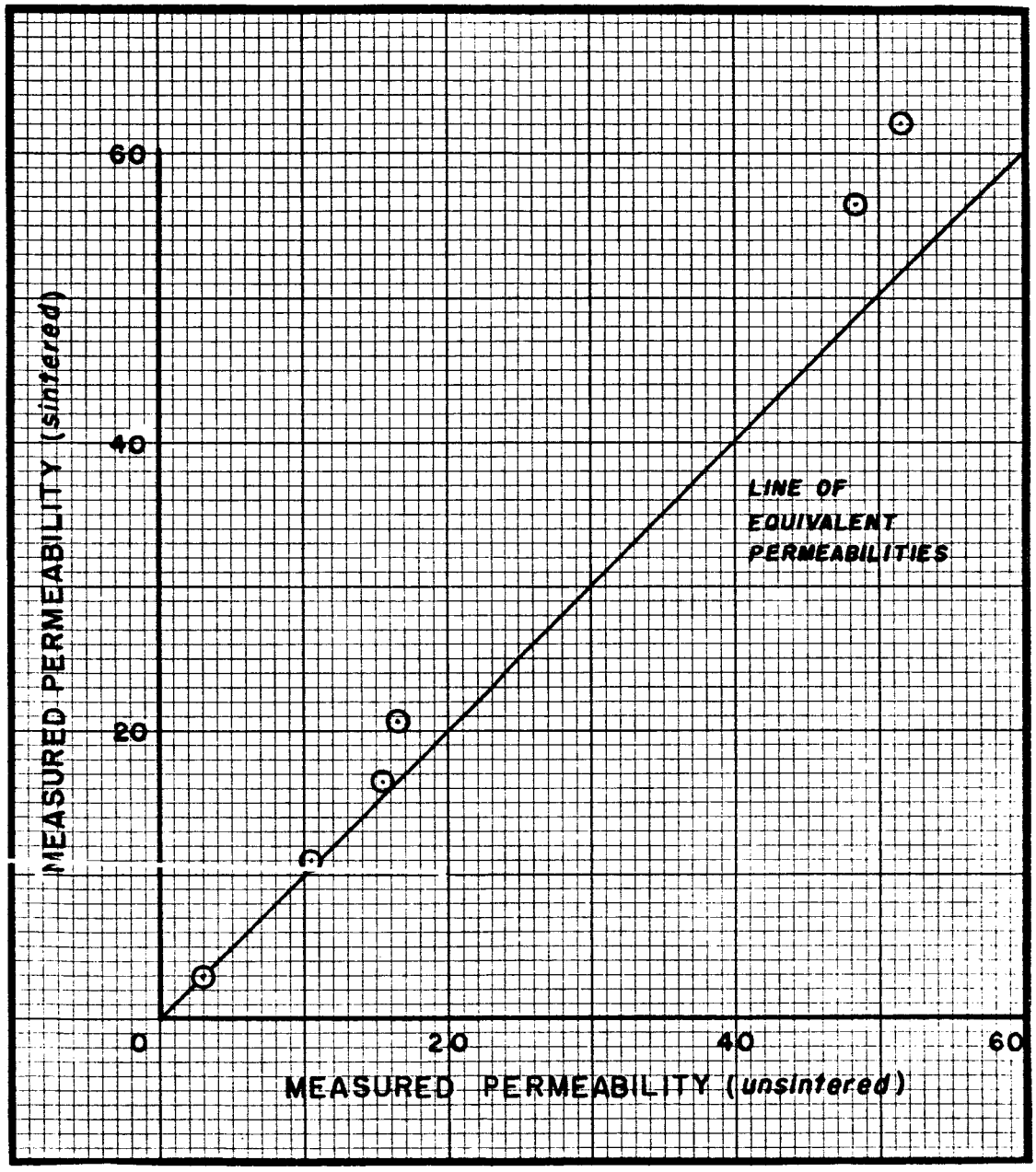

Figure 3.2. Effects of Sintering on Media Permeabilities.

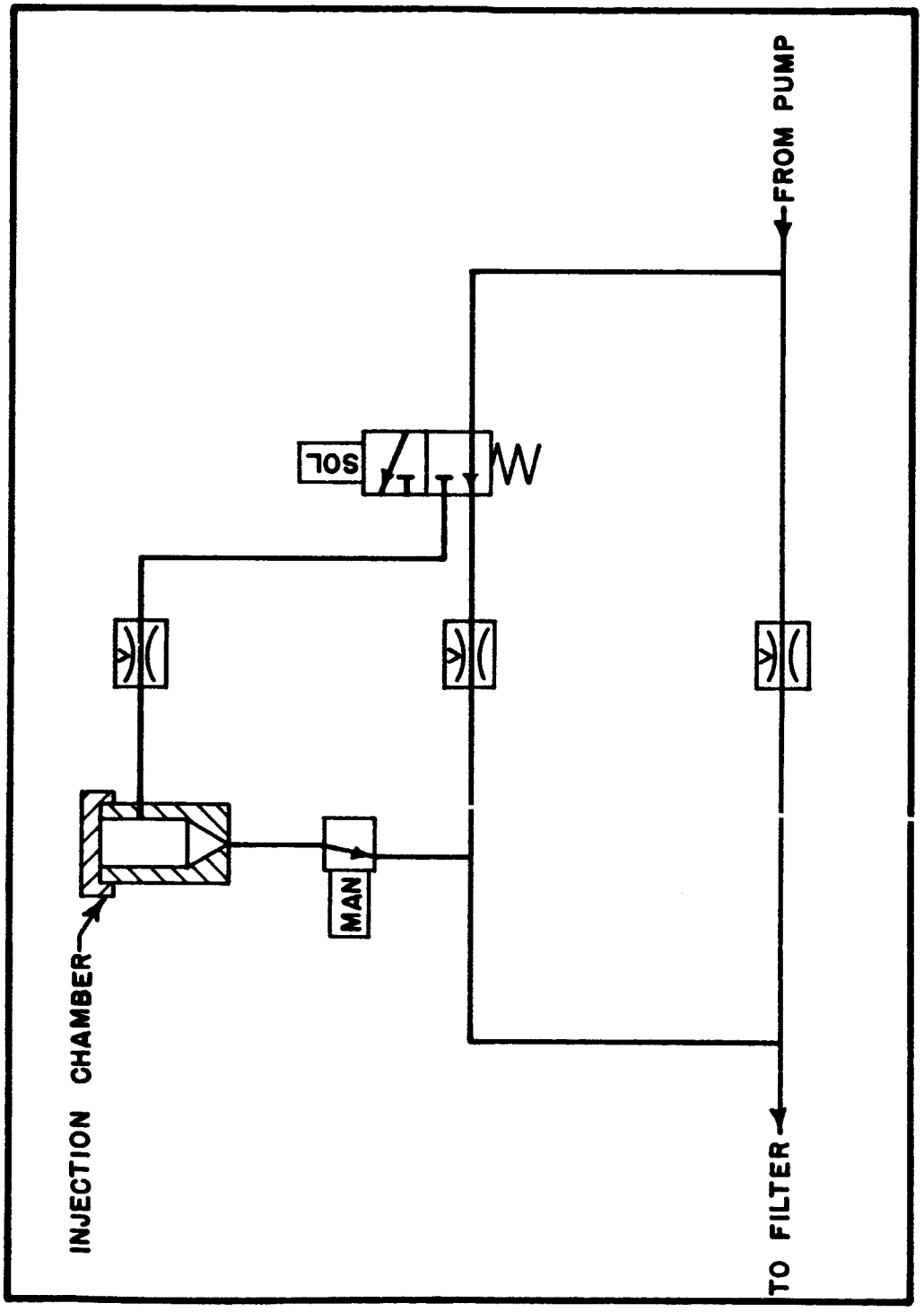

Figure 3.3. Auxilliary Injection System.

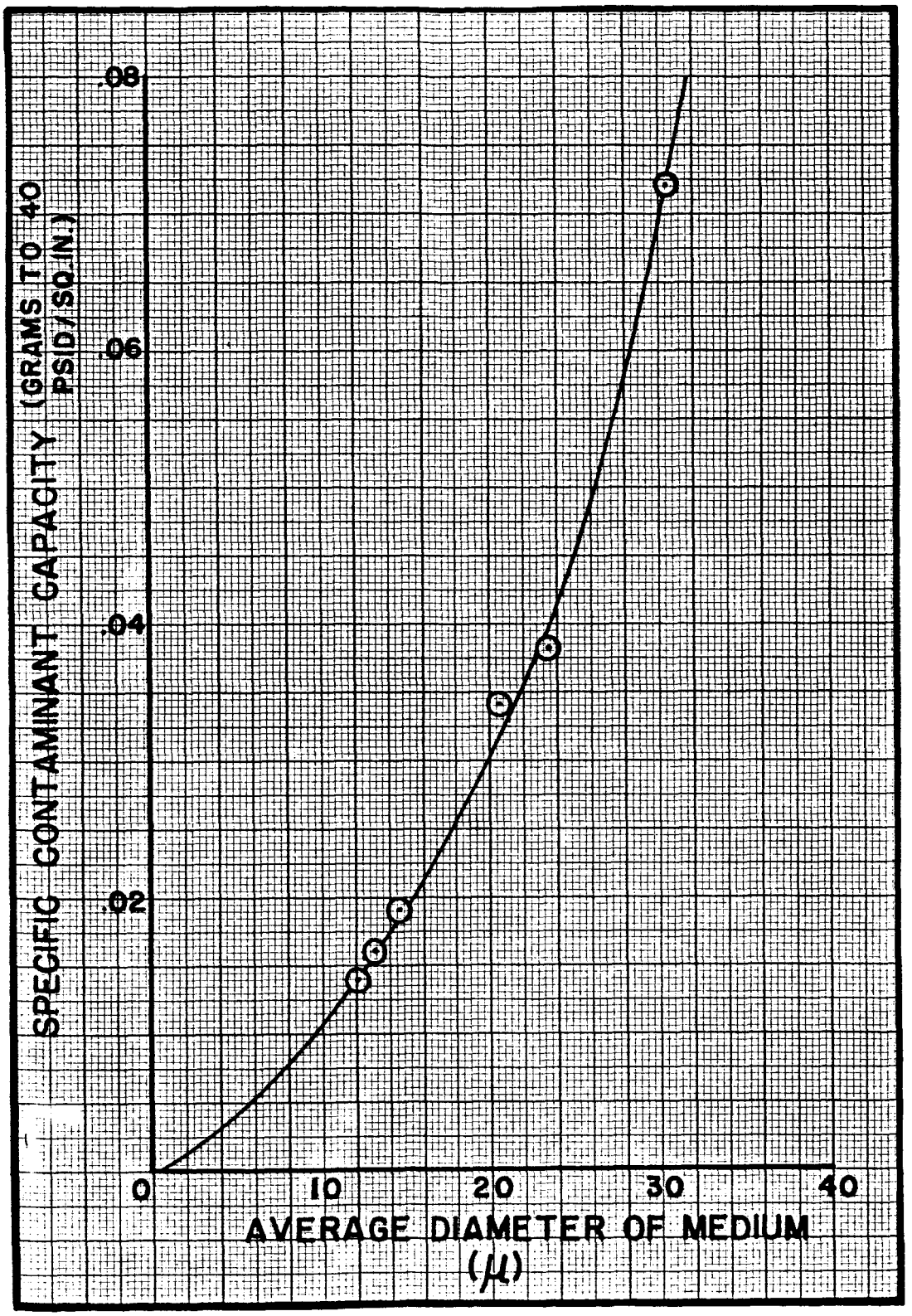

Figure 3.4. Specific Contaminant Capacity as a Function of Media Diameter.

TABLE 3.2

Sample Number	Average Dia. (Microns)	Contaminant Capacity (to 40 psid)	Specific Contaminant Capacity
1	12.0	.045	.014
2	13.0	.050	.016
3	14.5	.059	.019
4	20.5	.108	.034
5	23.5	.120	.038
6	30.5	.225	.072

of their poorer filtration efficiencies. This data in combination with that of the previous chapter can aid a designer in the selection of a filter element which will have a given contaminant capacity.

3.4 Effects of Flow Rate on Contaminant Capacity

The nature of the variation in specific contaminant capacity as a function of specific flow rate was examined. The test interval covered specific flow rates from 0.1 to 1.0 gpm/sq. in. A 2-inch diameter sample of 165 x 1400 wire cloth was used for the test program and AC Fine test dust was the contaminant. The test procedure was as follows:

1. The specific flow rate for the particular test was established at a temperature of 100°F.
2. An injection of 0.02 grams of contaminant was presented to the filter sample.
3. Following the injection, the flow rate was reduced to a reference flow rate of 0.1 gpm/sq.in. and the differential pressure was recorded.

4. The specific flow rate for the individual test was then re-established and another injection begun.

5. This procedure was repeated until the differential pressure at the reference flow rate reached 10 psid. This lower pressure was used as the arbitrary reference pressure rather than the 40 psid reference used in previous tests, because at the higher specific flow rates the 100 psid range of the Press-I-Cell would have been exceeded.

The pressures at the test flow rate before and after each lowering to 0.1 gpm/sq. in. were the same; therefore, no adverse effect on the contaminant retained on the filter was present. Figure 3.5 is a graph of the contaminant capacity curves at the reference flow rate. Table 3.3 gives the capacities and specific capacities to 10 psid for each of the 5 specific flow rates which were used. (See also Figure 3.6.)

The results show an increase in specific capacity with an increase in specific flow rate. This increase is attributed to the fact that the higher fluid velocities through the pores of the medium force some contaminant through the medium which would be retained at lower fluid velocities. Efficiency tests to substantiate this hypothesis are in a preliminary phase, but no applicable data is currently available.

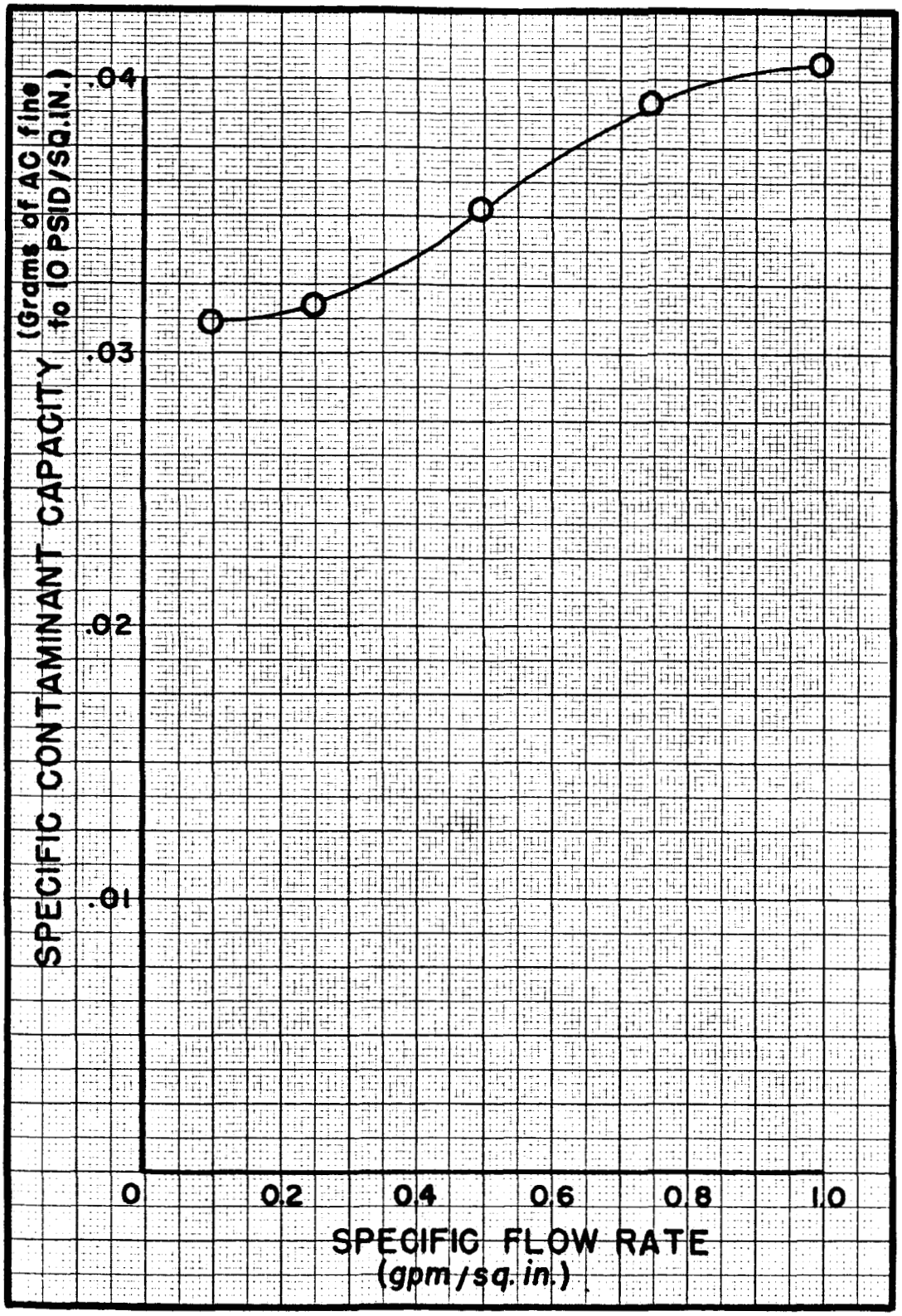

Figure 3.5. Contaminant Capacity Curves at Various Flow Rates.

TABLE 3.3

CONTAMINANT CAPACITY AS A FUNCTION OF FLOW RATE

Specific Flow Rate (gpm/sq.in.)	Contaminant Capacity to 10 psid (grams)	Specific Capacity to 10 psid (gms/sq.in.)
0.10	0.098	.0312
0.25	0.100	.0318
0.50	0.111	.0353
0.75	0.123	.0392
1.00	0.128	.0407

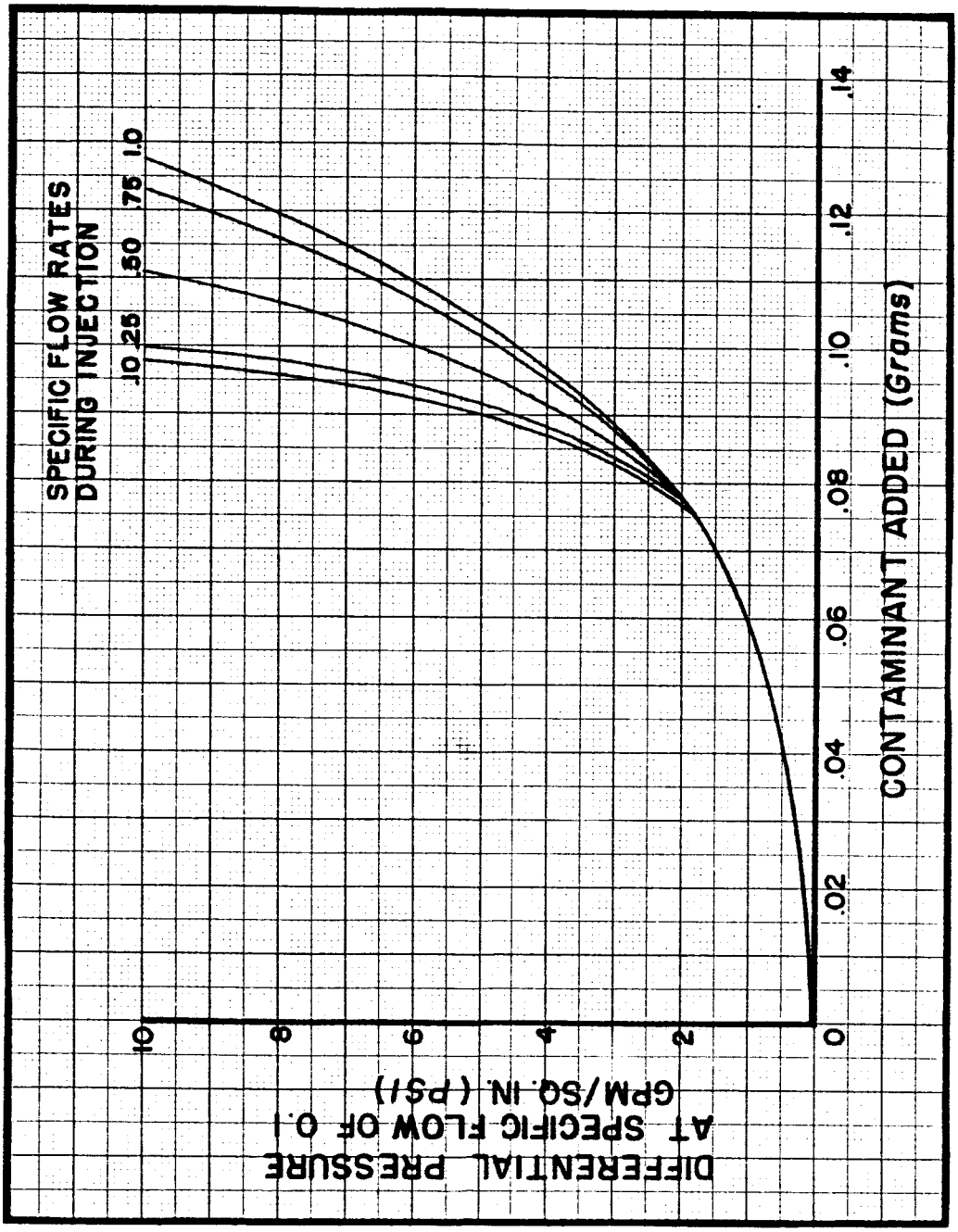

Figure 3.6. Specific Contaminant Capacity as a Function of Specific Flow Rate.

CHAPTER IV

THE FILTRATION TEST STAND

4.1 Introduction

A test stand was required which would permit measurement of the efficiency of wire cloth media under conditions

1. of various steady flow rates,
2. of partial contaminant loading of the test filter,
3. which satisfy the requirements associated with the testing of Mil-F-8815 elements.

To more closely simulate the in-service loading of a filter medium, a means was required for injecting contaminant upstream of the filter continuously for periods of the order of 30 minutes, while the flow rate and contamination level of the oil was maintained constant. The principle problem was to ensure uniform dispersion and suspension of the added contaminant in the oil presented to the test filter.

4.2 Description of the Test Stand

Figure 4.1 shows the functional diagram of the stand. Oil can be pumped from the sump reservoir to the main reservoir through a low micron depth filter. Oil can be circulated through the rest of the system by air pressure in the main reservoir. The valving permits flow from the main reservoir to

1. go directly to the test section,
2. go to the test section via the contaminant mixing chamber,

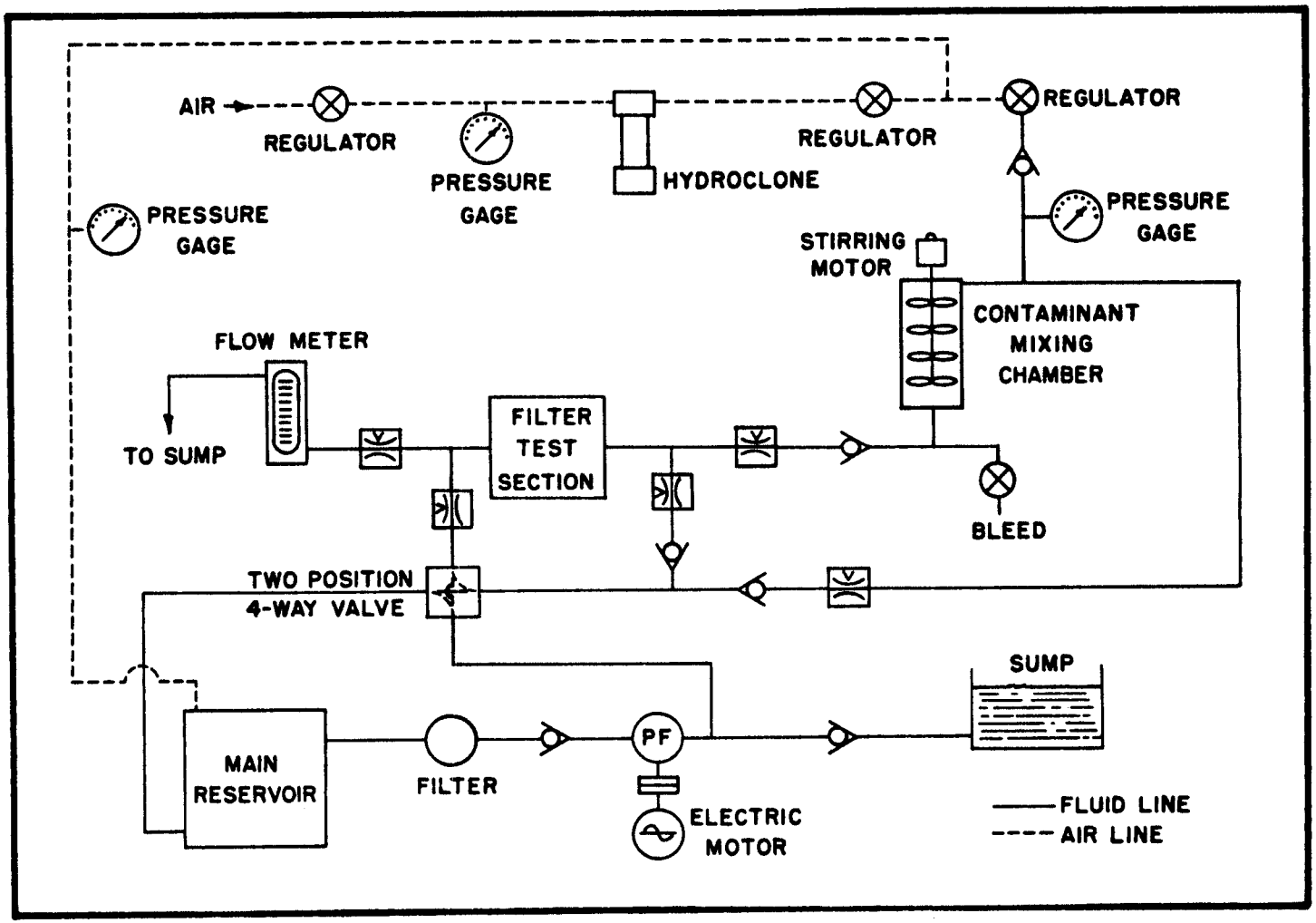

Figure 4.1. Schematic of Filtration Test Stand.

3. reach the test section from both routes simultaneously.

The discharge from the test section can be directed to the sump reservoir via the flow meter when testing, or returned to the suction side of the pump when circulating for clean-up purposes.

Contaminant can be added to the mixing chamber and dispersed and held in suspension by the stirrer. Contaminated oil can be presented to the test filter by applying air pressure to the mixing chamber. The rate at which contaminated oil is admitted to the test section is controlled by the air pressure in the mixing chamber and by the valving. The rate can be held constant while the flow rate through the filter is varied, by suitable mixing of the flows from the mixing chamber and the main reservoir.

Sampling valves are included in the circuit immediately upstream and downstream of the test section so that upstream and downstream samples can be taken simultaneously at any time during a test. Evaluation of the samples by gravimetric analysis and particle counting gives the data required to establish the efficiency of the test filter. Ideally, the upstream sample should be directly comparable with the contamination condition in the mixing chamber. The loading condition of the test filter when the samples are taken is described by the pressure drop across the filter. The sampling valves are of the bleeder-type described in the 1964 report. Figure 4.2 shows a front view of the test stand.

4.3 Evaluation of the Test Stand

Tests were conducted to examine the effectiveness of the filtration system of the stand. After a period of circulation through the main filter, oil samples revealed the background contamination level shown in Table 4.1.

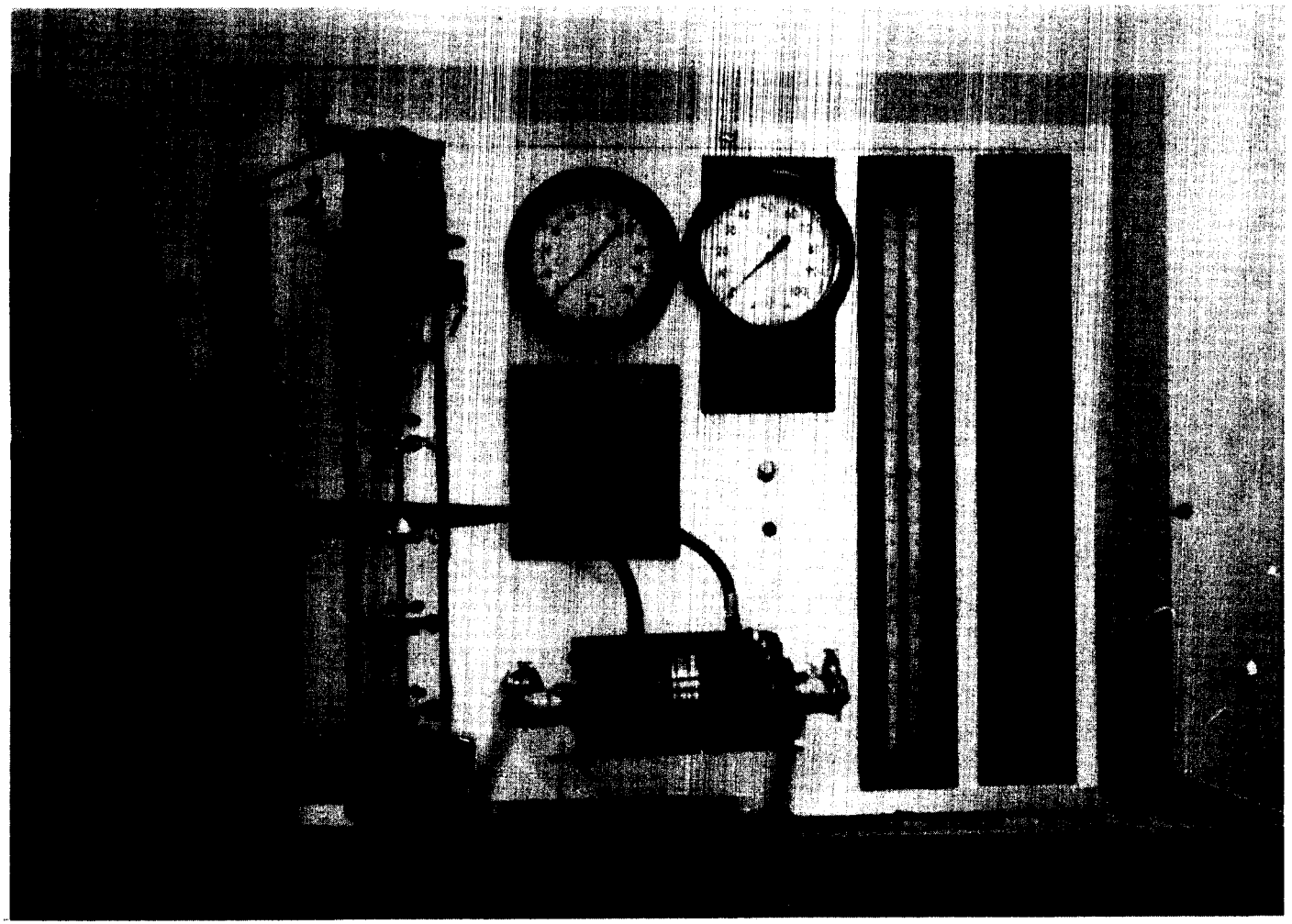

Figure 4.2. Photograph of Filtration Test Stand.

TABLE 4.1

BACKGROUND CONTAMINATION

Particle Size Range Micron	Number of Particles/Milliliter					
	Series 1			Series 2		Overall Average
	Mix. Chamber Bleed	Upstream Sampler	Downstream Sampler	Mix. Chamber Bleed	Upstream Sampler	
6 - 10	78	96	76	100	61	82
10 - 15	24	23	32	39	20	28
15 - 20	17	4	5	7	4	7
> 20	1	1	1	2	1	1
Gravimetric, mg/l	5.5	7.4	5.5	5.5	6.1	6

Samples were taken at the mixing chamber and at the test section. The results compare favorably with the background levels of other test stands in the laboratory, and are considered to be satisfactory.

Tests were conducted to examine the effectiveness of the contaminant mixing and injection systems. Samples of AC test dust were placed in 150 ml. bottles, triple filtered (0.45μ) oil was added to the bottles, and the contaminant was dispersed by shaking and by insertion of the bottle in an ultrasonic bath. The slurry was poured into the mixing chamber which was initially nearly full of system oil. The stirrer was run continuously. Table 4.2 shows the contamination level results obtained when 0.1 gram of AC Fine test dust was added to the mixing chamber. The contaminated oil in the mixing chamber was admitted to the system at a steady rate which required about 40 minutes to empty the chamber. The samples were taken progressively, at the periods indicated. The results indicate that

1. the contamination level of the oil at the test section (upstream sampler) is substantially the same as the level in the mixing chamber (mixing chamber bleed),
2. the contamination level remains substantially constant for periods of up to 40 minutes and hence reflects the effectiveness of the mixing process.

Similar tests were conducted using AC Coarse dust, and a 30-40 micron cut from AC dust. Figure 4.3 shows the gravimetric analysis for each case, for samples taken at the test section as the mixing chamber was emptied into the system when all of the flow is from the mixing chamber. The consistency of the contamination levels achieved is apparent.

TABLE 4.2

UNIFORMITY OF CONTAMINATION LEVEL

Particle Size Range Micron	Number of Particles/Milliliter						
	Stirring Time 5-10 minutes		Stirring Time 20 minutes		Stirring Time 40 minutes		Overall Average
	Mixing Chamber	Upstream Sampler	Mixing Chamber	Upstream Sampler	Mixing Chamber	Upstream Sampler	
6 - 10	6,439	7,019	7,622	7,610	6,774	6,572	7,173
10 - 15	1,102	1,555	1,782	1,557	1,709	1,426	1,522
15 - 20	168	307	359	261	280	357	289
> 20	50	125	146	84	117	118	107
Grav. mg/l	50.5	39.2	36.7	34.8	38.6	35.7	39

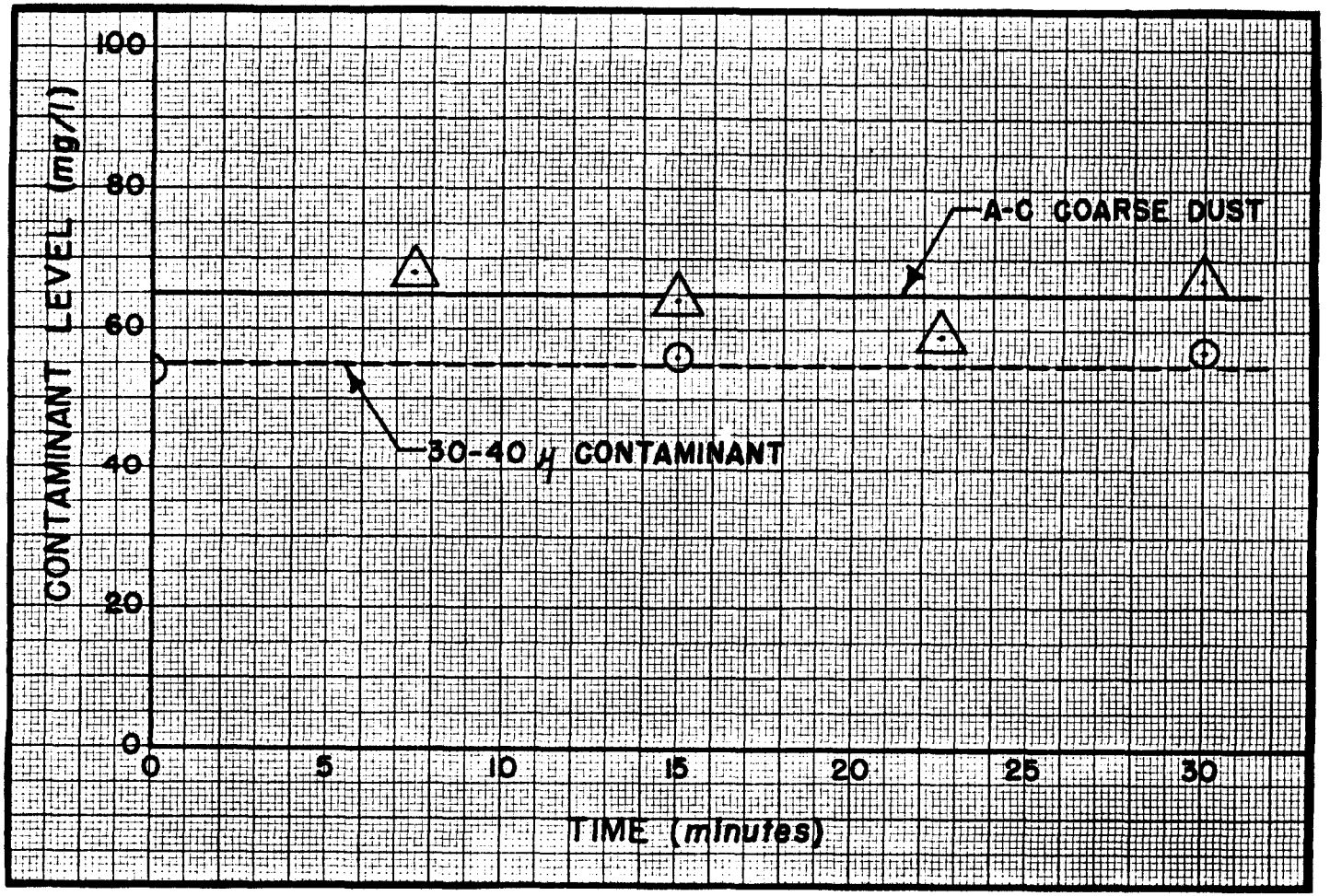

Figure 4.3. Gravimetric Level Vs. Time.

The Media Sample Holder (1964 report) was fitted to the test section, with a flat sample of 165 x 1400 dutch twill wire cloth fitted in the housing to give an effective filtration area of π in^2. AC Coarse test dust was added to the mixing chamber. After mixing, the contaminated oil was presented to the test filter at a specific flow rate of 0.05 gpm/in^2 of filter surface. The solid line of Figure 4.4 shows the pressure drop-time relationship obtained. The data points shown were obtained from a conventional contaminant capacity test in which incremental quantities of AC Coarse test dust were periodically injected upstream of the test filter. The shapes of the contaminant capacity curves obtained by the two different methods are similar.

4.4 Use of the Test Stand

The efficiency of wire-cloth media at various stages of the life cycle associated with contaminant capacity is at present being investigated. The results presented here should be regarded as indicative only.

A flat sample of 165 x 1400 wire cloth was fitted to the test housing, which in turn was placed in the test section of the Filtration Test Stand. 0.15 gram of AC Fine test dust was added as a slurry to system oil in the mixing chamber and dispersed by stirring to produce uniformly contaminated oil. Oil from the mixing chamber was admitted to the test section together with filtered oil from the main reservoir, in the ratio 1:1. Flow rate through the test filter was maintained at 0.05 gpm/in^2 of filter area. The pressure drop-time relationship for the test filter was recorded. Samples of oil downstream of the test filter were taken near the start of the test ($\Delta P \cong 0$) and near the end of the test ($\Delta P \cong 40$ lb/in^2), when the filter was considered to be fully loaded. A sample upstream of the filter was taken for reference purposes.

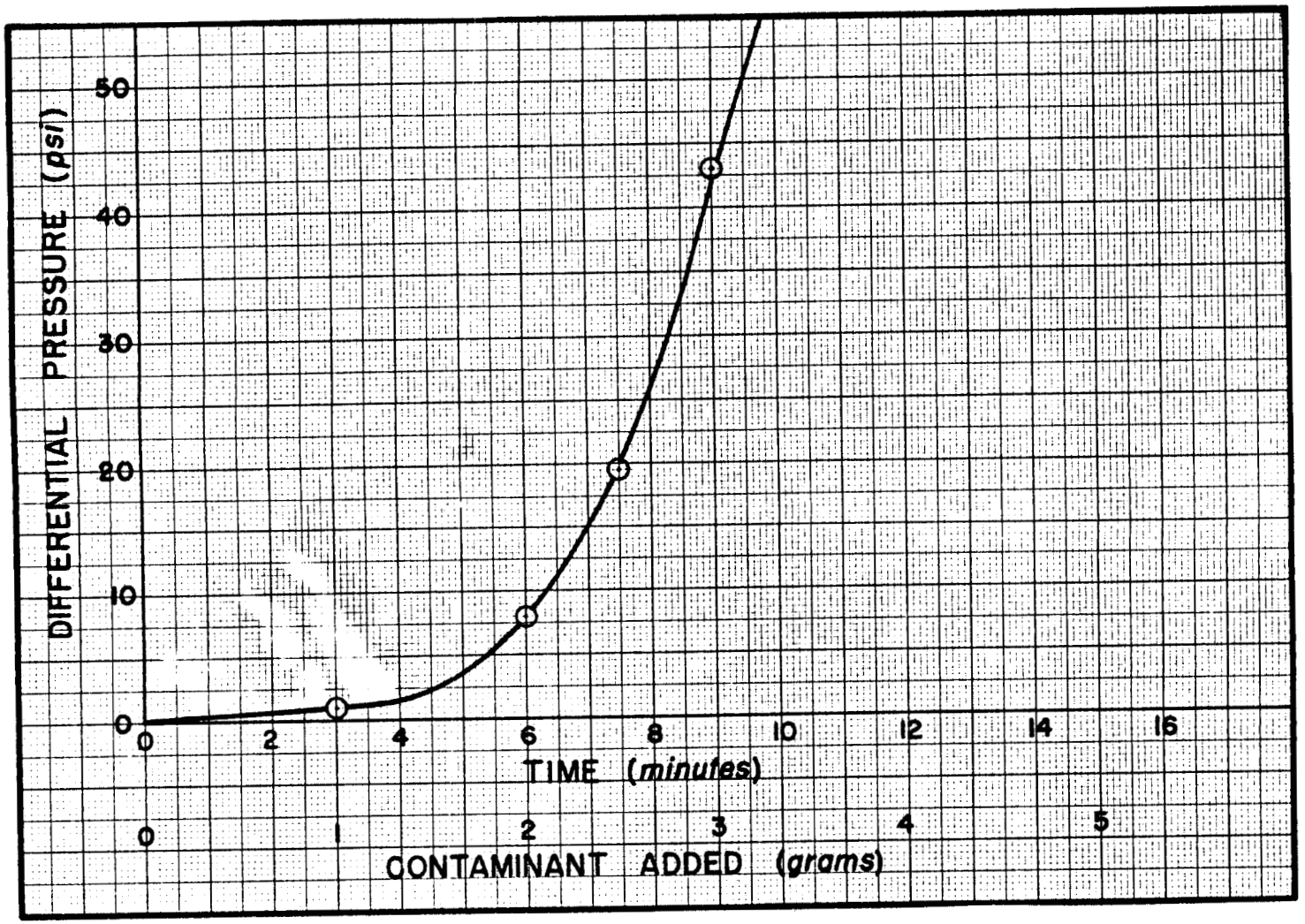

Figure 4.4. Pressure-Time Relationship for 165-1400 Dutch Twill Medium Using AC Coarse Test Dust.

The level of contaminant in the mixing chamber was 0.15 gm/3ℓ = 50 mg/ℓ. The rate at which contaminant was presented to the test filter can be established using the known flow rate from the mixing chamber. Figure 4.5 shows the pressure drop-contamination characteristic obtained. The specific contamination capacity (weight of contaminant to produce ΔP = 40 lb/in^2) is 0.041 gm/in^2 of filter surface area, which agrees closely with the results obtained for the same media by the incremental injection method (Section 3.3).

Table 4.3 shows the particle counts obtained from the samples taken during the test, together with the calculated efficiency values. Figure 4.6 shows the efficiency of the media near the start and near the end of its useful life. The efficiency shows a small but distinct tendency to increase with use.

4.5 Conclusions

The test stand performance is satisfactory in that it

1. permits cleaning of the system to a low background contamination level,
2. permits continuous presentation at the test filter of oil at a controlled contamination level for long periods, up to 40 minutes,
3. permits a range of flow rates through the filter,
4. permits evaluation of the contaminant loading cycle of a filter,
5. enables the filtration efficiency of a test filter at given flow rates to be measured for any part of the contaminant loading cycle of the filter.

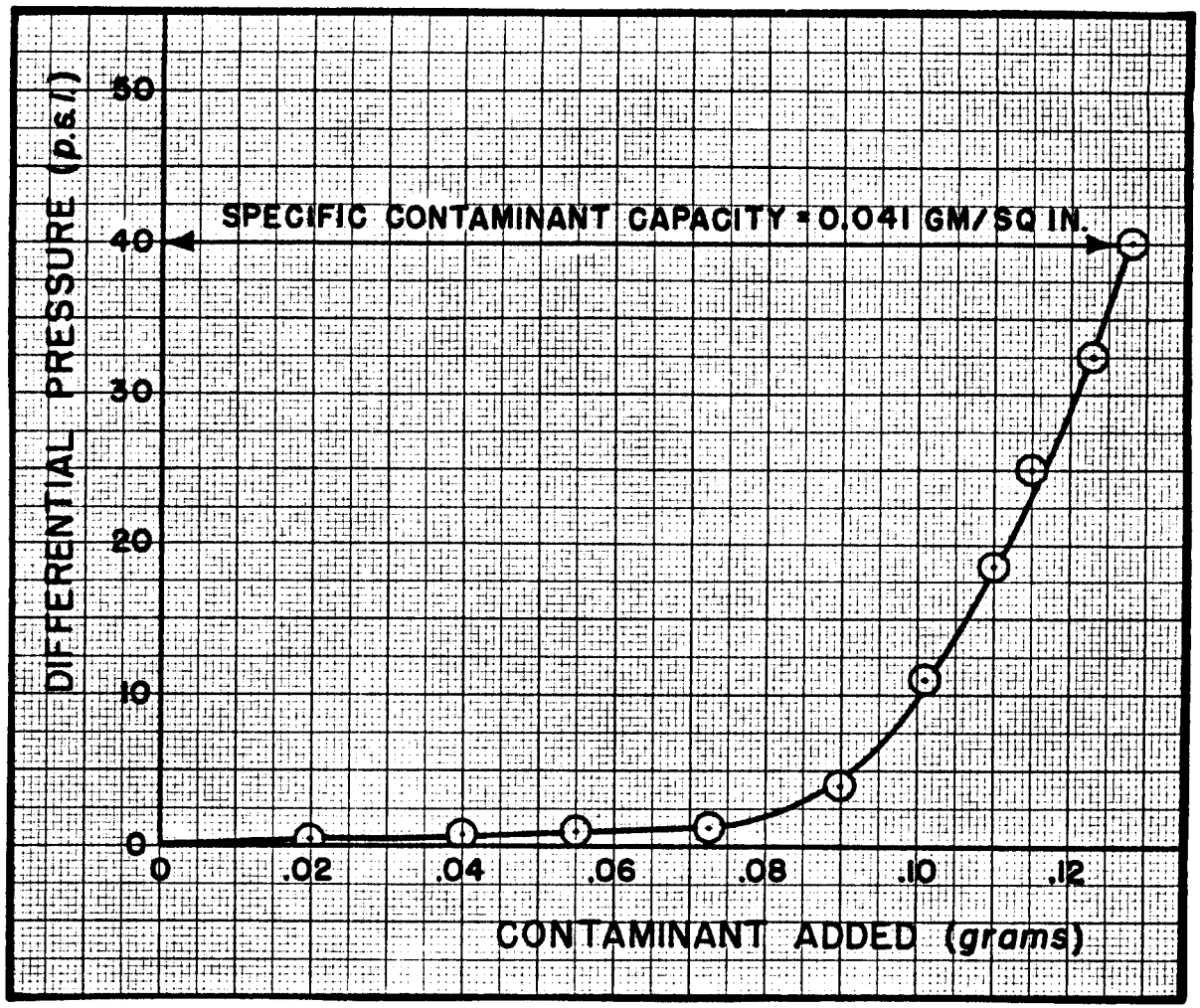

Figure 4.5. Contaminant Loading Curve for 165 x 1400 Dutch Twill Medium.

TABLE 4.3

EFFICIENCY DURING CONTAMINATION LOADING CYCLE

Particle Size Range Micron	Number of Particles Per Milliliter			Efficiency $= \frac{N_{up} - N_{down}}{N_{up}}$	
	Initial Downstream	Final Downstream	Upstream	Initial %	Final %
6 - 10	6,196	4,535	6,729	8	32
10 - 15	567	529	917	38	42
15 - 20	39	17	219	82	92
20 - 25	37	1	39	--	97
25 - 30	2	1	16	88	94
30 - 35	1	0	7	86	100
> 35	1	0	5	80	100

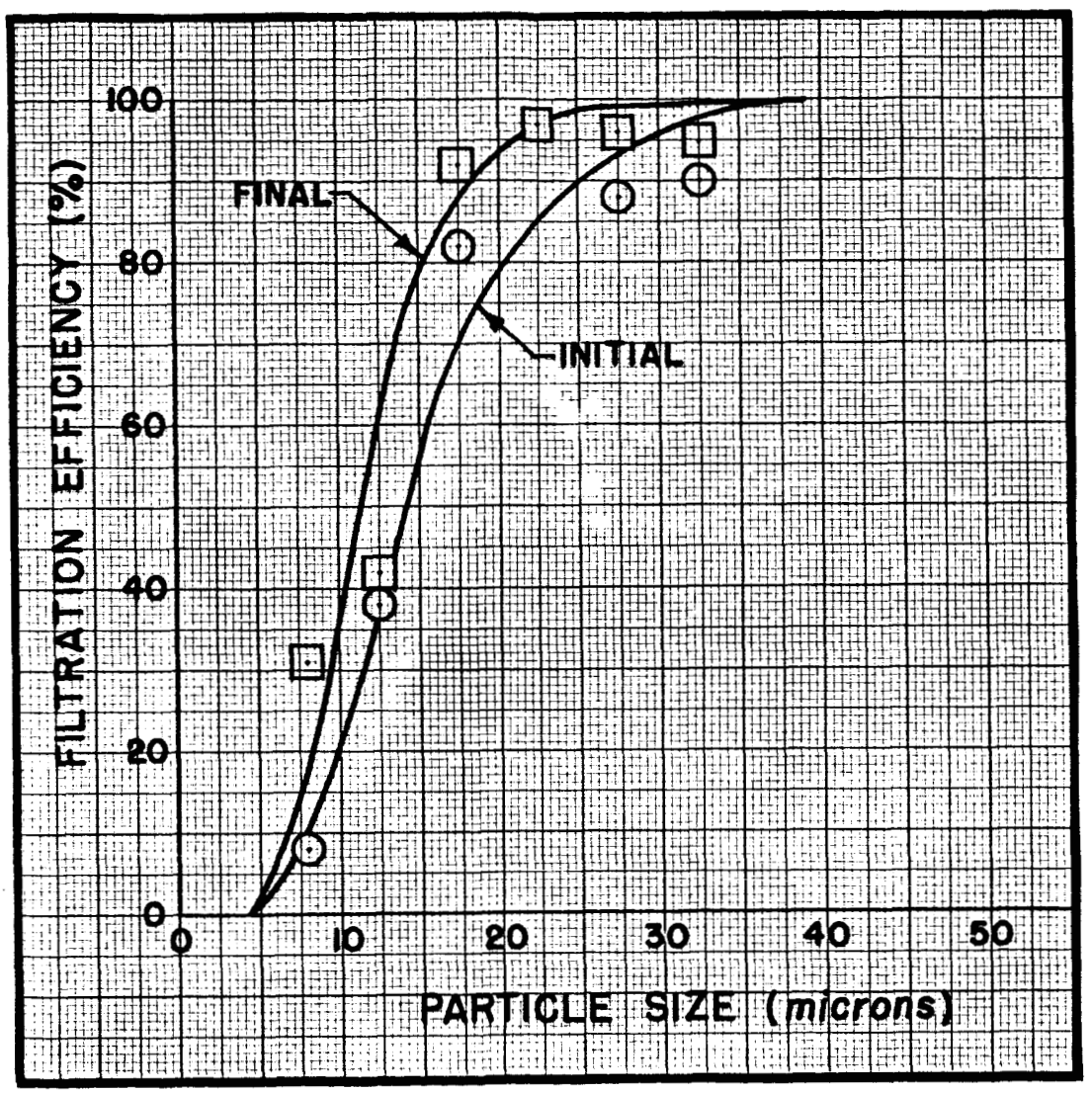

Figure 4.6. Variations in Efficiency with Contaminant Loading.

CHAPTER V

DEVELOPMENT OF A HIGH-PRESSURE SYSTEM OIL-SAMPLING DEVICE

5.1 Introduction

A requirement existed for a device suitable for taking oil samples direct from a working high-pressure system. The device should:

1. prevent any environmental error due to on-site sampling,
2. be simple to operate, and operable by normal on-site personnel,
3. provide samples suitable for transporting long distances for laboratory analysis.

Work described in the 1964 report concerning the sampling of oil from low-pressure systems for contamination analysis produced several general requirements for sampling techniques. There were:

1. The sampling device and procedures should provide demonstratively accurate and repeatable samples.
2. Any sample containers used should be cleaned and prepared in a clean room environment, and protected from atmospheric contamination during the sampling period.
3. An established adequate flushing period of the sampling device should be utilized prior to the taking of a sample.

5.2 The High Pressure Sampler

Figure 5.1 shows the design and operation of the sampling device which was developed. Figure 5.2 shows a photograph of the sampler, with an indication of its physical size. The device consists of a high pressure

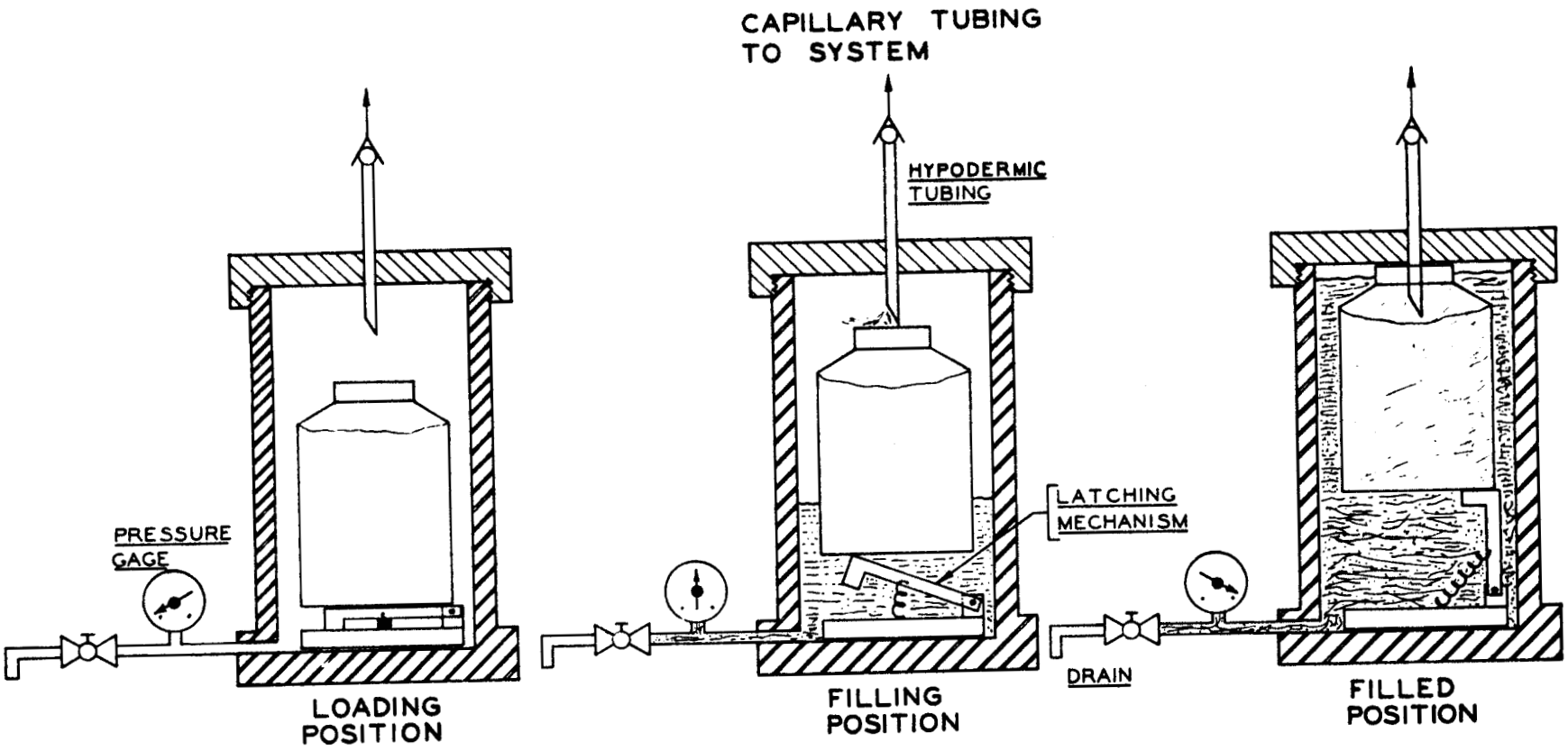

Figure 5.1. Operational Schematic of High Pressure Sampling Device.

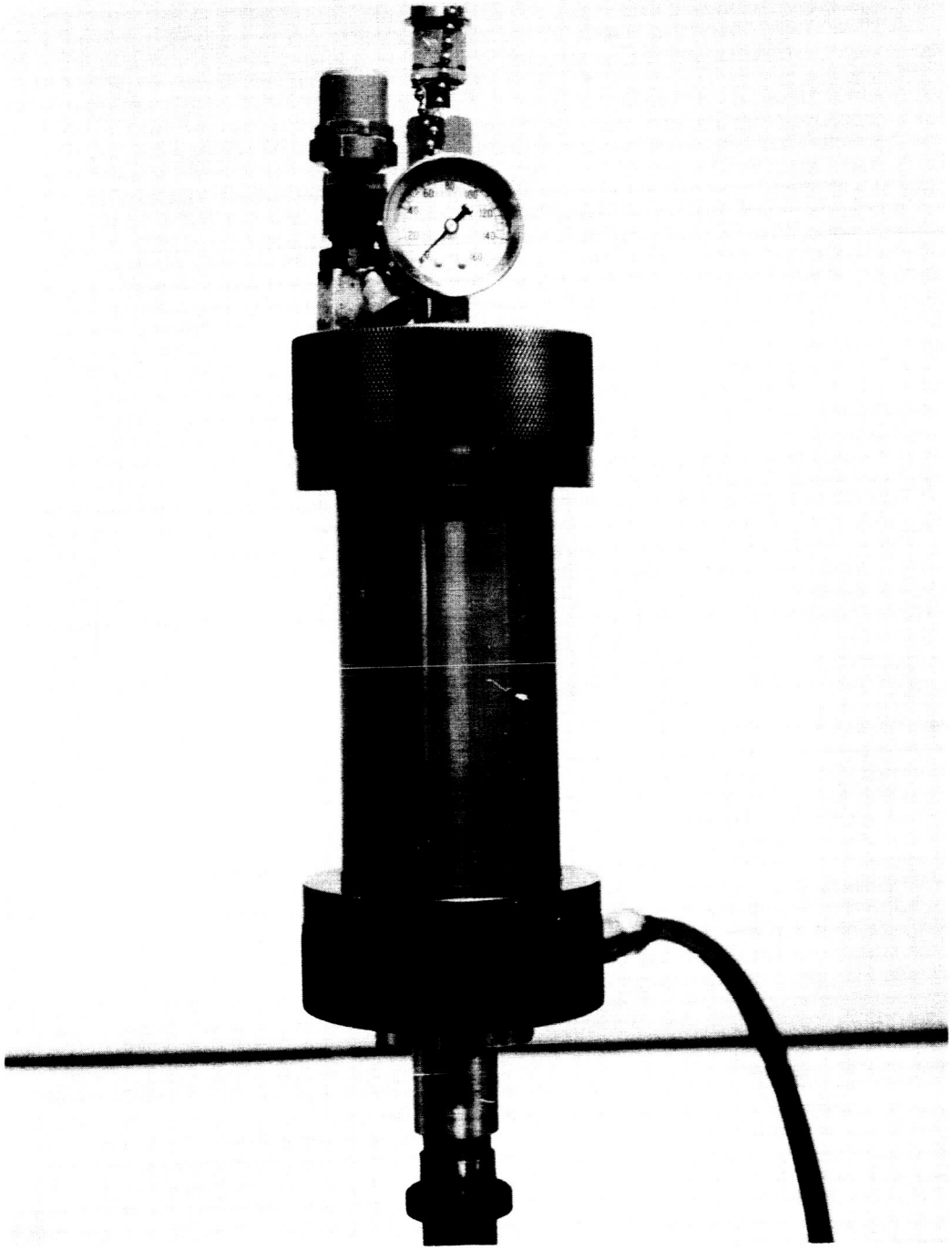

Figure 5.2. High Pressure Sampling Device.
(Gage has 2 in. O.D.)

vessel into which is placed a precleaned 500 ml. sample bottle sealed with a non-generating film. The sampler is connected to a suitable tapping point in the system being sampled, via a length of stainless steel hypodermic tubing. The purpose of the hypodermic tubing is to reduce the flow rate from the system to the sampler by causing a large pressure drop without restricting the flow of contaminant particles. A sharpened tube of 0.024 in. I.D. and 6 in. length was found to be suitable for sampling a 3,000 lb/in^2 system. The downstream end of the hypodermic tubing projects through the end cap of the sampler as shown on Figure 5.1. When a sample is required, a valve at the system tapping point is opened to permit flow to the sampler. The initial fluid reaching the sampler fulfills two purposes:

1. It provides the necessary flushing of the line and fittings connecting the system to the sampler.
2. It floats the sample bottle until the sharpened end of the hypodermic tubing pierces the film.

When a seal is pierced, the bottle is filled with a sample of the system fluid. The latching mechanism (Figure 5.1) holds the bottle in the floated upright position to keep the flushing fluid from entering the bottle, the upper part of the bottle being surrounded with air which has been compressed as the flushing fluid level rises in the sampler. A non-return valve is included in the line connecting the system and sampler, to offset the possibility that air trapped under pressure in the sampler could be admitted to the system being sampled if system pressure was reduced.

When the sample has been taken, the sampler can be disconnected from the system, the pressure inside it can be released, and the sample bottle

removed for analysis. Completion of the sampling is indicated by a constant pressure reading on the pressure gauge fitted to the sampler casing. A new sample bottle can be placed in the sampler for immediate re-use.

The sampler can be used for sampling low-pressure fluid systems. However, it is necessary to include a valve in the cap in order to release the air pressure caused by entry of the flushing fluid. Otherwise, the air pressure may become equal to the system pressure, and flow to the sampler would cease.

5.3 Laboratory Evaluation of the Sampler

The performance of the high-pressure sampler was compared with the results obtained by proven methods of sampling.

Test No. 1. A high-pressure test stand was equipped with a quick-disconnect fitting of the type to be used for joining the sampler to a system in the field. A throttling valve was fitted downstream of the quick-disconnect fitting, followed by a "tee" fitting. This arrangement enabled a high-pressure sample to be taken through the quick-disconnect fitting by the sampler at the same time as a low-pressure sample was taken directly from the line at the "tee" fitting. The gravimetric results obtained when various quantities of AC Fine test dust were injected into the system are shown in Table 5.1 to have good correlation.

Test No. 2. The high-pressure sampler was placed in series with an isokinetic sampler, as shown on Figure 5.3. The good performance of isokinetic sampling was demonstrated in the 1964 report, where it was shown to be accurate within 5% over a wide range of flow rates. Needle valves installed between the two samplers were used to reduce the 2000 lb/in^2

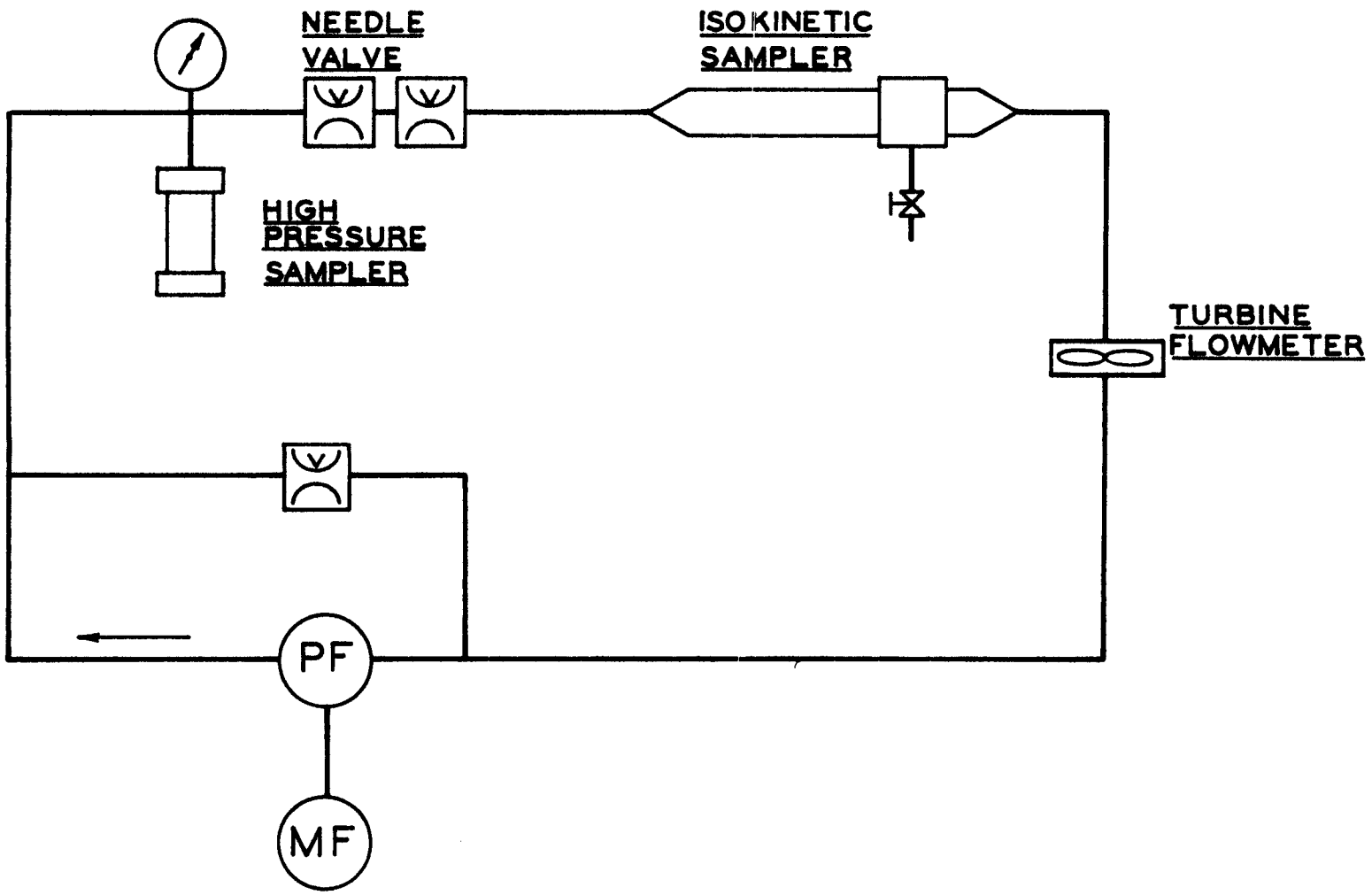

Figure 5.3. Circuit Schematic Used in Evaluating High Pressure Sampler.

TABLE 5.1

Sample No.	Contaminant Level--mg/l	
	High-Pressure Sample	Low-Pressure Sample
1	6.5	6.7
2	5.3	4.8
3	10.0	10.8
4	12.5	9.2
5	25.5	26.3
6	21.5	21.5

pressure used for the high-pressure sampling to 100 lb/in^2 for the isokinetic sampling.

Fluid samples taken simultaneously from a contaminated system were evaluated with a HIAC particle counter. Table 5.2 shows the results of the two tests which were conducted.

The results of the laboratory tests indicate that the high-pressure sampler will withdraw a representative sample of fluid from a high-pressure system.

5.4 Field Use of the Sampler

The high-pressure sampler is at present being used to monitor the contamination conditions associated with the life cycle of hydraulic pumps in some aircraft control systems. Figure 5.4 shows a set of three samplers connected to the pump suction, the pump discharge, and the pump case drain on an aircraft system. Some results obtained to indicate the levels of contamination to be expected are shown in Table 5.3. Additional case

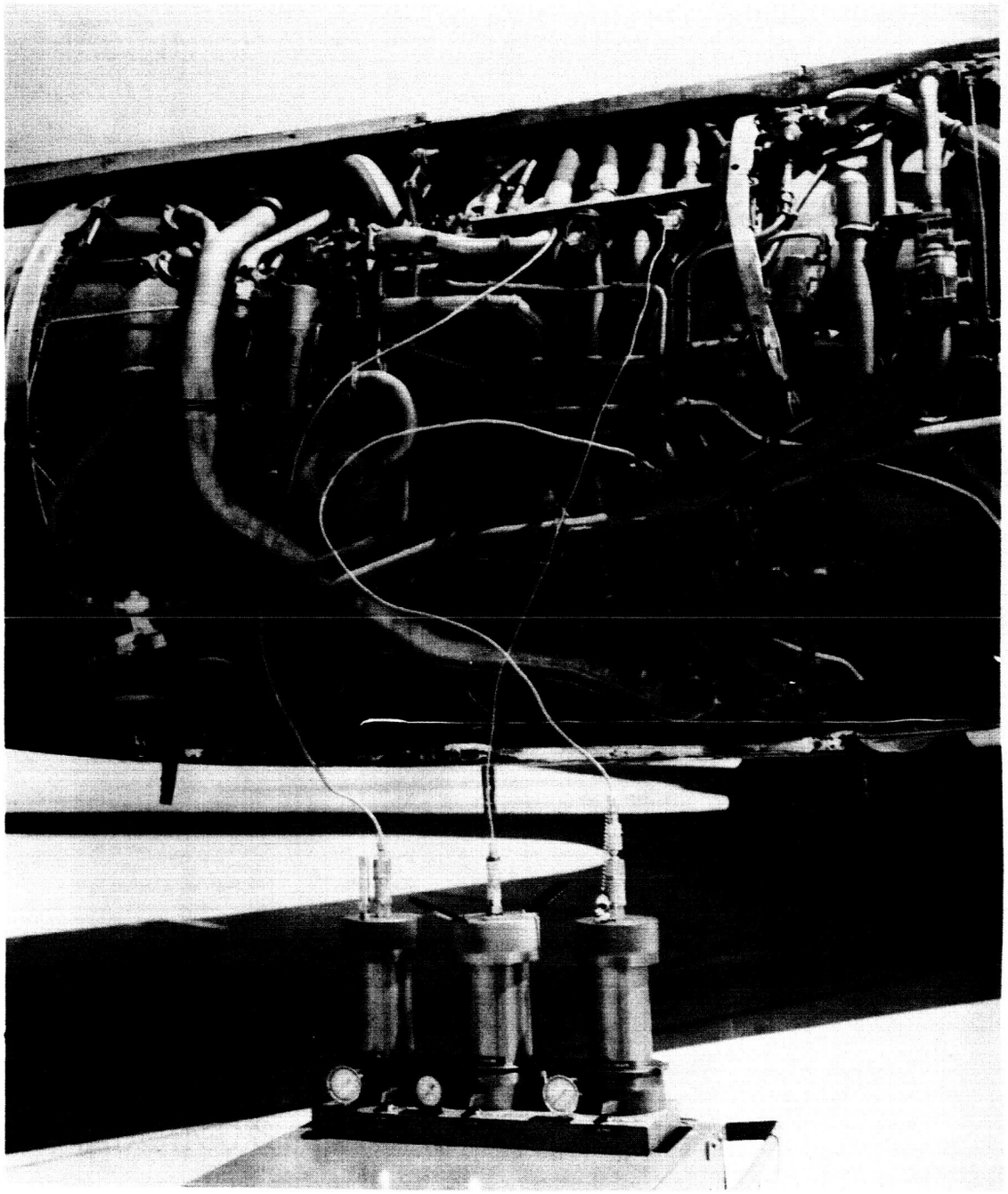

Figure 5.4. High Pressure Sampler Connected to Aircraft System.

TABLE 5.2

Particle Size Range Micron	Number of Particles/ml. of Sample			
	Test No. 1		Test No. 2	
	Isokinetic	H.P. Sampler	Isokinetic	H.P. Sampler
6 - 10	2,858	2,734	2,369	2,392
10 - 15	663	699	559	541
15 - 20	78	98	67	66
> 20	39	66	43	37

TABLE 5.3

Gravimetric Analysis, mg/l					
Aircraft No. 1			Aircraft No. 2		
Suction	Discharge	Case Drain	Suction	Discharge	Case Drain
6.0	5.7	7.5	6.0	5.5	9.0
6.0	5.0	6.5	6.0	5.5	8.9
		7.5			9.5
		8.0			11.4
		8.0			8.0
		7.5			

drain samples were taken to determine the consistency of the sampling procedure over an extended period of time.

A sample taken at the suction is used to represent the contaminant level reference input to the pump. A sample taken at the case drain is

used to represent the contaminant generation of the pump. A gravimetric generation ratio (G_R) and a particle size generation ratio N_x are defined as:

$$G_R = \frac{\text{Gravimetric Weight of the Case Drain Sample}}{\text{Gravimetric Weight of the Suction Sample}}$$

$$N_x = \frac{\text{Number of Particles Above Size x Microns in the Case Drain Sample}}{\text{Number of Particles Above Size x Microns in the Suction Sample}}$$

G_R and N_x should each be unity for a pump which is not generating contamination, and should increase from unity as the pump experiences wear. Figure 5.5 shows the form of wear relationship to be expected from a pump in service. The generation ratios are relatively large initially after installation of the pump, and fall off as the pump becomes "run-in." A steady state region of normal pump wear is reflected by the constant generation ratio. The generation ratio starts to increase again as the pump begins to wear out.

Figure 5.6 shows the data presently available for one aircraft system. N_6, N_{10}, N_{15} refer to the number of particles in the samples greater than 6, 10, and 15 micron respectively. The decaying trend of the N_x-time data reflects the wearing in of the newly installed pump. The high values of N_x for $t = 0$ reflects the high initial contamination generation of the new pump. The samples were taken at relatively coarse intervals of time (t - 0, 35 hours, 70 hours) to fit the normal service procedures for the aircraft. There is insufficient data at present to indicate whether the pump has entered a region of normal wear.

Figure 5.7 shows the actual particle counts for the aircraft system associated with Figure 5.6.

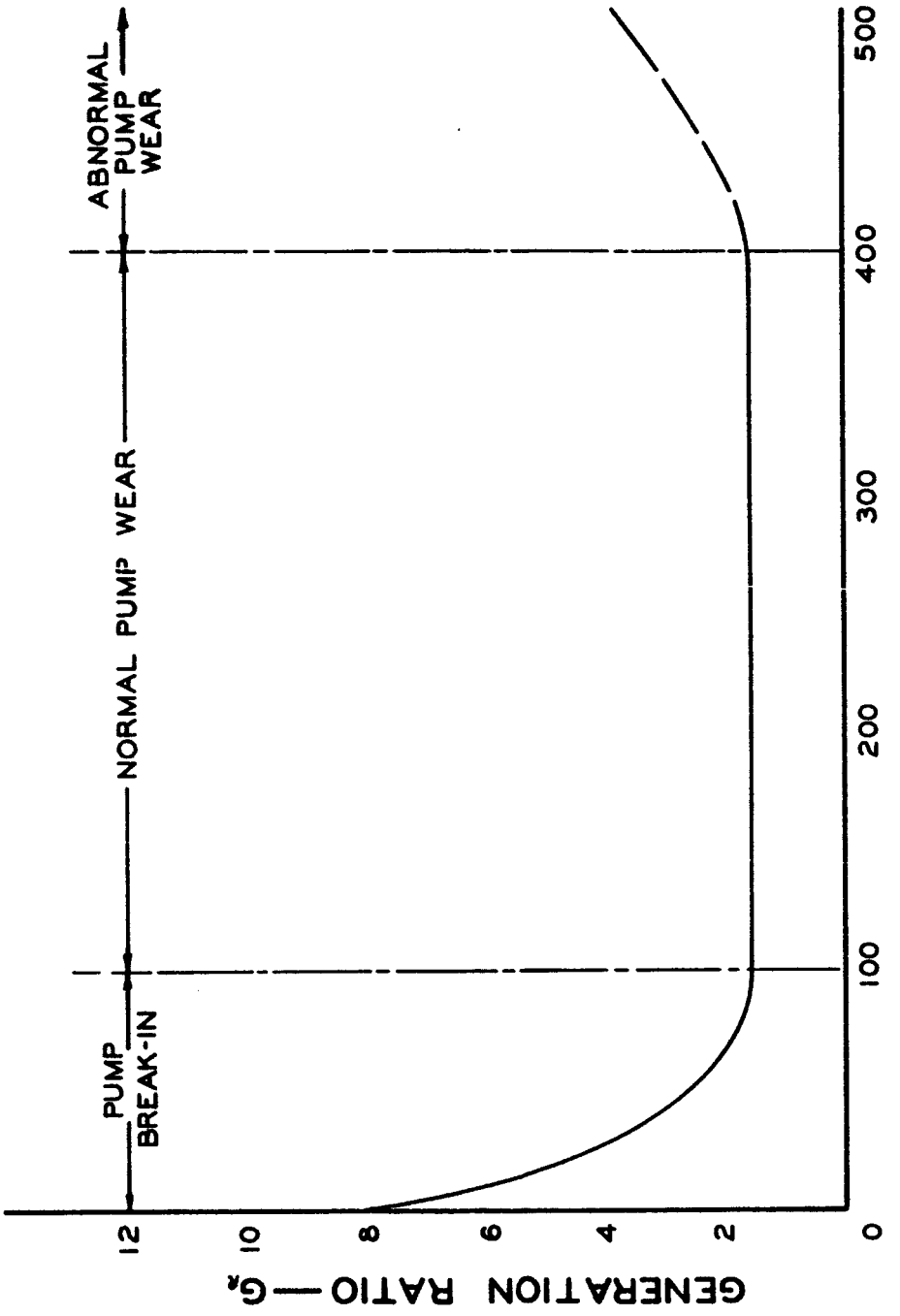

Figure 5.5. Characteristic Pump Curve.

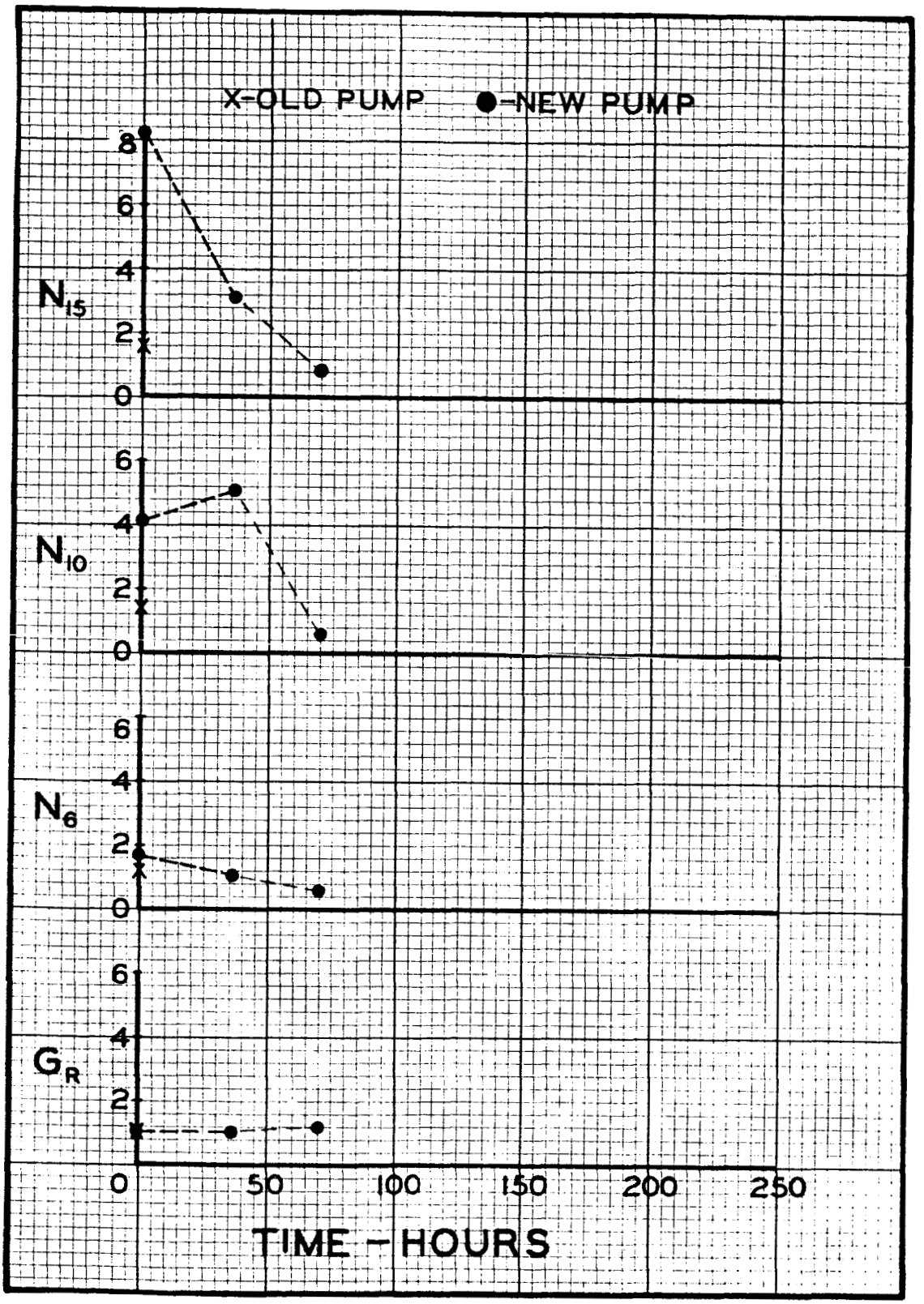

Figure 5.6. Generation Ratio-Time Data From Aircraft Pump.

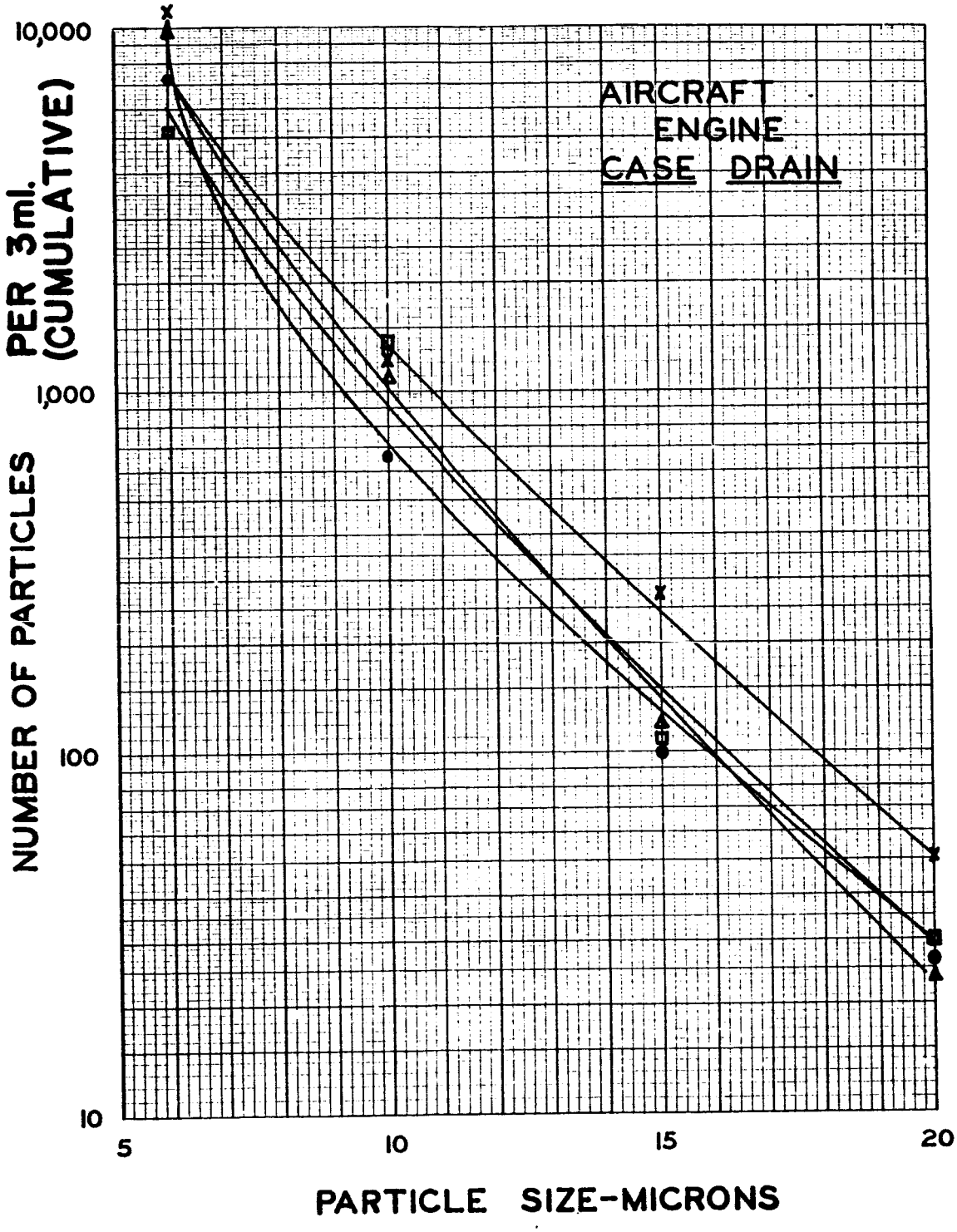

Figure 5.7(a). Particle Size Distribution Curve (Case Drain).

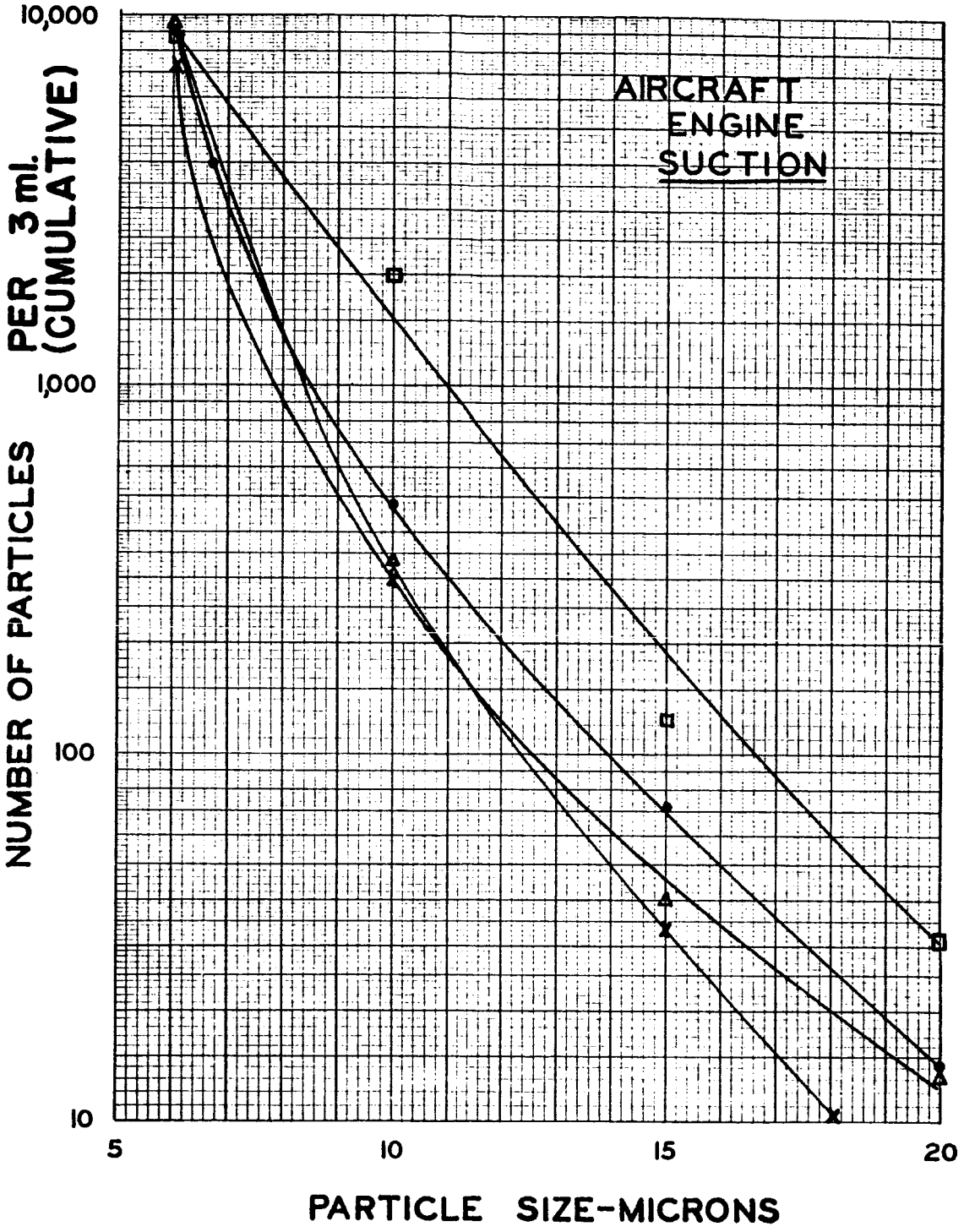

Figure 5.7(b). Particle Size Distribution Curve (Suction).

The types of contaminant found in the aircraft systems included

1. a small number of metallic particles in the 0 - 5 micron range with a large number of silica type particles in the suction samples,
2. a large number of metallic particles in the 5 - 20 micron range in the case drain samples.

Gravimetric analyses varied in the range 3 - 27 mg/l for the suction samples, and 3.5 - 31 mg/l for the case drain samples.

5.5 Conclusions

1. A device suitable for taking oil samples from a working system has been developed.

2. Laboratory testing shows that the sampler withdraws a representative sample of fluid from a working system.

3. Sufficient field tests have been conducted to show that samples can be taken by service personnel for later evaluation by an experienced laboratory staff.

4. The device is simple, rugged, quick-to-use, and does not require specific environmental control during its use.

CHAPTER VI

USE OF THE SILTING INDEX METHOD FOR CONTAMINATION LEVEL ANALYSIS

6.1 Introduction

The common methods used for assessing the contamination level of oil systems--optical assessment and particle counting, particle counting instruments, and gravimetric procedures--do not reveal the true contribution to contamination of particles smaller than about 5 microns. It is known that particles smaller than 5 microns are present in system oil in very large numbers. It is considered also that contaminant in the low size range can play a significant part in the contamination effect on component performance.

Contaminants larger than 5 microns tend to form a relative loose open cake on the surfaces of a filter media, in a somewhat random manner. Particles smaller than 5 microns tend to block the filter flow passages. As the flow passages become blocked, flow of oil through them tends to decay. Under conditions of constant pressure drop across the filter, the rate of decay is mathematically predictable. The Silting Index is a dimensionless parameter which describes the decay of flow under constant pressure drop through a standard membrane filter. In describing such decay in flow, the Silting Index is a measure of the contamination level in the < 5 micron range of the oil being examined.

The Silting Index Apparatus is essentially a graduated cylinder with a 0.8 micron membrane filter disk fitted to one end. The oil sample

to be examined for silting properties is placed into the cylinder. A constant pressure is applied to force the oil through the membrane filter. The times required for three successive pre-determined volume increments of oil to pass through the filter are noted. The first incremental volume (V_1) is small, so that the flow rate indicated by its time of flow approximates the flow rate to be expected for uncontaminated oil. The second and third incremental volumes $(V_2$ and $V_3)$ are chosen so that $V_3 = 2V_3$. The Silting Index is defined as

$$S = \frac{t_3 - 2t_2}{t_1}$$

where t_1, t_2, and t_3 are the times required for volumes V_1, V_2, and V_3 respectively to pass through the membrane filter.

The precise construction of and procedure to be used with a Silting Index Apparatus is described in SAE-ARP 788 (1963). The parameter S has a firm mathematical base, as described by Van Loon (1964)[1] or in Publication XX6801300 of the Millipore Filter Corporation. The higher the value of S, the greater the tendency of the fluid to silt.

The Silting Index apparatus and procedure are simple and independent of fluid properties such as viscosity and temperature, as long as such properties are held constant during a test. The method appears to be a logical compliment to the older methods of contamination level analysis, with special use in the low size range of contaminant which the previous methods could not adequately cover.

---

[1] Van Loon, J. K., "Silting Index," Hyd. and Pneum., March, 1964.

6.2 An Evaluation of Silting Index for Mil-H-5606 Oil

A Silting Index Apparatus manufactured by Millipore Filter Corporation was obtained. The apparatus is shown diagramatically on Figure 6.1. A syringe is mounted vertically in a support frame. A 13 mm. diameter membrane filter holder is connected to the bottom of the syringe via a 3-way valve. The valve positions permit

1. the syringe to be connected to the supply line with the filter isolated,
2. the syringe to be connected to the filter holder with the supply isolated.

The fluid to be examined can be drawn into the cylinder up to the "Fill" mark by withdrawing the syringe plunger. A 0.8 micron membrane filter (Millipore AAWP 013 00 or equivalent) is fitted into the filter holder. The weight is placed on the syringe plunger to generate a constant pressure in the fluid. The valve is opened to cause flow from the syringe through the filter. The times required for the level of fluid to fall from "Fill" to "V_1" (t_1), to V_2 (t_2), and to V_3 (t_3) are noted and used to give the Silting Index

$$S = \frac{t_3 - 2t_2}{t_1}$$

The timing operation of the apparatus was automated to eliminate the inaccuracies inherent in hand timing. The timing unit circuit is shown on Figure 6.2, while Figure 6.3 shows the timing unit and Silting Index Apparatus complete. The timing unit contains 3 clocks which are operated from 4 mercury contact fixed to the plunger weight. A mercury pool is placed beneath the contacts to trigger then when the plunger

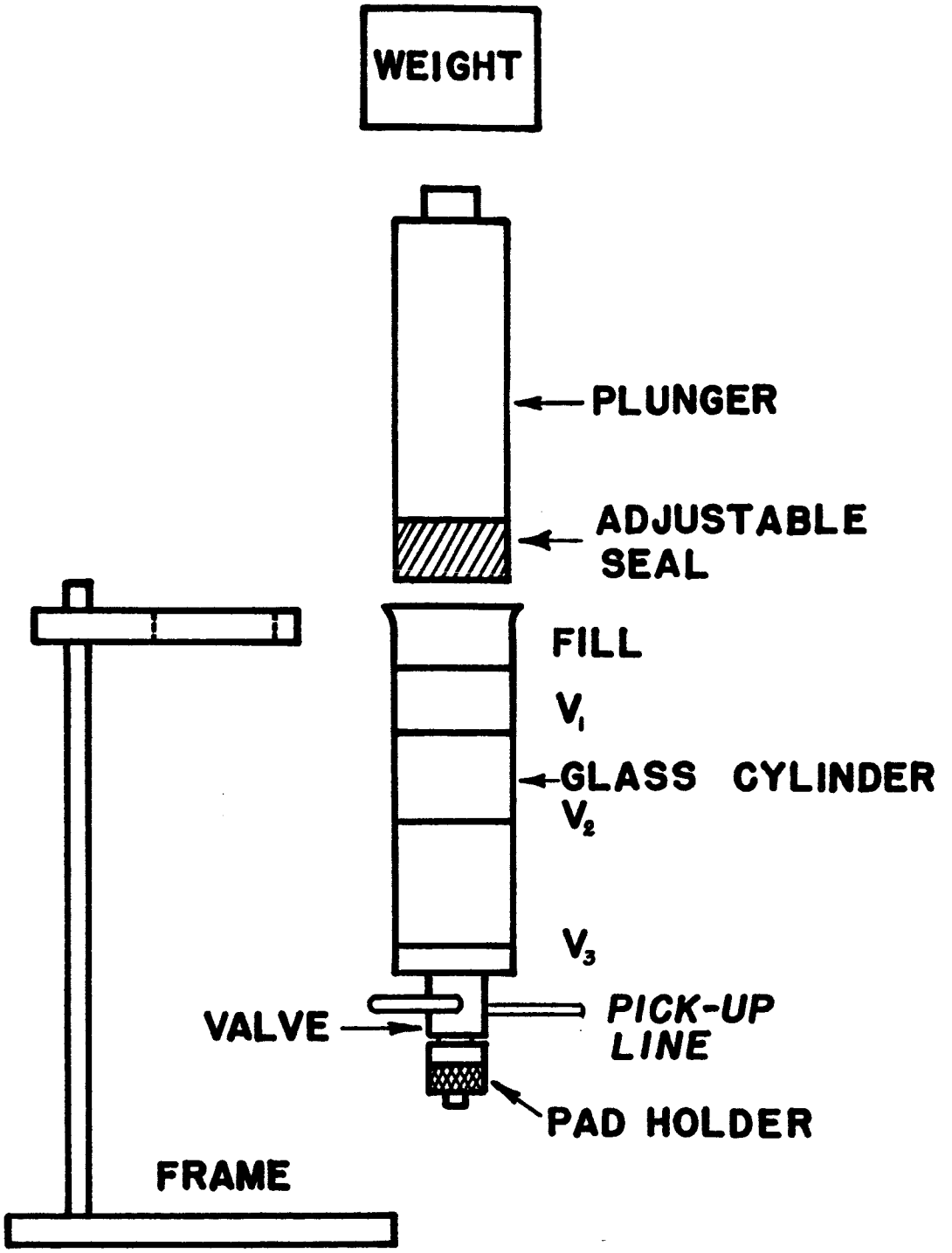

Figure 6.1. Diagram of Silting Index Apparatus.

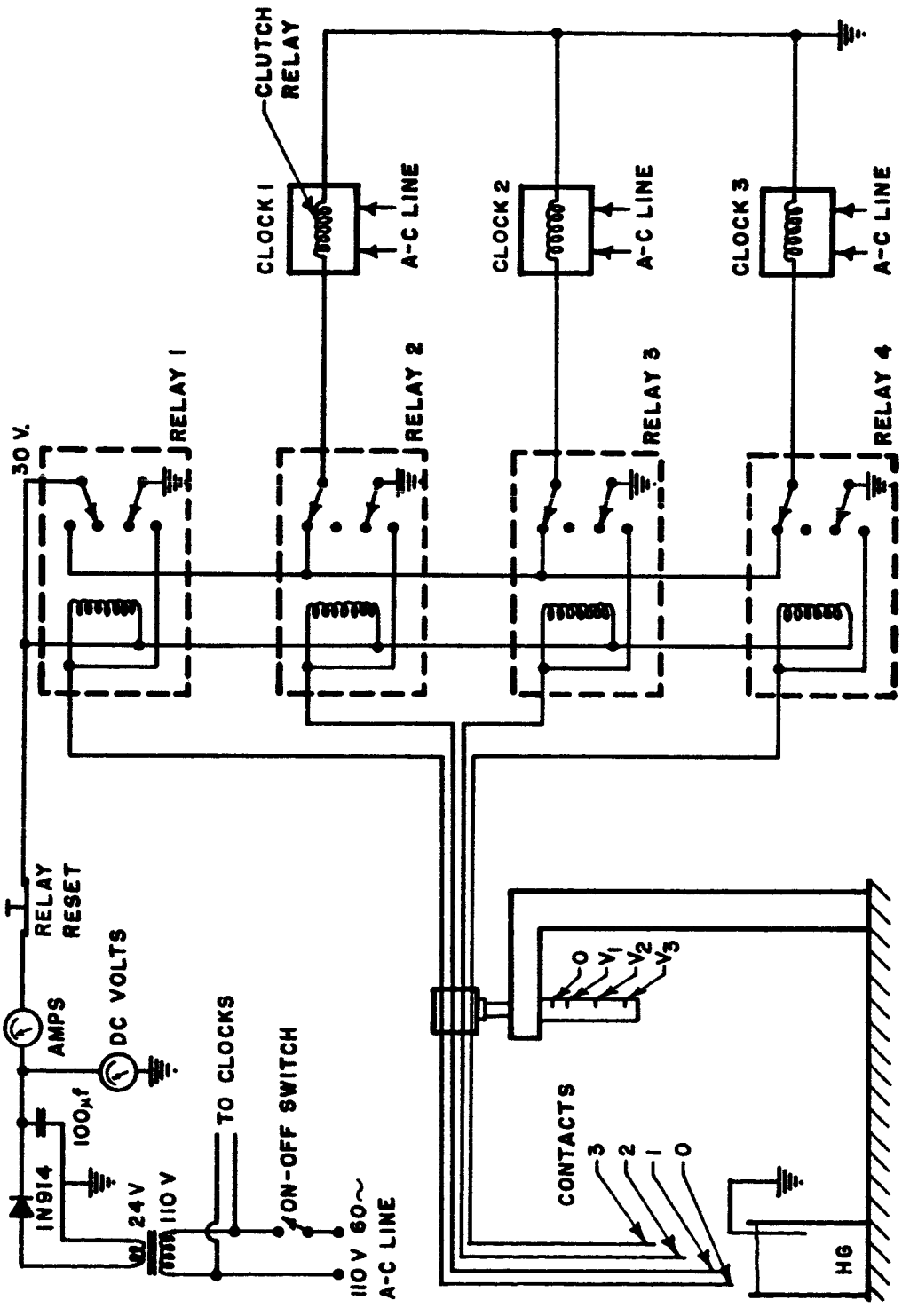

Figure 6.2. Circuit Schematic for Siting Index Timing Unit.

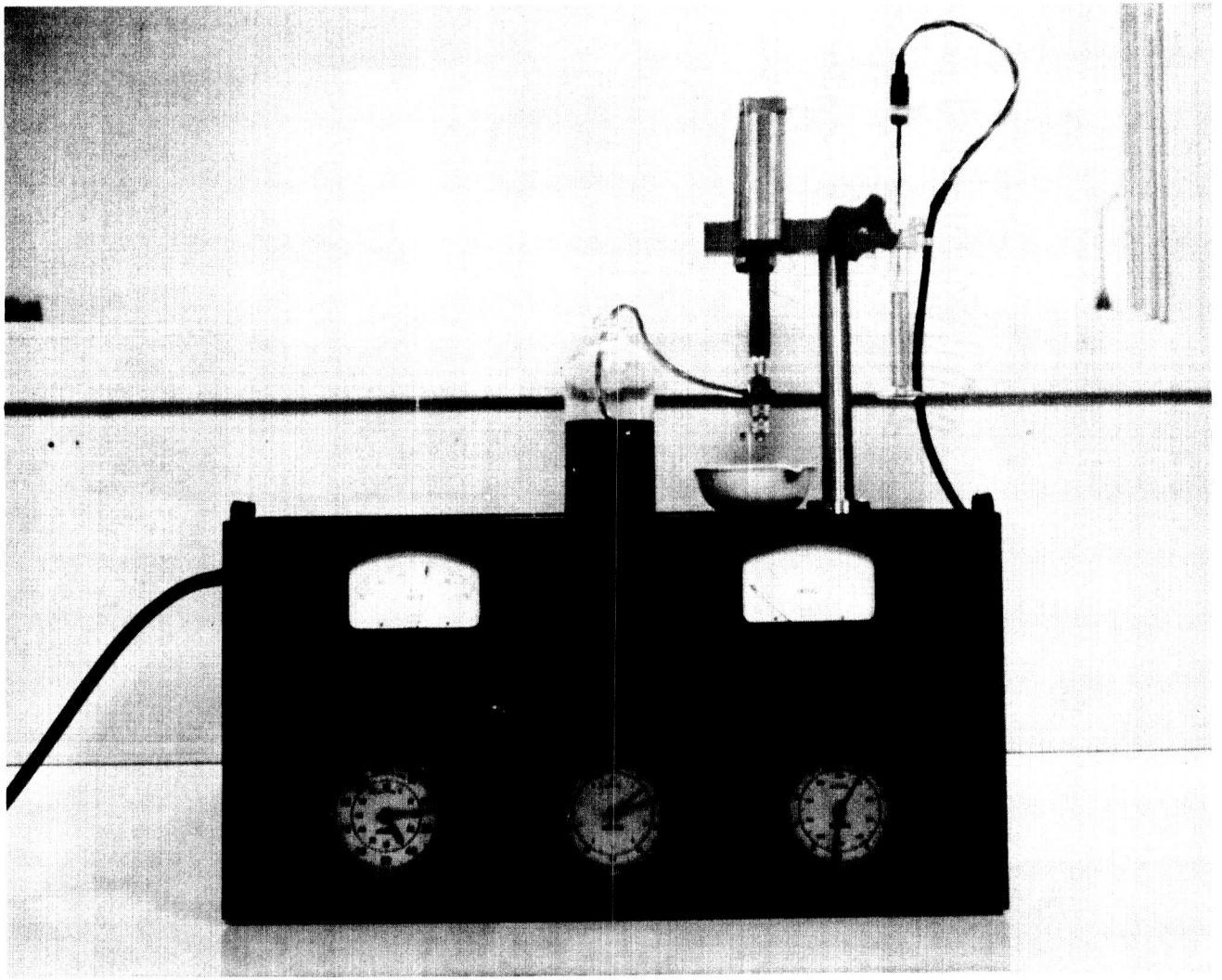

Figure 6.3. Timing Unit for Silting Index Apparatus.

reaches the appropriate position in the syringe cylinder. The sequence of operation is

Contact 0: Starts all clocks when the plunger is in the start or zero position.

Contact 1: Stops clock 1 at the plunger position V_1, thus recording time t_1.

Contact 2: Stops clock 2 at the plunger position V_2, thus recording time t_2.

Contact 3: Stops clock 3 at the plunger position V_3, thus recording time t_3.

6.21 The Repeatability of Silting Index Evaluations

An initial series of tests was conducted using 1 micron rated membrane filters, and MIL-H-5606 oil taken from a working system. The results, shown in Table 6.1 varied over a relatively wide range. To examine the consistency of pore size and distribution in the 1 micron membranes used, a series of readings was made using oil which had been triple-filtered through a 0.45 micron membrane. The readings obtained when a series of tests were made using a single-filter membrane are shown in Table 6.2 to be reasonably repeatable. As to be expected, the Silting Index is zero in each case, indicating the high cleanliness of the oil relative to the filter. Table 6.3 shows the readings obtained when the triple-filtered oil was passed through different 1 micron rated filters. While the Silting Index is zero in each case, the individual readings vary widely indicating the inconsistency of the filter pads used. This type of inconsistency explains the scatter of results in Table 6.1. The tests indicate the necessity to use the recommended 0.8 micron filter pads,

TABLE 6.1

Source: Contaminated 5606 Hydraulic Fluid,
New 1.0μ Filter Pad Used for Each Test

Run	T_1	T_2	T_3	Silting Index
1	2.29	14.8	85.0	24.1*
2	3.72	33.3	221.3	41.7
3	2.90	22.0	130.1	29.7
4	1.88	6.2	80.3	36.0

$$*S.I. = \frac{t_3 - 2T_2}{t_1}$$

TABLE 6.2

Source: Triple Filtered (0.45μ) 5606 Hydraulic Fluid,
Same Filter Pad Used for Each Test

Run	T_1	T_2	T_3	Silting Index
1	1.98	9.3	18.7	0
2	1.99	9.1	18.3	0
3	2.00	9.1	18.2	0
4	1.90	8.7	17.7	0
5	1.77	8.3	16.7	0
6	1.89	8.6	17.1	0
7	1.85	8.6	17.1	0
8	1.99	8.7	17.3	0
9	1.87	8.5	17.0	0
10	1.95	8.7	17.5	0

TABLE 6.3

Source: Triple Filtered 5606 Hydraulic Fluid,
New Filter Pad Used for Each Test

Run	T_1	T_2	T_3	Silting Index
1	6.10	28.5	56.4	0
2	3.91	15.9	30.8	0
3	7.29	32.5	64.0	0
4	2.50	11.0	22.0	0

which are manufactured with close control on pore size for use with the Silting Index Apparatus.

6.22 The Effect on Silting Index of Filter Pad Pore Size

The Silting Index test was conducted with a range of filter pad sizes, using MIL-F-5606 containing 30 mg/l of the 0-5 micron portion of AC Fine test dust as the test fluid. The results, shown on Figure 6.4 indicate that filter pads of pore size greater than 1.2 micron are insensitive to silting under the prescribed conditions. The standard Silting Index pad of 0.8 micron rated pore size is also fairly insensitive giving very low values for Silting Index. The smaller pore size pads were increasingly sensitive, giving large values for Silting Index. The results indicate that the use of a particular pad size, such as the recommended 0.8 micron pad in the present case, limits the flexibility of the Silting Index test by limiting the range of contaminant levels to which the test is sensitive.

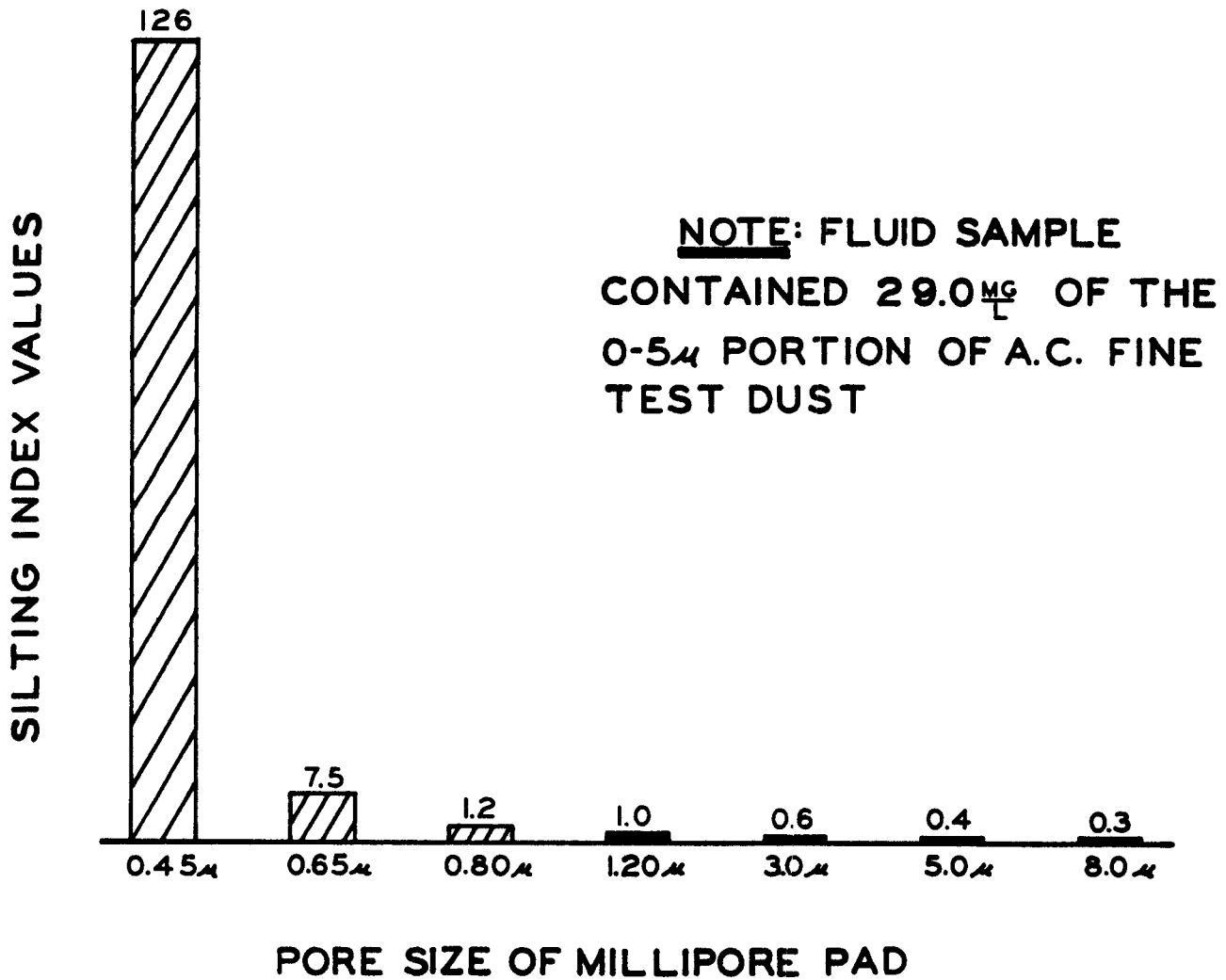

Figure 6.4. Effect of Filter Pad Size on Silting Index.

6.3 Relationship Between Silting Index and Gravimetric Analysis

Simultaneous gravimetric and silting index evaluations were made on samples of oil contaminated to different levels with the 0-5 micron portion of AC Fine test dust. The results, Figure 6.5, show reasonably a relationship of the form

$$\log_{10} S = aG + b, \text{ or } \qquad S = e^{(cG + d)}$$

where a, b, c, and d are constants, and G is the gravimetric level. It appears that Silting Index can be correlated to gravimetric analysis for low micron contamination. It is considered likely that additional contaminant of larger sizes will not appreciably affect a Silting Index evaluation. However, large particles will increase a gravimetric evaluation, and hence it is likely that the correlation of Figure 6.5 is applicable only to low micron contamination conditions.

Figure 6.6 which shows a similar semi-log plot for 0-20μ contamination, illustrates the poorer correlation for the larger size contaminant.

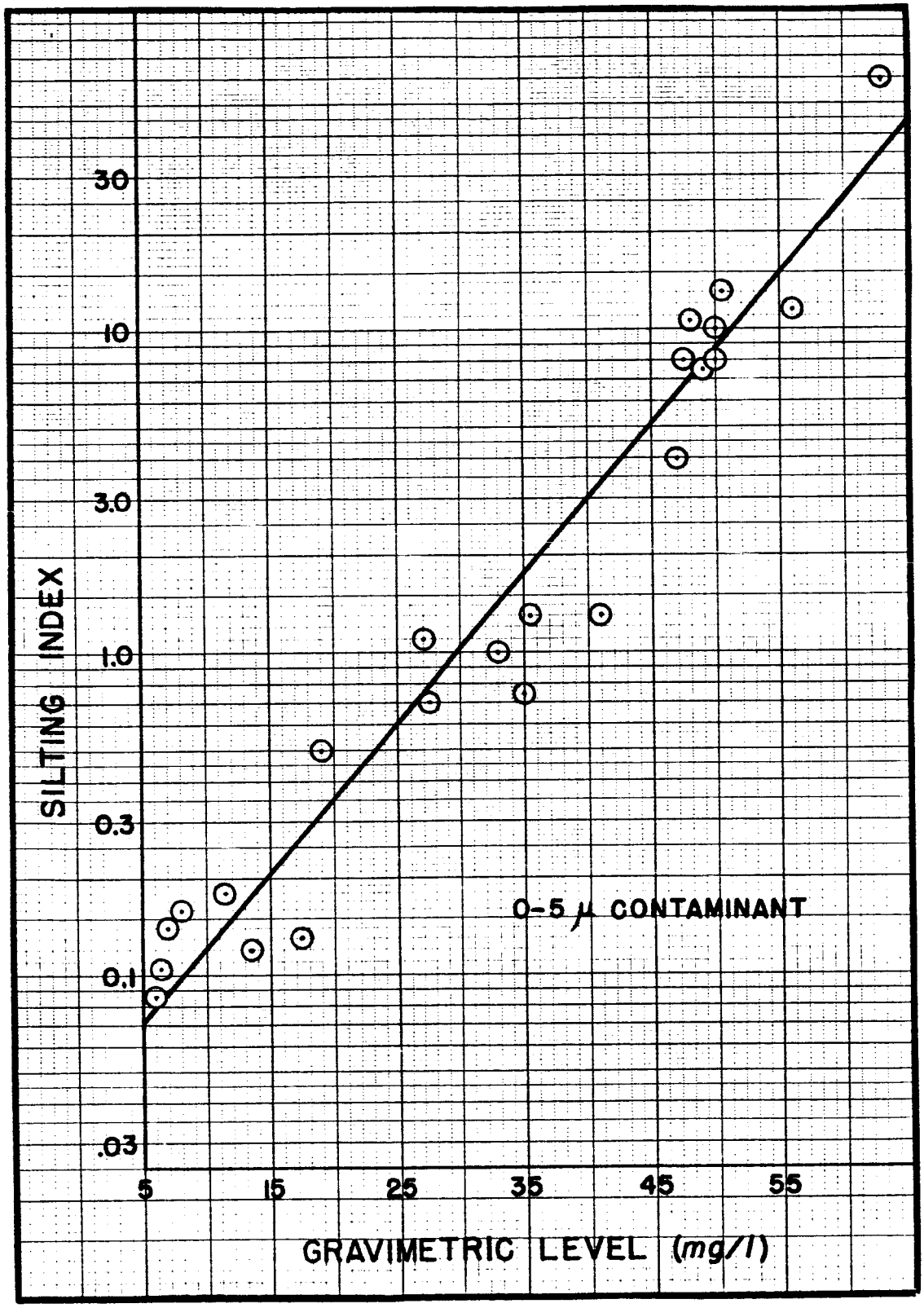

Figure 6.5. Silting Index Vs. Gravimetric Level for 0-5μ Contaminant.

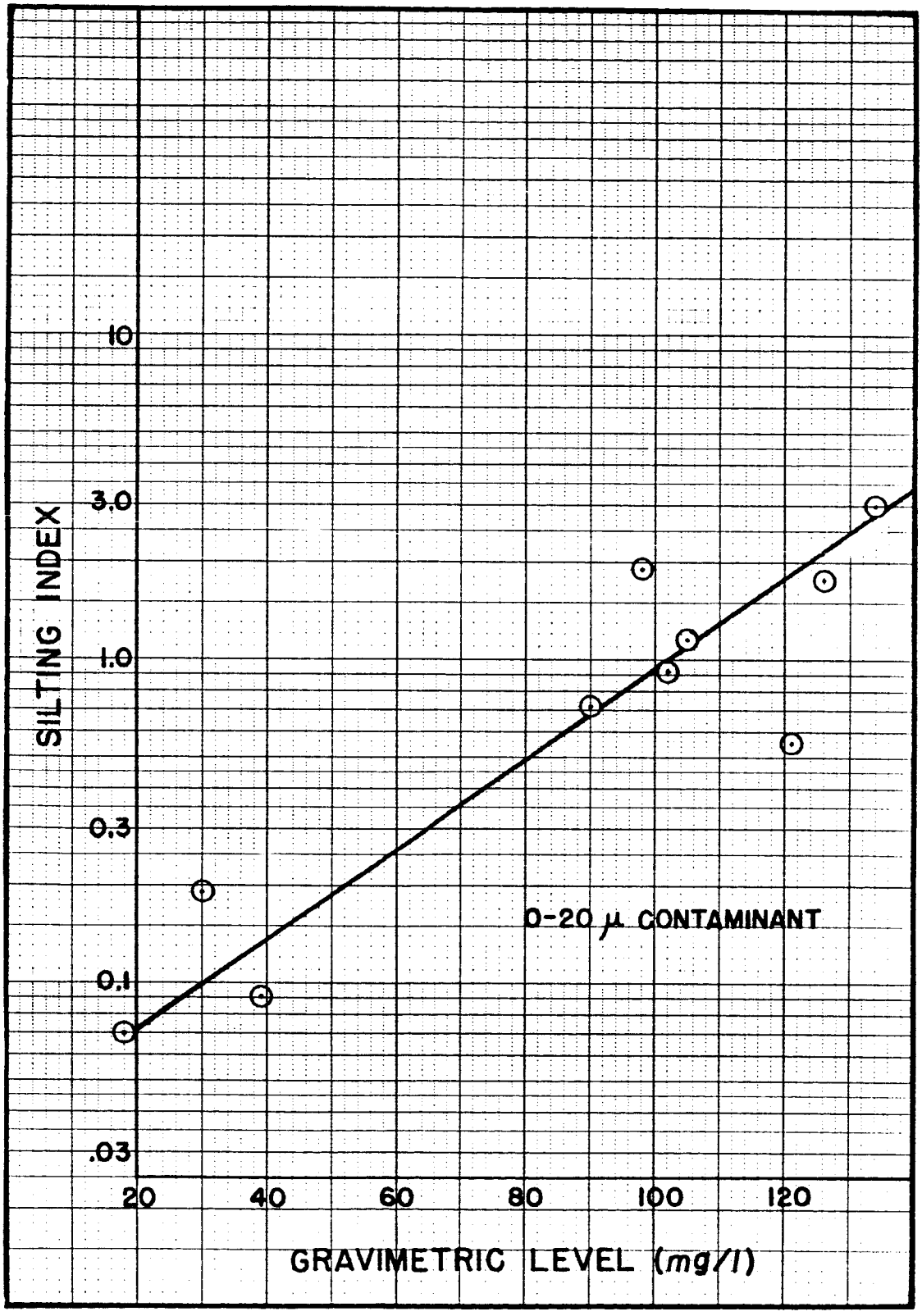

Figure 6.6. Silting Index Vs. Gravimetric Level for 0-20μ Contaminant.

APPENDIX A

NOMENCLATURE

a	Volume of solid particles removed per unit volume of filtrate.
A	Surface area of filter element and cake normal to direction of flow.
B	A constant associated with cake filtration which describes particle shape and orientation in the cake and the length of flow path/thickness ratio of the cake.
C	Constants associated with linear P - W curves.
g	Acceleration due to gravity.
h	The length of the pores of a filter medium.
K	The plugging constant associated with a filtration mechanism.
L	Length of pore of filter medium.
n	An exponent associated with the mechanism of filtration.
Q	flow rate of fluid through a filter.
r	Effective initial pore radius of a filter element.
R_m	Resistance to flow of the filter element.
S_o	Specific surface of particles of contamination.
t	Time.
V	Volume of filtrate passed through filter.
w	Weight of solid particles deposited in filter cake per unit volume of filtrate.
W	Total weight of solid particles presented to a filter.
W_o	Total weight of solid particles in a filter cake.

α Specific resistance to flow of a filter cake.

ΔP Pressure drop across a filter.

ΔP_o Pressure drop across a filter when uncontaminated fluid is flowing through it.

ϵ Porosity or void fraction of a filter cake.

ρ_s Density of contamination particles.

μ Dynamic viscosity of the fluid flowing through the filter.

APPENDIX B

FILTER EVALUATION TEST STAND

The Filter Evaluation Test Stand is a multi-purpose unit which is used to perform contaminant capacity and pressure versus flow tests on filter elements. The Evaluation Stand used for the tests in this report is the third unit constructed at OSU; and, therefore, the design concepts included in it represent the experience gained in using the two previous test stands.

A schematic diagram of the test stand is shown in Figure B.1. The stand is equipped with a vari-drive motor and pump unit with flow capabilities up to 45 gpm. The temperature of the system fluid is maintained to within $\pm$ 0.5°F of the desired temperature for a given test. The circuit includes a 0.5 micron nominal control filter which maintains a contaminant level in the test fluid well below that which would "load" any of the elements being evaluated. The flow rate through the filter under examination is measured by a Fischer and Porter turbine meter and displayed on a digital counter. The differential pressure across the element and housing is measured with a 0-200 psi Heise gage that is subdivided into 0.2 psi increments. The pressure measurements are made in accordance with SAE ARP 24A. Figure B.2 is a photograph of the control panel of the test stand.

The contaminant injections are made by means of a bypass circuit which is shown in the schematic. This bypass circuit can be electrically

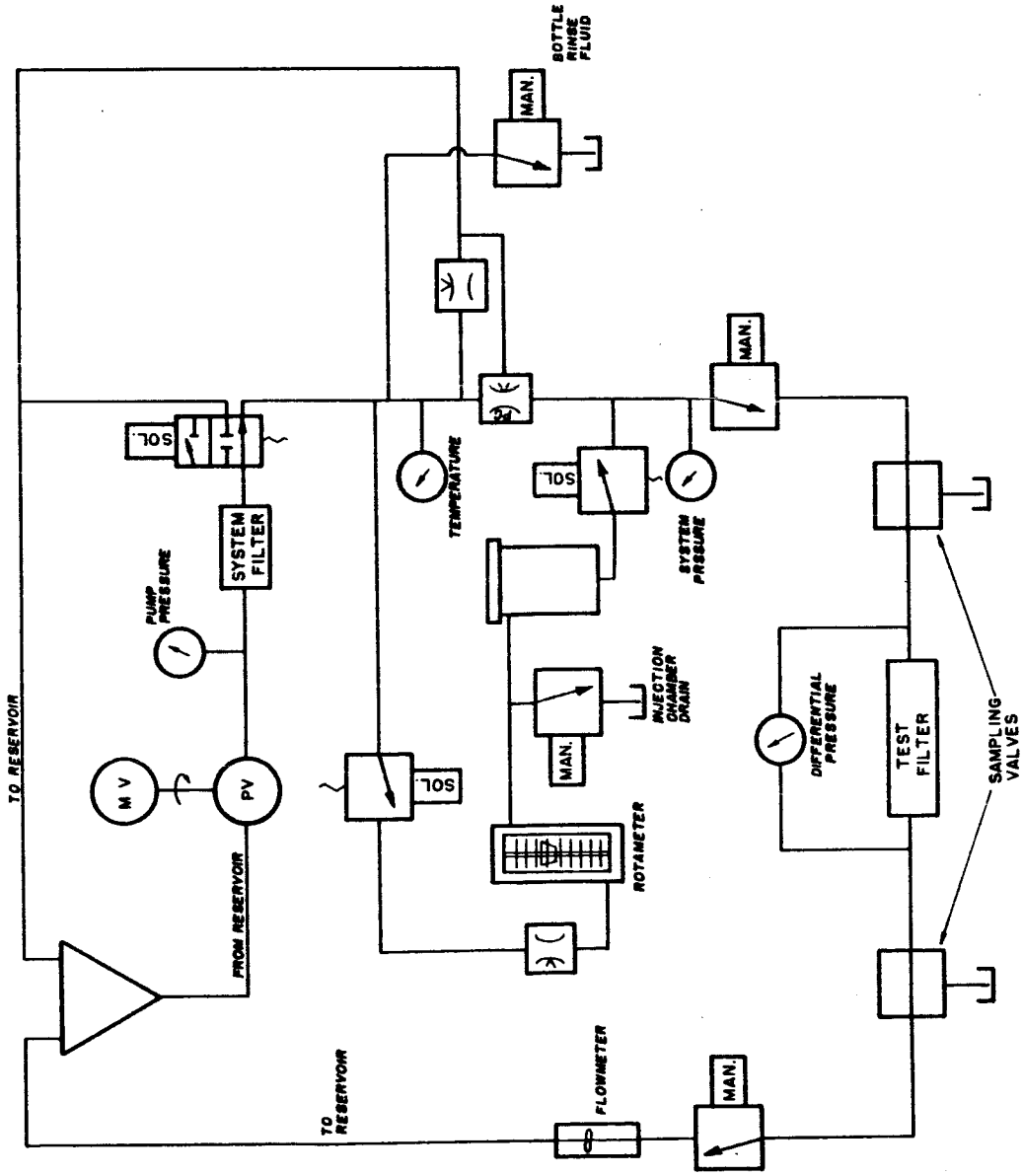

Figure B.1. Schematic Diagram of Filter Evaluation Test Stand.

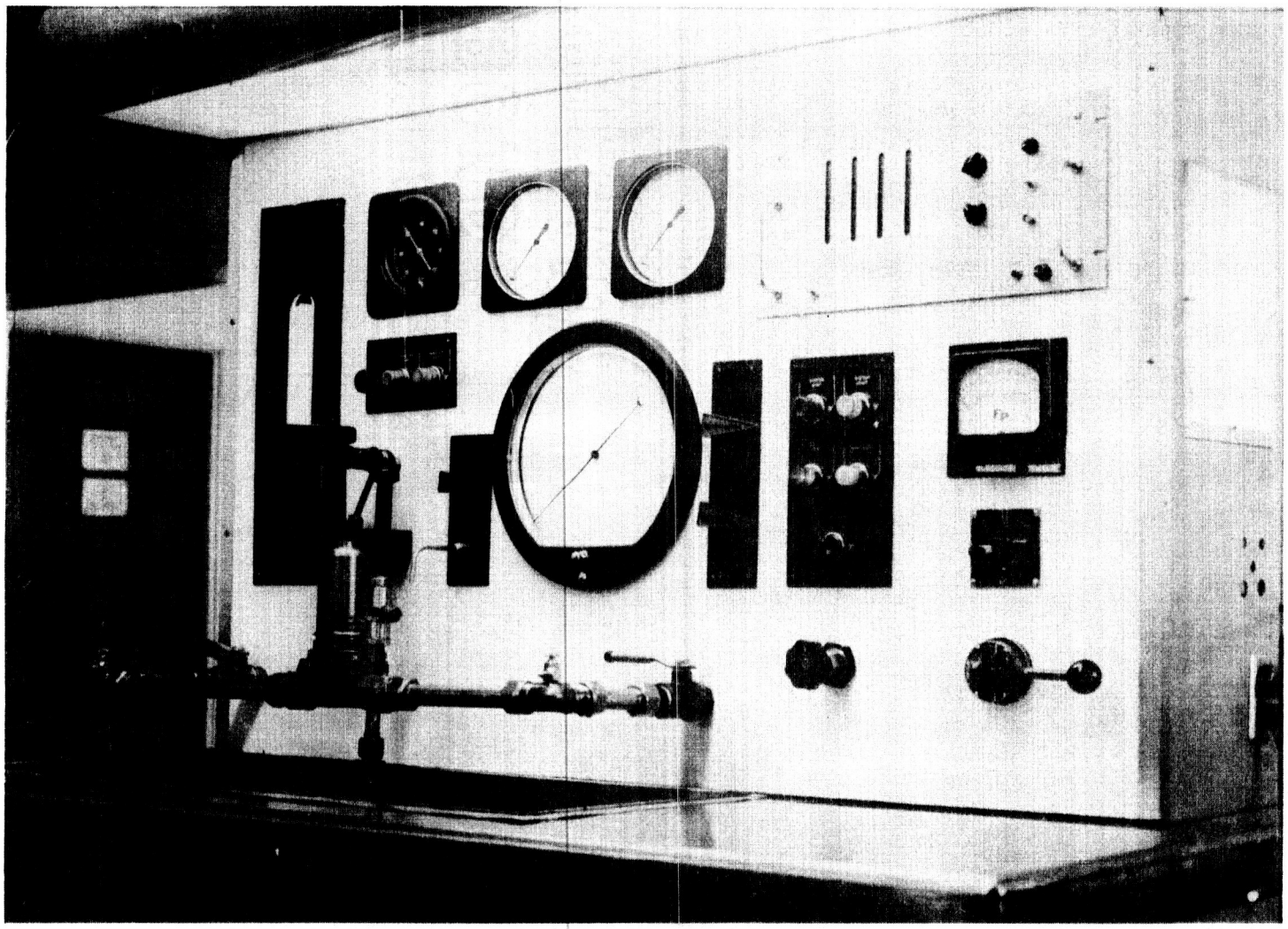

Figure B.2. Photograph of Filter Evaluation Test Stand.

isolated from the system flow by actuating a solenoid valve, located upstream of the injection chamber, and an air operated ball valve, located downstream of the chamber. The chamber itself has a conical shape which provides no trap for the contaminant that is added to it. The volume of the chamber is approximately 1 liter. The test contaminant is added to the injection chamber in the form of a slurry. This slurry is prepared by placing the desired weight of contaminant into an ultrasonically cleaned 125 ml bottle. The bottle is then filled with clean system fluid from an outlet on the stand and then it is placed in an ultrasonic bath to disperse the contaminant in the fluid. This slurry is then immediately added to the injection chamber by removing the chamber top and draining 200 ml. of fluid. After pouring the slurry into the chamber, the bottle is then refilled and shaken and the rinse fluid and residual contaminant is added to the chamber. Upon closing the chamber the upstream and down stream valves are then opened allowing a portion of the system flow to pass through the chamber and carry the suspended contaminant into the main flow upstream of the test filter.

The bypass flow continues for a time period which is sufficient for all of the contaminant to reach the filter. A total volume 3 times that of the chamber volume is adequate. The bypass flow rate is controlled with a needle valve and measured with a rotameter. The flow rate through the injection chamber is regulated to approximately one-tenth of the rated flow of the element under test. Consequently, the injection time must be varied to allow for adequate flushing. An electrical timer which may be set from 0 to 5 minutes is included in the electrical system

of the injection circuit. At the end of the timed interval, the bypass circuit is again isolated from flow and a new contaminant sample can be added. In most cases, an injection can be made at 1½ minute intervals. Following each injection the pressure differential is measured and recorded. This procedure is continued until the differential pressure across the element reaches a predetermined level.

There are several requirements which have been found to be of extreme importance in order to conduct contaminant capacity tests which are meaningful and reproducible. These requirements are satisfied in the design of this stand and the procedures outlined above. These requirements in summary are as follows:

1. A constant flow rate and temperature through the filter must be maintained throughout the test.
2. The contaminant must be thoroughly dispersed in the test fluid. The addition of dry contaminant without dispersion results in the aglomeration of the contaminant and often can give erroneous results.
3. Thorough flushing of the injection system after each addition of contaminant is mandatory for reliable test results.
4. "Contaminant traps" between the injection chamber and the test filter should be eliminated.

APPENDIX C

FILTER ELEMENT AND MEDIA CLEANING PROCEDURES

The nature of many of the tests reported in this document has required that filter elements and filter media be restored to a clean status following a contaminant capacity test. Previous investigations at OSU have demonstrated that wire cloth can be cleaned to its initial cleanliness level by the proper use of ultrasonics in conjunction with suitable cleaning solvents. The cleaning procedure used for cleaning the elements and media tested in this study is as follows:

1. The contaminated unit is placed in petroleum ether for degreasing and then is allowed to dry.
2. The unit is placed in a beaker containing water and a liquid detergent and the beaker is placed in an ultrasonic bath.
3. After vibration, the unit is rinsed with water, dried, and shaken again in a beaker of triple-filtered (0.45μ) trichloroethylene.
4. After rinsing with petroleum ether (triple-filtered) the unit is allowed to dry.

The adequacy of this procedure was demonstrated by the fact that the pressure drop across the cleaned unit could be restored to its initial value. Also, the contaminant capacity of the cleaned unit was restored. The ultrasonic unit which was used was a Westinghouse Model MT-2 having an energy level slightly in excess of 10 watts/sq.in.

OKLAHOMA STATE UNIVERSITY
OF AGRICULTURE AND APPLIED SCIENCE
INSTRUCTION RESEARCH EXTENSION
1891

THE COLLEGE OF ENGINEERING